Determining appropriate loss coefficients for use in the nozzle-model of a stage-by-stage turbine model

Prepared By:

Alton Cadle Marx

MRXALT001

Department of Mechanical Engineering

University of Cape Town

Supervisor: Prof. Wim Fuls

January 2019

Submitted to the Department of Mechanical Engineering at the University of Cape Town in partial fulfilment of the academic requirements for a Masters of Science degree in Mechanical Engineering

Key Words: Turbine loss coefficient, Flownex, Stage-by-stage turbine nozzle-model,

Loss coefficient algorithm

Declaration

I, Alton Cadle Marx, know the meaning of plagiarism and declare that all the work in the document, save for that which is properly acknowledged, is my own. This dissertation has been submitted to the Turnitin module (or equivalent similarity and originality checking software) and I confirm that my supervisor has seen my report and any concerns revealed by such have been resolved with my supervisor.

Signed by candidate

_____

Alton Cadle Marx

Abstract

A previously developed turbine modelling methodology, requiring minimal blade passage information, produced a customizable turbine stage component. This stage-by-stage turbine nozzle-model component was derived from the synthesis of classical turbine theory and classical nozzle theory enabling the component to accurately model a turbine stage. Utilizing Flownex, a thermo-hydraulic network solver, the turbine stage component can be expanded to accurately model any arrangement and category of turbine.

This project focused on incorporating turbine blade passage geometrical information, as it relates to the turbine specific loss coefficients, into the turbine stage component to allow for the development of turbine models capable of predicting turbine performance for various structural changes, anomalies and operating conditions.

The development of turbine loss coefficient algorithms as they relate to specific blade geometry data clusters required the investigation of several turbine loss calculation methodologies. A stage-by-stage turbine nozzle-model incorporating turbine loss coefficient algorithms was developed and validated against real turbine test cases obtained from literature.

Several turbine models were developed using the loss coefficient governed turbine stage component illustrating its array of capabilities. The incorporation of the turbine loss coefficient algorithms clearly illustrates the correlation between turbine performance deviations and changes in specific blade geometry data clusters.

Acknowledgements

I would like to express my sincere gratitude to the following individuals and organizations:

- The Eskom Power Plant Engineering Institute (EPPEI) program and the UCT ATProM team.

- Everyone who assisted in making this study possible, notably Prof. Pieter Rousseau and my engineering managers; Joe Roy-Aikins and Kapil Sukhnandan.

- My industrial mentor, Gary de Klerk, for his guidance that lead me towards my post-graduate studies.

- My wife, Candice Marx, for her endless love, encouragement and willingness to proofread engineering jargon.

- My supervisor, Prof. Wim Fuls, without who's outstanding professional guidance, continuous patience and enthusiastic discussions, this study would not be possible.

- My late grandfather, Brian Samuel, Weil ich dir so viel verdanke.

Table of Contents

List of Figures

List of Tables

List of Nomenclature

General Symbols

h	Enthalpy	kJ/kg
s	Entropy	kJ/kg·K
ρ	Density	kg/m^3
μ	Dynamic Viscosity	kg/ms
p	Pressure	MPa, kPa
c_p	Specific Heat at Constant Pressure	kJ/kg·K
c_v	Specific Heat at Constant Volume	kJ/kg·K
k_s	Surface Finish	mm
u	Blade Speed, Turbine Rotational Speed	m/s, rpm
T	Temperature	˚C / K
V	Volume	m^3
v	Working Fluid Velocity	m/s
Δv	Difference in Working Fluid Velocities	m/s
w	Work	MW, kW

Subscripts

co	Carry-over
s	Ideal, Isentropic
$0,1,2,3\ldots$	Position Indication
r	Relative
Stg	Stage
x, y, z	Turbine Stage Indication

Superscripts

$'$	Stator Blade Row / Fixed Blades / Nozzles
$''$	Rotor Blade Row / Moving Blades / Buckets

Dimensionless Parameters

k_{co}	Carry-over ratio	
x_{Df}	Dryness Fraction	
ζ	Enthalpy Loss Coefficient	
η	Efficiency	%
Ma	Mach Number	
n_{Bld}	Number of Blades per Row	
N	Number of Stages	
C_D	Restrictor Contraction Coefficient	
C_L	Restrictor Loss Coefficient	
Y	Pressure Loss Coefficient	

Dimensionless Parameters Continued

R	Degree of Reaction	%
Re	Reynolds Number	
RF	Reheat Factor	
k	Specific Heat Ratio	
c_w	Change in Flow Velocity Ratio	

Blade Geometry Symbols

D_m	Mean diameter	m, mm
D_n	Hub diameter	m, mm
D_s	Tip diameter	m, mm
l	Blade height	m, mm
υ	Blade diameter hub to tip ratio	
S_{Wdth}	Blade width	m, mm
S_{chrd}	Blade chord length	m, mm
δ_{gap}	Blade row gap width	m, mm
δ_{Bld}	Maximum blade thickness	m, mm
δ_{Te}	Trailing edge thickness	m, mm
O	Throat width	m, mm
τ	Blade tip clearance	m, mm
ω	Shrouded tip leakage mass flow ratio	
Υ	Shrouded tip leakage velocity ratio	
φ	Unshrouded tip leakage mass flow ratio	
K_τ	Unshrouded correction coefficient	
D_{LSB}	Last Stage Blade interconnection diameter	m, mm
l_{LSB}	Last Stage Blade interconnection length	m, mm
d_{LSB}	Last Stage Blade interconnection thickness	m, mm
w_{LSB}	Last Stage Blade interconnection width	m, mm
f_{hcc}	Height of the curvature of the camberline	m, mm
C_{Line}	Camberline	m, mm

Angles

α_0	Inlet Angle	°
α_1	Outlet Angle	°
α_{Inc}	Incidence angle	°
β_s	Blade stagger angle	°

Areas

A_{BldGap}	Blade spacing area	m^2
A_{Flow}	Overall flow area	m^2

Abbreviations

AGARD	The Advisory Group for Aerospace Research and Development
AT	Acceptance Test
GT	Gas Turbine
HBD	Heat Balance Diagram
HP	High Pressure Turbine
IP	Intermediate Pressure Turbine
LSB	Last Stage Blade
LP	Low Pressure Turbine
LS	Live Steam
LTA	Life Time Assessment
RHS	Reheat Steam
rpm	Revolution per Minute
ST	Steam Turbine

Chapter 1 Introduction

1.1 Background

Power production performance modelling and simulations have become a vital everyday component of the energy engineering sector. The evaluation of seemingly unrelated performance variations of power plant components as they relate to distant structural anomalies has become common practice. This has been made possible by the tedious evolution from the complex hand calculation performed in the past to the present spectrum of computerized applications that has many shapes, structures and formats.

Turbine performance modelling plays a key role in power production performance evaluations. Although turbines very simply put only convert energy from one format to another the modelling thereof is a slightly more complex matter. For this reason, many methodologies exist to accurately model turbines. A dominant theme throughout literature is the determination and prediction of turbine efficiency and loss quantification.

Combining turbine performance modelling with plant operation data and turbine specific design information it becomes possible to identify location specific anomalies and suggest improvements to affected turbine sectors. This, in turn, could inform maintenance procedures, assist in accurate lifetime assessments (LTA) of steam path components (such as blading, seals and diaphragms) and thus benefit overall turbine operation and performance.

Small anomalies can contribute to significant performance losses and develop into more severe problems that can affect the lifespan of components and the entire turbine. Evaluating performance consistency across the stages of a turbine allows for the isolation of specific problem areas within the turbine.

This study builds upon a previously developed turbine modelling methodology, requiring minimal blade passage information, that produced a customizable turbine stage component [1]. This stage-by-stage turbine nozzle-model component was derived from the synthesis of classical turbine theory and classical nozzle theory enabling the component to accurately model a turbine stage. Utilizing Flownex, a thermo-hydraulic network solver, the turbine stage component can be applied to accurately model any arrangement and category of an axial turbine.

This study aims to incorporate additional turbine blade passage geometrical information, as it relates to the turbine specific loss coefficients, into the turbine stage component. This inclusion will allow for the development of turbine models capable of predicting turbine performance for various structural changes, anomalies and operating conditions, without requiring assumptions or calibrations of the loss coefficient.

1.2 Research objectives and limitations

A need was identified for the investigation and determination of the most beneficial loss coefficient sets that would provide the greatest possible advance to the existing stage-by-stage turbine nozzle-model component [1]. For this reason, this study is focused on the development of turbine loss coefficient algorithms, as they relate to specific blade geometry data clusters, whilst maintaining a minimal geometric data input requirement.

Listed below are key approach orientated objectives that define the backbone of the study:

- Investigation of turbine loss methodologies.
- Determine appropriate loss coefficients for design conditions.
- Determine the best loss coefficient or correction factor for off-design conditions.
- Investigate the implementation possibility of Carry-over and Reheat factor.
- Develop a comprehensive loss coefficient calculation algorithm.
- Implement algorithms into the nozzle-model and test model's structural soundness.
- Construct a case study model in Flownex for validation and verification purposes
- Construct a case study model of an existing operational steam turbine to illustrate modelling ability for both design and off-design conditions.
- Utilizing a developed steam turbine model, display the ability to predict offset performance conditions resulting from turbine component variance.
- Demonstrate how the new loss coefficients can help to quantify the impact of design and operational variation on the overall turbine performance.
- Develop a practical user-friendly interface and listing procedure for the loss coefficient algorithm script architecture in the nozzle model.

The greatest impediment for the study was the availability of sensitive design information. Due to the intellectual property rights that govern the majority of the turbine design and manufacturing sector, obtaining information has been limited. This limiting factor restricts the extent and range of the validation and testing of the loss coefficient algorithms. Unfortunately, while some data have been obtained, the source and some specifics may not be disclosed.

Additionally, this study only extends to axial flow gaseous turbines: air, steam.

1.3 Dissertation outline

This dissertation is comprised of a further eight chapters consisting of the following content:

Chapter 2: Literature Review

Establishes an overview of turbine fundamentals, designs and performance modelling as to orient the reader to the general focus area of this study. This is followed by an in-depth review of key focus areas, notably carry-over and reheat factor, turbine loss coefficients and turbine blade design.

Chapter 3: Research Methodology

Builds on the focus areas discussed in Chapter 2 by analysing how all the various components fit together, before providing a numerical evaluation required for the development of the loss coefficient algorithm. The implementation of the loss coefficient algorithm into the stage-by-stage turbine nozzle-model component completes the chapter.

Chapter 4: Algorithm Validation

Acts as a validation case study that compares the published AGARD air turbine test case, utilizing the loss coefficient algorithms, against comparable turbine models and the original turbine test case measurements.

Chapter 5: Design and Off-Design Evaluation

Evaluates the ability of the stage-by-stage turbine nozzle-model component, governed by turbine loss coefficient algorithms, to model an actual steam turbine. The case study compares the performance of the turbine model against the actual turbine for both design and off-design conditions.

Chapter 6: Turbine Blade Design Deviation Impact

Investigates the information that can be obtained for a single turbine stage model with focus placed on specific turbine blade geometry data clusters as they relate to turbine loss coefficients. Four different case study are evaluated: Blade profile design improvement, Blade profile degradation, Blade shrouding variations and LSB Interconnection impact.

Each case study examines the impact that deviating from an original blade design has on stage performance.

Chapter 7: Conclusion & Recommendation

This chapter concludes the dissertation, drawing together significant findings, performance correlations, model features and capabilities made possible by the turbine loss coefficient algorithm implementation. Recommendations for further investigation completes the chapter.

Chapter 2 Literature Review

According to the International Energy Agency [2], approximately 75% of the world's energy is produced by power plants dependent on gaseous turbines. An example of this is illustrated by a layout of a conventional coal-fired power station depicted in Figure 2-1. Steam turbines are utilized for the energy conversion between the boiler and the generator.

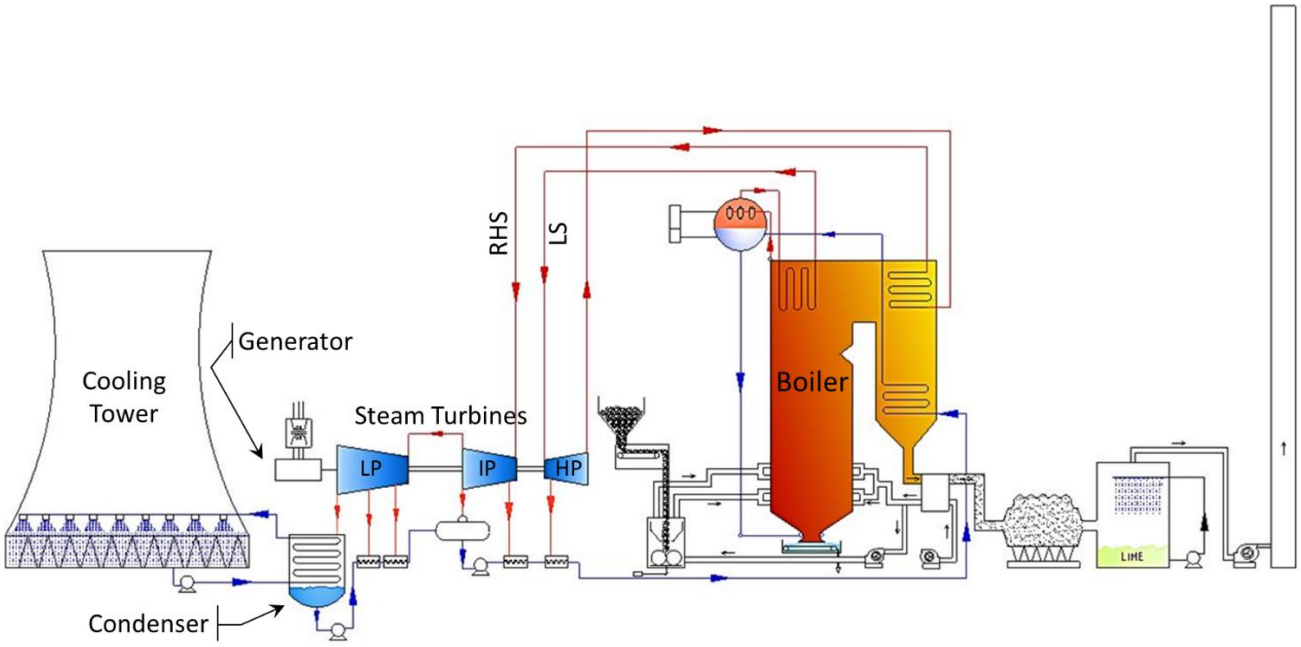

Figure 2-1: Coal-fired Power Station Illustration - Adapted from [3]

In a similar framework, a gas power plant converts energy from a combustion chamber to a generator via a gas turbine. The literature review will proceed by discussing key turbine fundamentals, such as turbine energy conversion. From energy conversion, it becomes possible to evaluate turbine performance and the modelling thereof.

2.1 Turbine fundamentals

A turbine extracts pressure and thermal energy from a working fluid and converts it into mechanical work. The mechanical work, in turn, is converted into electrical power as the turbine shaft drives the generator [4]. Steam and gas turbines are both classically categorized as heat engines. When energy conversion consists of heat energy being extracted from a working fluid, the working fluid will expand at a corresponding rate.

An alternative view is to define a turbine as a turbomachine. A turbomachine transfers energy to (e.g. Pumps) or from (e.g. Turbines) a continuously moving fluid by means of singular or set of moving

blade rows. For turbines the moving blade rows are defined as a rotor assembly, consisting of a shaft with blades intricately connected to each other and the shaft.

In addition to the rotor assembly gas, steam and hydro turbines consist of a stator assembly, that constricts and guides the working fluid. The stator assembly consists of a casing with stationary blade rows intricately connected [5]. The combination of both stator and rotor set is termed a turbine stage. Figure 2-2 presents a cross-section drawing of a modern turbine rotor and stator assembly.

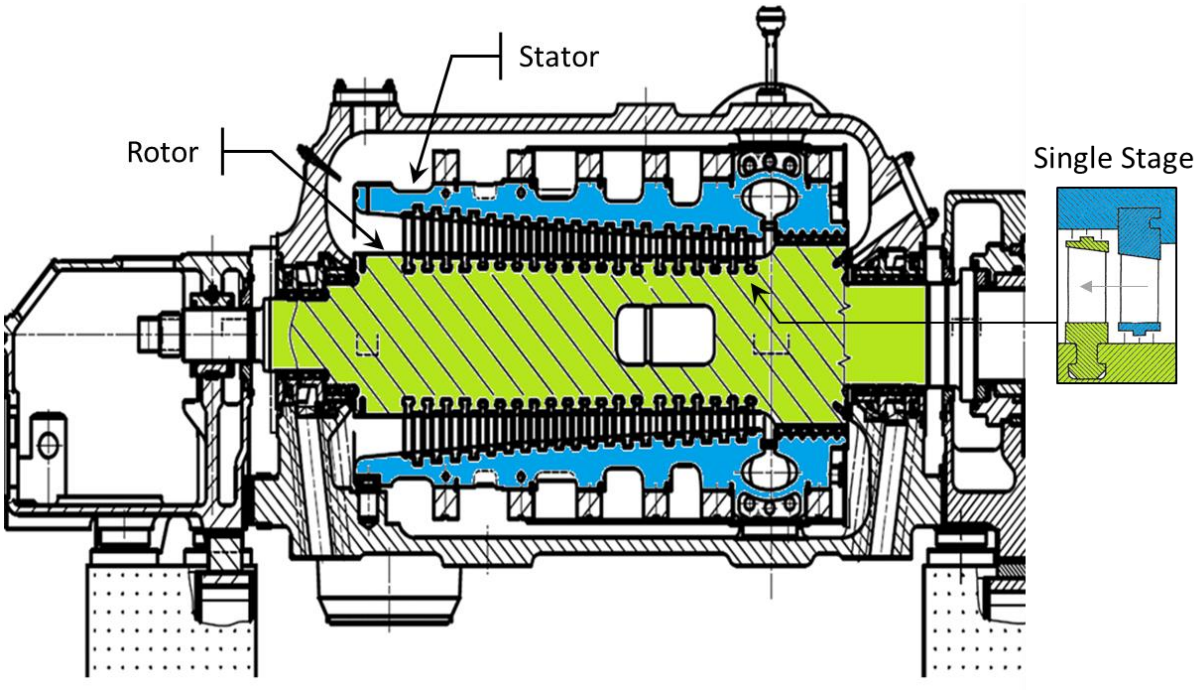

Figure 2-2: HP Steam Turbine Cross Section - Adapted from [6]

Several design conditions and physical parameters dictate the complexity of turbine design. For this reason, it is important to understand how energy is converted in turbines and how to define turbine classifications.

2.1.1 **Turbine classification considerations**

Turbine cascade development is a vital design consideration. As the working fluid enters the turbine (from a boiler or a combustion chamber) it consists of high pressure and temperature at a given mass flow rate. The working fluid then passes through a turbine stage causing the working fluid to expand. This expansion must be accommodated for in the turbine design. For each stage, the working fluid expands at a ratio defined by the specific volume condition.

As the pressure decrease, the volume will increase and vice versa. For most cases, it can be assumed that gaseous working fluids in turbines hold to polytropic expansion during operation [7]. Thus, holding to the gas law stated in equation [2.1.1].

$$p_1 \cdot V_1^k = p_2 \cdot V_2^k \qquad [2.1.1]$$

The value of the specific heat ratio (k) is determined as an isentropic ideal gas relation for both gas and steam turbines. Equation [2.1.2] defines the isentropic condition in terms of the specific heat at constant pressure (c_p) and constant volume (c_v).

$$k = \frac{c_p}{c_v} \qquad [2.1.2]$$

For steam turbines specifically there exists low-pressure operating conditions where the steam moves across the vapour line requiring a unique calculation, this is accomplished with Zeuner's relation [2.1.3]. This relation utilizes the initial dryness fraction value (x_{Df}) of the steam. During the occurrence of this phase change in the steam there exist a unique phenomenon namely supersaturation that will be discussed in section 3.3 .

$$k = (1.035 + \frac{x_{Df}}{10}) \qquad [2.1.3]$$

Table 2-1 provides values of specific heat ratio for steam and gas turbines under different physical conditions. The specific heat ratio plays a significant role in both turbine design and performance analysis.

Table 2-1: Specific Heat Ratio Values [7]

Working Fluid	Specific Heat Ratio (k)
Air[1]	1.4
Most Combustion Gasses	1.333
Superheated Steam	1.3
Saturated Steam	1.135
Wet Steam	See equation [2.1.3]

The rate of expansion, on the other hand, has several input considerations (e.g. bleed points or reheats) but is always driven by the fixed mass flow rate that must move through the turbine. The increase in volume per stage requires longer blading and hence a larger casing diameter.

[1] The Specific heat ratio (k) of Air is 1.4 for moderate temperature. Slight changes in the specific heat ratio of Air occur with changes in temperature.

This sizing increase per stage for a high-pressure steam turbine in comparison with a low-pressure steam turbine section is displayed in Figure 2-3 and Figure 2-4 respectively.

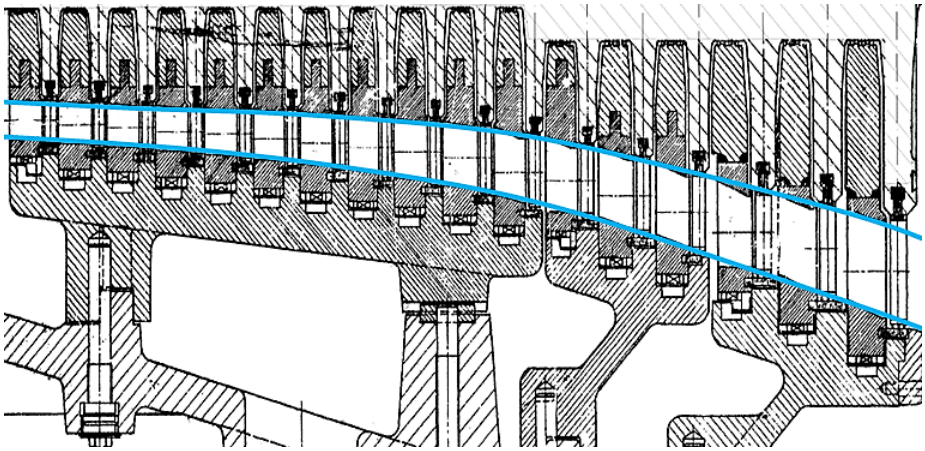

Figure 2-3: HP ST Cascade Sizing Indication - Adapted from [6]

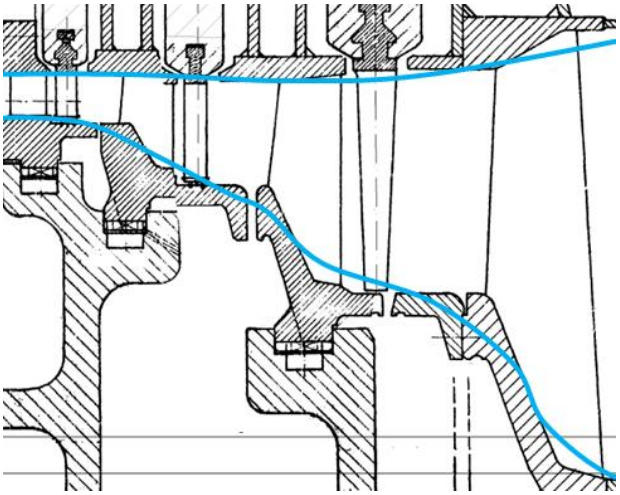

Figure 2-4: LP ST Cascade Sizing Indication - Adapted from [6]

The number of stages (N) of a turbine can be determined as the ratio of total enthalpy drop ($\Delta h_{Total(ss)}$) across a turbine compared to the desired average ideal enthalpy drop of a single stage ($h_{Design(s)}$).

$$N = \frac{\Delta h_{Total(ss)}}{h_{Design(s)}} \quad [2.1.4]$$

Equation [2.1.4] assumes an identical design enthalpy drop across all stages of a turbine. When calculating the number of stages as a design step the value is rounded down if the cost was the primary criteria whilst rounding up if efficiency is more important [8]. The enthalpy drop of a stage indicates the loading per stage. Some other design considerations may result in an un-even stage loading as is found especially in low-pressure turbines.

Notably, the reheat factor, discussed in section 2.2.4 could be used by turbine designers for turbine stage loading design evaluation [9].

Thermal expansion must be mentioned as a design consideration for turbine cascade development. As metals expand when heated so will turbine cylinders and rotors. Turbine thermal expansion predominately occurs during the start-up operational phases of a turbine. The thermal expansion generated from the heat exchange between the working fluid and the composition materials of a turbine will induce metal stresses. These stresses related to the turbine operational lifetime expectancy design consideration [10].

The laws of linear expansion state that for a given rise in temperature, the larger the original size of metal, the greater its expansion [11]. The following linear thermal expansions are defined for turbine design:

- Differential expansions: the difference in expansion between the rotor and the stator.
- Relative expansion: the rate of expansion between the rotor and the stator of the turbine.
- Absolute expansion: This is the total expansion of the turbine shaft and casing trains from the fixation point(s).

Differential expansion must be carefully controlled during the operation of turbines. During turbine warming, the rotor will heat faster than the turbine casing due to the differences in their respective physical design parameters. The clearance between the stator and rotor turbine blades are very small to minimize losses. Hence precautions must be taken to prevent contact [12].

Thermodynamic design considerations alone do not account for the mechanical integrity of turbine design. Mechanical reliability and safety design considerations must be implemented alongside all other design factors such as thermal, performance and cost.

The mechanical design limitations associated with the working fluid pressure and density transformations, across a turbine and its stages, determine the principal design layout of a turbine unit. Larger pressure differentials invoke higher material stresses, greater component deflections and more axial thrust. The magnitudes of the mechanical design limitations are determined and evaluated as they account for the final sizing and arrangement of a turbine and its components [11].

Three common pressure region sizing classifications are used: High-Pressure (HP), Intermediate-Pressure (IP) and Low-Pressure (LP). The combination, type and number of classifications are all dependent upon requirements and the design preference of the specific manufacturer. Nuclear turbines tend to have much larger LP turbines, whilst smaller industrial turbines combine HP and IP sections into one turbine casing.

Notably, gas turbines are often comprised of high-temperature ceramic blades with intercooling thus voiding pressure region sizing classification. Blade intercooling has not been included in this study.

The turbine train in Figure 2-5 consists of a single HP turbine, a double flow IP turbine and two double flow LP turbines. All the turbines are connected onto one rotating a shaft that drives the generator.

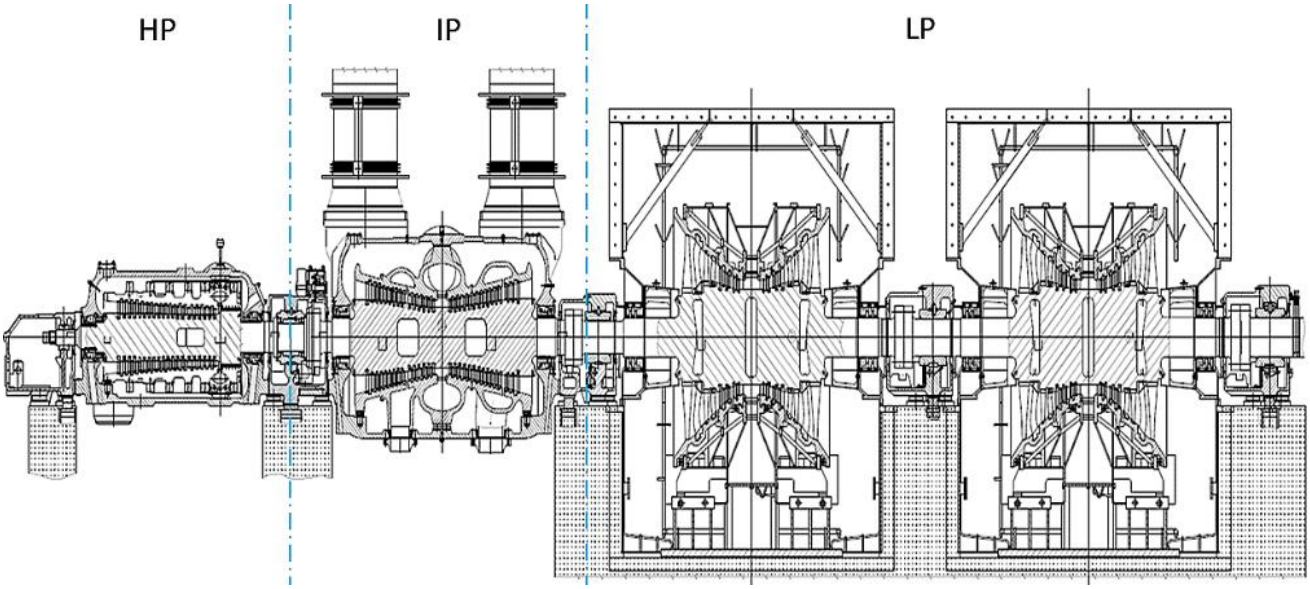

Figure 2-5: HP/IP/LP Steam Turbine Layout - Adapted from [6]

Table 2-2 provides a comparative overview of the three steam turbine classifications.

Table 2-2: HP/IP/LP Comparison – Adapted from [13]

High-Pressure Turbines	**Intermediate-Pressure Turbines**	**Low-Pressure Turbines**
Highest steam temperatures and pressures	Primarily only found on power stations with reheat	Exhausts to lower pressure (Condenser vacuum)
Largest thermal expansion	Exhausts to LP turbine	Often operates in wet steam conditions
Efficiency Range: +/- 88%	Efficiency Range: +/- 92%	Efficiency Range: +/- 85%
Mostly single flow direction design	Varies single or double flow based on design requirement	The blades twist between reaction and impulse design

The last point to mention is that of extraction points which are used to extract steam from the turbine to the feed-heaters. The number and sizing of extraction points are all dependent upon plant thermal requirements and turbine design considerations. Before assessing the detail of turbine blade design a brief clarification is required between impulse and reaction turbines.

2.1.2 **Turbine blade design nomenclature**

Turbine blade design is normally strictly controlled proprietary information of manufacturers. Thus, obtaining exact geometric data for turbine blade profile designs is no easy task. However, provided with some detail design information and the right set of extraction methods it is possible to refine theoretical profile designs to closely match actual turbine blade designs [8, 12].

It is not the intention of this study to perform a detailed breakdown of turbine blade detail design reverse engineering but merely to provide an introduction to the topic. With such knowledge, it would be possible to make valid geometry assumptions using minimal information. Figure 2-6 illustrates a cross-section view of two turbine stages. From this illustration, important geometrical information can be obtained that will inform the development of the turbine blade cross-section, illustrated in Figure 2-7.

The following observable geometries and correlations inform turbine design:

- The size of tip leakage and the design of shroud seals.
- The gradual growth of blade width to accommodate for the increase in blade loading.
- The size difference between the stator and the rotor blade width (Impulse or reaction design).
- The ratio between the hub, mean and tip blade diameters.
- The gradual increase in mean blade diameter and blade height is to compensate for the volumetric expansion of steam flow along the steam path.
- Number of stages and location of extraction points (observed in Figure 2-3)

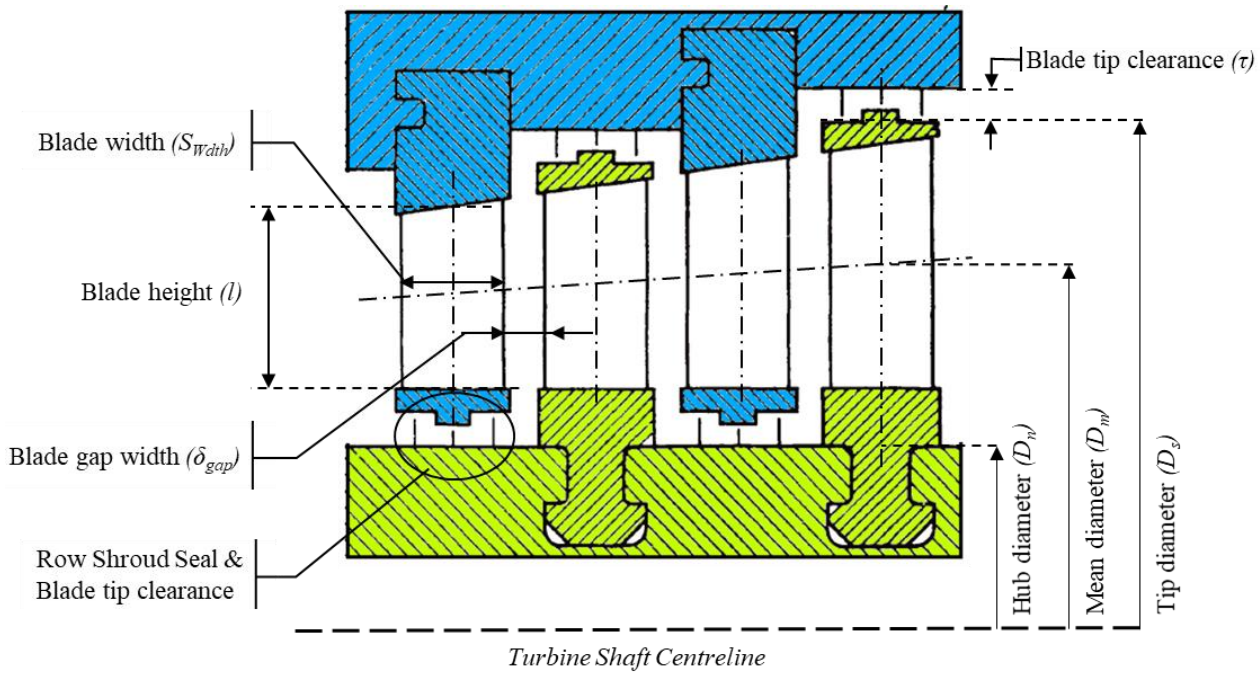

Figure 2-6: Turbine Cross-Section Geometry Indication

It should be noted that an actual turbine cross-section contains significantly more detailed information than illustrated in Figure 2-6.

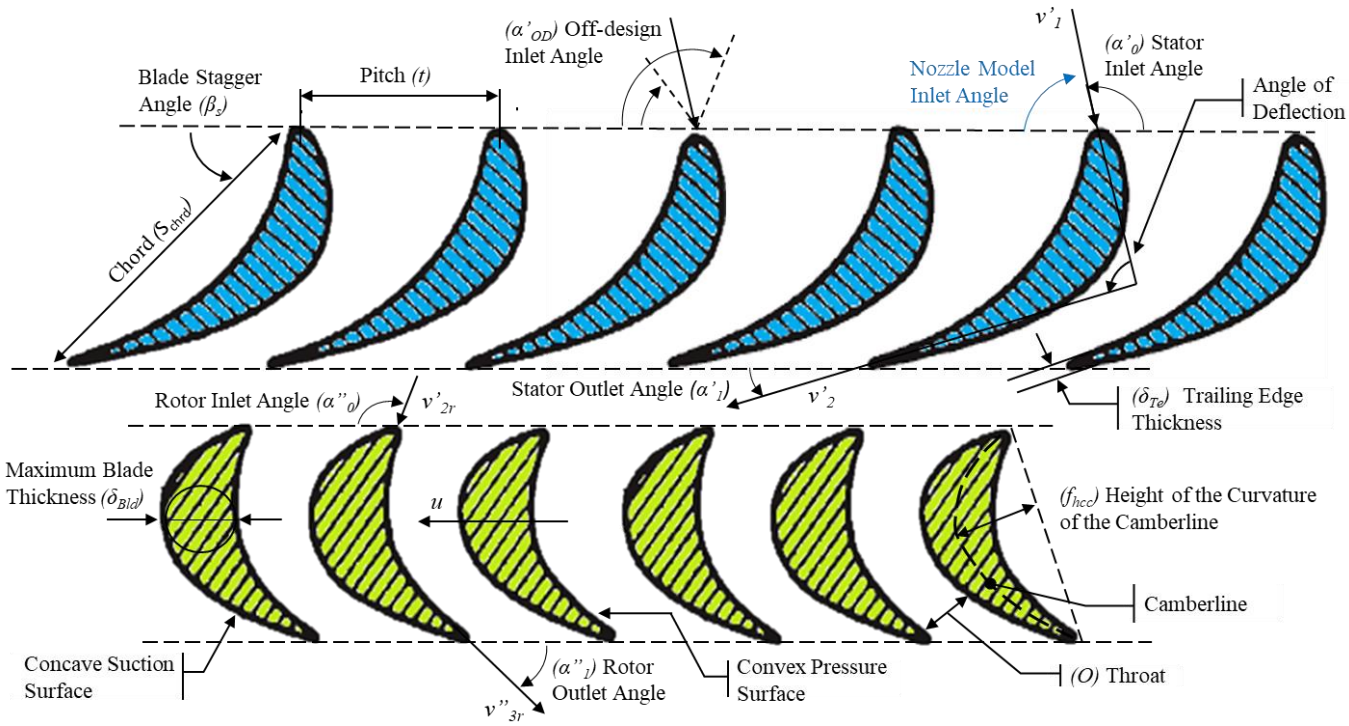

Figure 2-7: Turbine Blade Cross-Section Geometry Indication

Figure 2-7 illustrates a turbine blade cross-section, providing blade profile geometrical information for a turbine stage. All the properties indicated are applicable to each blade profile design. The transition from Figure 2-6 to Figure 2-7 is largely made possible by the interconnectivity of turbine blade design geometrical properties.

Construction methods illustrated in Figure 2-8 in combination with empirical data sets, such as the guide for pressure distributions along the suction and pressure surfaces of turbine blades [14], assist the development of a blade profile design.

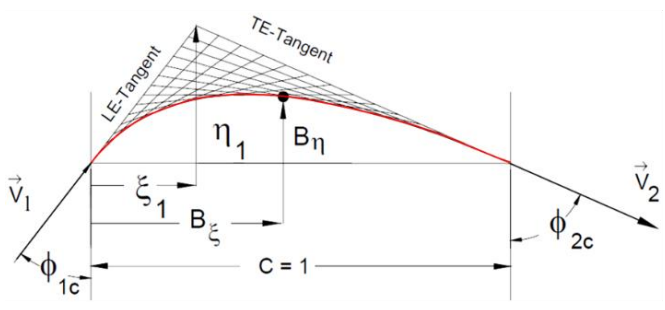

Camberline coordinate using Bèzier curve and deflection angle

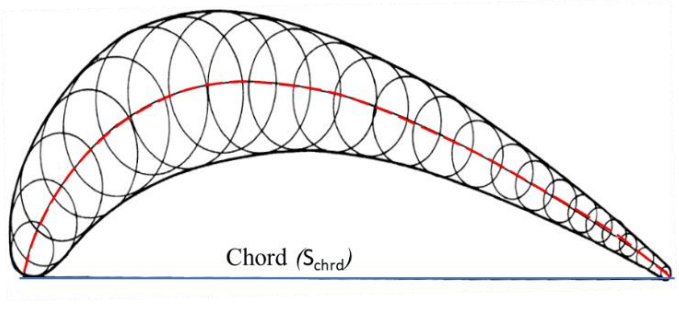

Superimposed fundamental blade profile on camberline

Figure 2-8: Turbine Blade Profile Design Guide - Adapted from [15]

The diagram presented in Figure 2-9 provides a process to identify various blade profile parameters.

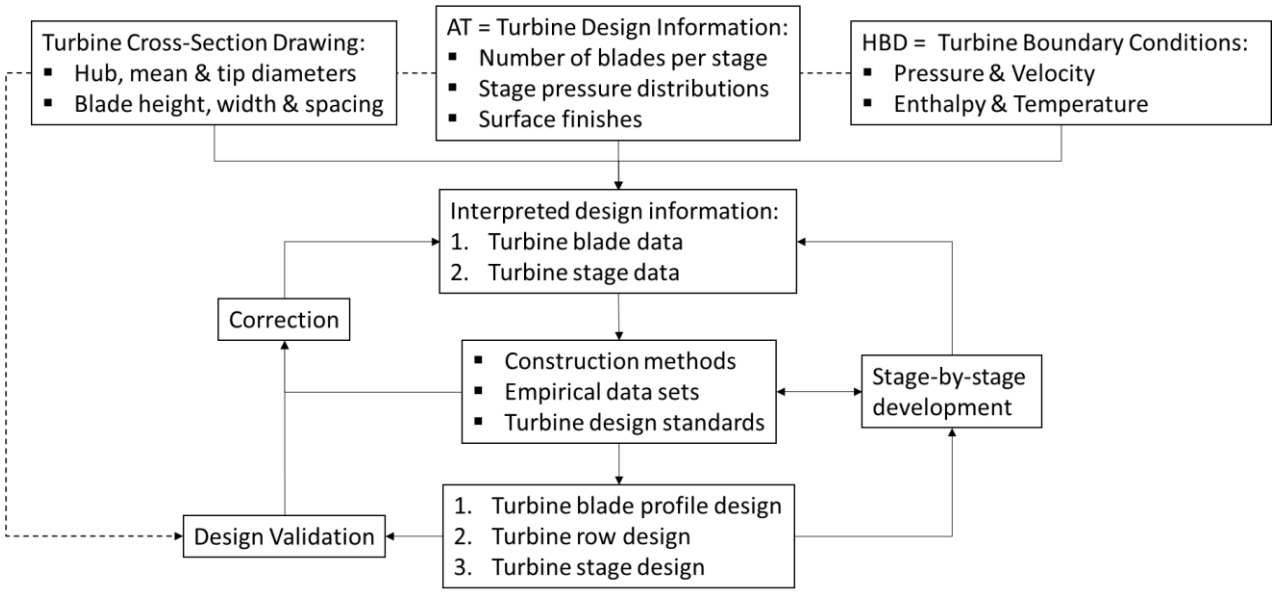

Figure 2-9: Blade Profile Parameters Identification Process

Once all the blade geometry properties are obtained and the blade row is assembled it is required for a turbine model that the blade spacing area (A_{BldGap}) be calculated:

$$A_{BldGap} = l_s \cdot t \qquad [2.1.5]$$

Equation **Error! Reference source not found.** averages the spacing area between blades assuming that deviation due to blade rotation and taper is relatively small for most blade design. Notably, a correction is required for the last stage blades. The overall flow area (A_{Flow}) per blade row is approximated by:

$$A_{Flow} = \pi \cdot l_s \cdot (D_m - n_{Bld} \cdot \delta_{Bld}) \qquad [2.1.6]$$

Although the overall flow area is not used in a specific calculation, it assists with the visualization of the turbine's cascade sizing design. For the determination of the actual overall flow area, the precise area position along the blade passage, together with the angle of the flow direction, would be required. This information is rarely obtainable from available turbine drawings.

The last blade parameter required is the Surface finish (k_s) of turbine blades. Surface finish quality is normally provided form all new turbines by manufacturers as part of an acceptance test. For turbines that have been in operation the simplest method to obtain surface finish quality is to perform a non-destructive inspection test during turbine maintenance [16]. If this is not possible several international standards on turbine surface finishes are available [17].

2.1.3 **Impulse and reaction turbines**

At a glance impulse and reaction turbines appear extremely similar as depicted in Figure 2-10. The fundamental difference becomes apparent when inspecting the energy conversion process utilized by each turbine type. This reveals the unique methods for determining working fluid velocities. The stage-by-stage turbine nozzle model uses these unique methods in its calculation structure.

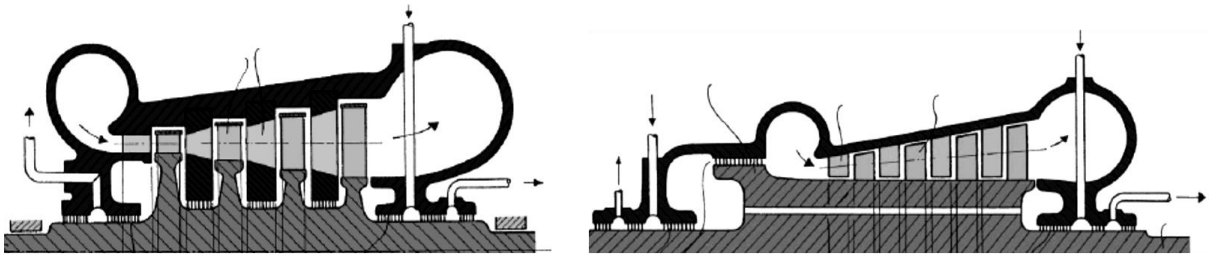

Impulse Turbine Reaction Turbine

Figure 2-10: Impulse and Reaction Turbine Comparison – Adapted from [11]

Impulse turbine blading

In an impulse turbine, the enthalpy and pressure drop through the stage takes place in the stator blades. Almost no pressure drop exists across the rotor.

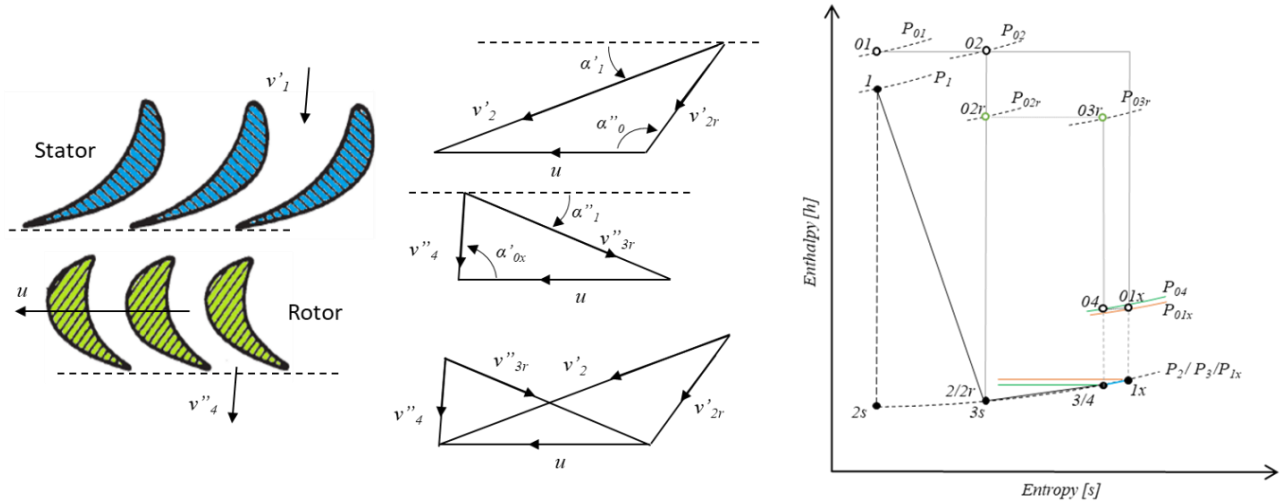

Figure 2-11: Impulse Turbine Velocity Triangle Diagram – Adapted from [18]

Figure 2-11 provides a velocity triangle visualization of the flow through an impulse stage. The working fluid enters the stator with an inlet velocity (v'_1):

$$v'_1 = \sqrt{2(h_{01} - h_1)} \qquad [2.1.7]$$

The working fluid exits the stator at an actual exit velocity (v'_2) at an exit flow angle (α) to the rotor. The actual exit velocity is subject to the losses that occur across the stator:

$$v'_2 = \sqrt{2 \cdot (h_{01} - h_2)} \qquad [2.1.8]$$

The fluid enters the rotor at a relative velocity (v'_{2r}) and flow angle (α_1). This considers the relative movement between the rotor blade speed (u) and the stators actual exit velocity (v'_2) at an exit flow angle (α). Utilizing the velocity triangle and the laws of trigonometry:

$$v'_{2r} = \sqrt{u^2 + v'^2_2 - 2 \cdot v'_2 \cdot u \cdot \cos(\alpha_1)} \quad [2.1.9]$$

The working fluid exits the rotor blades at a relative exit velocity (v''_{3r}). The rotor relative total enthalpy stays constant ($h_{03r}=h_{02r}$) so in a loss-less rotor, the relative rotor inlet velocity (v'_{2r}) and exit velocity (v''_{3r}) would be the same. The rotor relative exit velocity with losses and before work extraction occurs is:

$$v''_{3r} = \sqrt{2 \cdot (h_{02r} - h_3)} \quad [2.1.10]$$

The rotor absolute exit velocity after work extraction has taken place:

$$v''_4 = \sqrt{2(h_{04} - h_4)} \quad [2.1.11]$$

The working fluid enters the next stage stator with an inlet velocity (v'_{1x}) after incorporating carry-over losses:

$$v'_{1x} = \sqrt{2(h_{01x} - h_{1x})} \quad [2.1.12]$$

The carry-over effect this is discussed in section 2.2.4 .

For clarification, point 3, illustrated in all h-s diagrams presented, is a fabricated point associated with the calculation of the fictitious kinetic energy component discussed in section 2.3.3 .

Reaction turbine blading

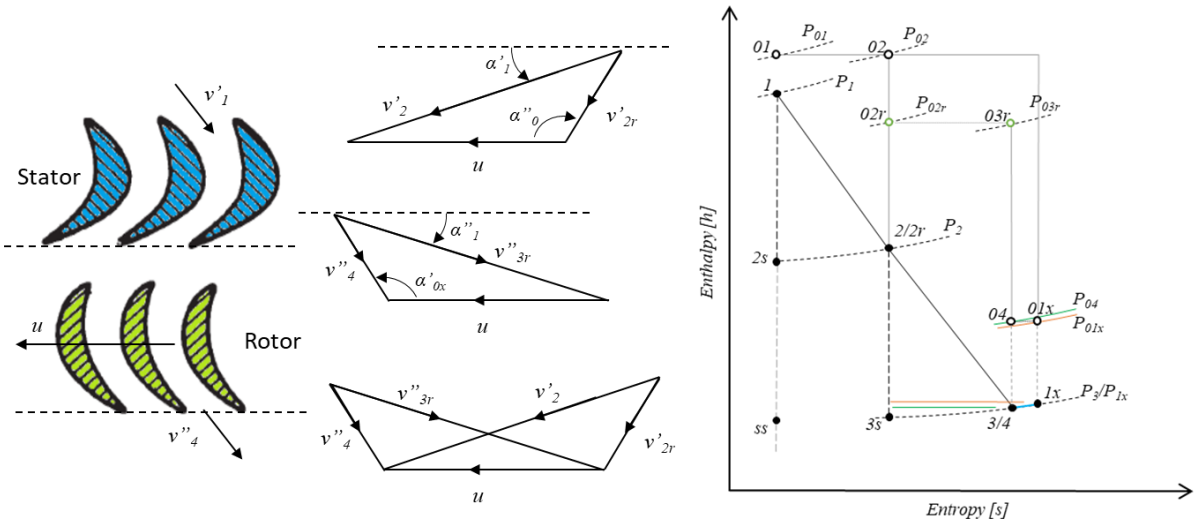

Figure 2-12: Reaction Turbine Velocity Triangle Diagram– Adapted from [19]

From Figure 2-12 it becomes apparent that the same velocity calculation methods used for an impulse turbine stage can be used to calculate the reaction turbine stage. The most significant difference is that v''_{3r} is substantially bigger than v'_{2r}, since the flow is further accelerated through the rotor passages. This difference is dependent upon the reaction ratio.

For a reaction turbine, the enthalpy conversion and pressure drop, across a stage, are split between the stator and rotor blades. The ratio of this spilt is determined by the degree of reaction (R) defined as:

$$R = \frac{\Delta h_R}{\Delta h_{Stg}} \qquad [2.1.13]$$

The degree of reaction is indicated as a percentage value. The conventional reaction turbines discussed in literature consists of all the stages having a nominal 50% reaction design. Actual turbines are often designed with a wide range of reaction values.

Design factors that may impact on the level of reaction per stage may be the available enthalpy within the working fluid, the turbine shaft length, material constraints, material and manufacturing costs and the manufacturers' proprietary designs preferences [8]. A 0% reaction stage experiences no change in enthalpy across the rotor, this differs from an impulse stage that experiences no change in pressure across the rotor [20].

2.2 Turbine performance

As the working fluid, be it steam or gas, flows through the turbine blade channel contained in the turbine casing, heat energy is converted into kinetic energy. Turbine designs have evolved over time to maximize the utilization of this energy conversion thus improving turbine performance.

2.2.1 Turbine performance visualization

Turbine performance is ideally characterized by an enthalpy-entropy diagram. The diagram illustrates the thermodynamic process, indicating the heat losses in relation to the functional energy converted (work output).

Figure 2-13 presents the turbine working fluid flow performance on an enthalpy-entropy (h-s) diagram for two consecutive stages. An equivalent turbine cross section was added, to the top right corner, as to orientate the reader to the physical locations depicted.

This configuration will assist in the clarification of concepts such as; loss coefficients, carry-over and off-design condition modelling. This section attempts to present a comprehensive visualization of turbine performance.

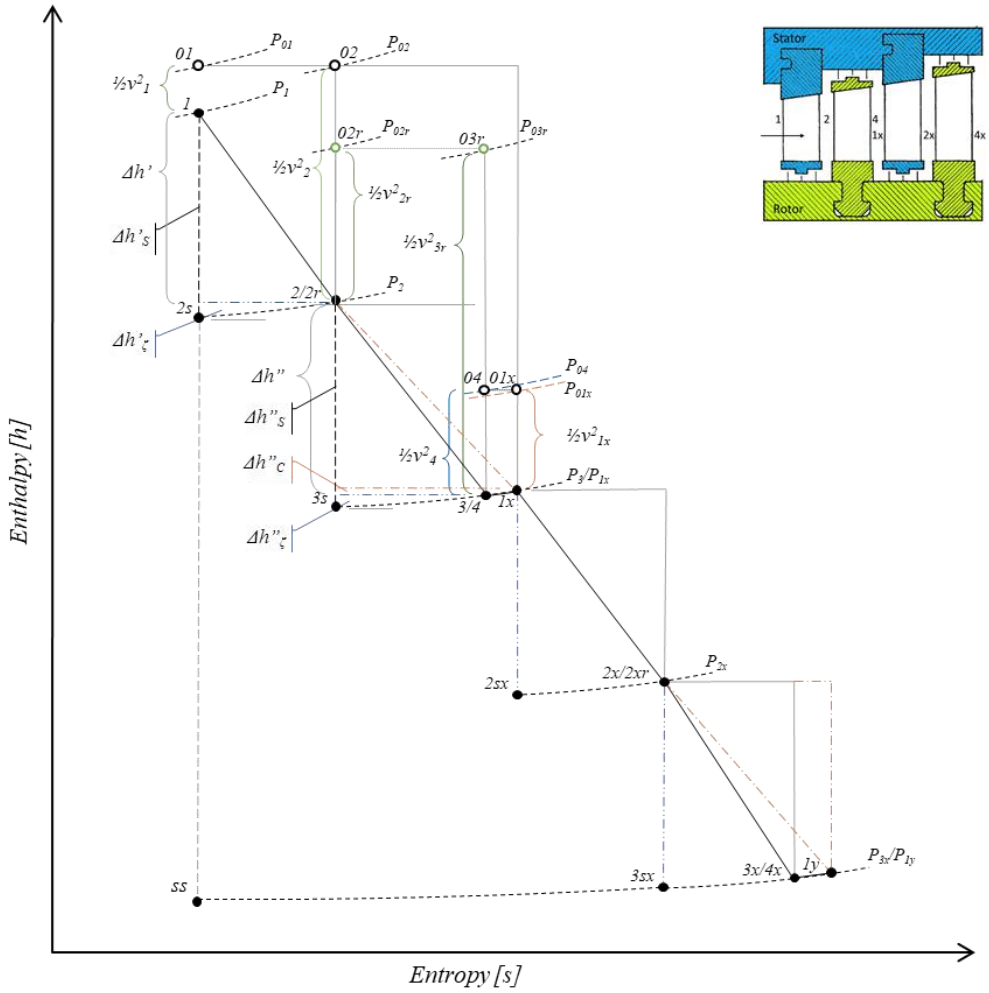

Figure 2-13: Two Turbine Stages Enthalpy-Entropy Diagram

An ideal turbine blade passage ($\Delta h'_s$ & $\Delta h''_s$) consists of no losses, whilst actual turbines ($\Delta h'$) experience losses. The nozzle losses ($\Delta h'\zeta$ & $\Delta h''\zeta$) are discussed in section 2.2.2 while the carry-over loss ($\Delta h''_c$) is discussed in section 2.2.4 . Turbine efficiencies are used to indicate the ratio between ideal and actual performance. Total-to-total, total-to-static and static-to-static are three efficiencies defined by classical turbine theory [20].

Total-to-total efficiency is the ratio between the actual work performed by a multistage turbine relative to the ideal work output whilst operating at fixed back pressure:

$$\eta_{tt} = \frac{h_{01} - h_{04}}{h_{01} - h_{04ss}} \qquad [2.1.14]$$

Total-to-static efficiency is the adiabatic efficiency that incorporates the loss of exit kinetic energy (exit velocity). Ideally suited for single stage or last stage blade calculations:

$$\eta_{ts} = \frac{h_{01} - h_{04}}{h_{01} - h_{3ss}} \qquad [2.1.15]$$

Static-to-static efficiency occurs when the inlet velocity of a stage equals the exit velocity:

$$\eta_{ss} = \frac{h_1 - h_3}{h_1 - h_{3ss}} \quad [2.1.16]$$

The isentropic nozzle efficiency for a single turbine stator and rotor row is defined as:

$$\eta' = \frac{h_{01} - h_2}{h_{01} - h_{2s}} \quad [2.1.17]$$

$$\eta'' = \frac{h_{02r} - h_3}{h_{02r} - h_{3s}} \quad [2.1.18]$$

Equation [2.1.17] (Stator nozzle efficiency) and [2.1.18] (Rotor nozzle efficiency) are used as a core framework property in the stage-by-stage nozzle-model component [1].

The following sections provide an overview of turbine losses and categorize them into the most widely acknowledged groups. This provides the premise for the evaluation of loss coefficients for both design and off-design conditions. Loss coefficients provide a turbine row and the stage specific analysis methodologies. To complete the required evaluation of a turbine, an overview of turbine performance evaluation is required. This is discussed in section 2.2.4 .

2.2.2 **Turbine loss coefficients**

The collective loss experienced by each row or stage can be characterized into the following loss categories depicted in Figure 2-14:

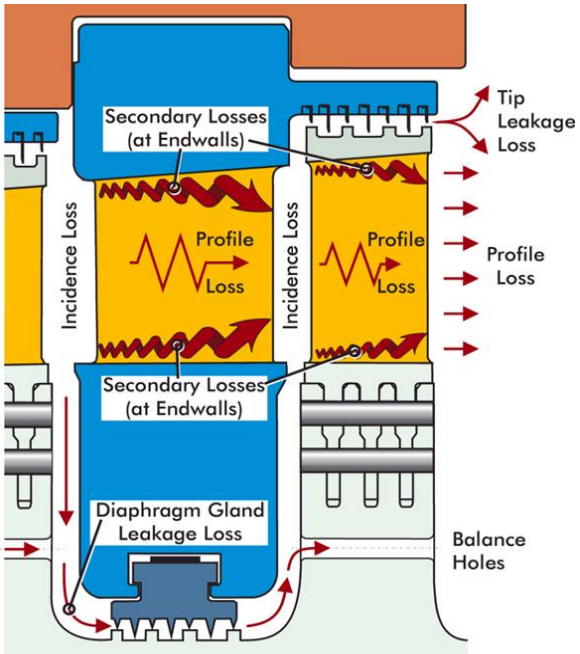

Figure 2-14: Turbine Loss Indication [13]

Profile Loss

Profile losses are primarily caused by interactions of the working fluid with the turbine blades' geometric design. As the working fluid enters the turbine row it makes contact with the blade profile. Almost instantaneously creating a boundary layer on the blade surface. This boundary layer develops from a laminar to a turbulent flow structure that has a percentage of separated flow occurring as a result of flow deflection during the transition.

The entropy of the turbine stage increases as kinetic energy is converted to heat within the boundary layer [21]. The change in entropy is accommodated by a drop in stagnation pressure. This can be visualized in Figure 2-13 (P_{01} to P_{02}).

Furthermore, the profile loss is increased by a "Trailing edge loss" and a "Shock loss". Trailing edge loss can be defined as the enthalpy loss resulting from the fluid mixing vortex caused by flow separation at the exit tip of the turbine blade passage, described as a wake. The largest contributor to trailing edge loss is the trailing edge tangential projection or trailing edge percentage. The larger the trailing edge percentage the larger the resulting wake.

Shock loss is the manifestation of shock wave expansion and propagation through the working fluid medium created by the rapid changes in geometry. These changes are caused by the collective effects of losses described on the working fluid and the change in blade profile geometry [22].

To summarize, the viscous forces generated by the working fluid in the boundary layer promotes the development of turbulent flow. As the turbulence increase and the overall flow continually separates and merges causing the respective friction to increase, decreasing the availability of the enthalpy in the turbine stage. Primary contributing factors are the blade surface finish, blade profile and the working fluid's velocity as it relates to the Reynolds and Mach numbers.

Secondary Loss

Secondary losses are mostly comprised of two components: The first is the loss incurred by the formation and dissipation of secondary flow vortexes. This loss is caused by the interaction of the secondary flow and primary flow. The vortexes, in turn, cause more mixing and thus more friction loss. Blade aspect ratio is a contributing factor towards secondary flow formation [23].

The second component is termed "Endwall loss". Endwall loss occurs when the secondary flow interacts with the blade boundary layer flow and blade surface (wall). This interaction causes the development of annulus wall boundary layers that in turn creates viscous turbulent flow between rows (wake) [23]. As Endwall loss is predominately three-dimensional in flow structure, it requires correction for one-dimensional modelling methodologies.

Tip Leakage Loss

Tip leakage loss occurs across the clearances between the stator blades and the shaft and the rotor blades and the turbine casing. The tip leakage loss is primarily created by the mixing of the working fluid flow through the blade passage and the flow across the respective tip leakage regions. The mixing occurs at the exit blade region and progresses into the blade spacing gap.

The loss severity is reliant on the pressure difference between interacting flows as well as the sizing of the clearances. A contribution to tip leakage loss severity is whether the blade is shrouded or unshrouded [11].

Incidence Loss

Incidence loss is caused by the deviation from the ideal inlet angle of the working fluid onto the blade profile. The incidence angle indicates the deviation from the design angle. The impact of this deviation results in the increase of the profile losses experienced. Dependent on the cause of the incidence the working fluid can be directed either towards the convex or concave side of the blade passage. Each incidence angle orientation has its own corresponding loss effect [24].

Moisture loss

Moisture loss is a steam turbine specific attribute, primarily occurring in the last stage blades of a low-pressure turbine and under the right conditions for water droplets to form. Wet steam is the term used to describe the condition of water droplet formation within steam as a working fluid. Moisture loss has been the focus of immense study [25]. For simplification, moisture loss will be broken into two categories: thermodynamic loss and mechanical loss.

Thermodynamic moisture loss occurs when sudden condensation occurs after the steam condition has crossed the saturation line. Described as the heat loss resulting from a phase transition between supercooling and equilibrium states [7].

Mechanical moisture loss is comprised out of two components. “Braking Loss” resulting from the difference in velocity profiles of the formed water droplets and the unchanged steam. As both phases are bound by the same velocity triangles yet have a different velocity constitution the heavier liquid particles will obstruct and slow the lighter vapour particles.

As a secondary effect of the braking loss, “Drag Loss” occurs because of the frictional loss generated between the water droplets and steam. The larger the water droplets the larger the mechanical loss [26].

Other Losses

For the purpose of this study, two additional losses are investigated, specifically “Fan loss” and “Last Stage Blade losses”. Fan loss is a correction coefficient that incorporates the additional losses incurred due to the blade spacing not being constant over the row radius from hub to tip [27].

Last stage blade losses specifically add losses incurred due to the unique interconnection designs of last stage blade. Uniquely “Exhaust loss” is specifically excluded as it relates to overall heat cycle performance.

It should be noted that the turbine losses discussed do not define all possible classifications or combinations of losses. The exact combination of losses is dependent upon the specific methodology’s requirements.

A comparative loss coefficient study was conducted and is discussed in the next sections for design and off-design conditions. The selected loss coefficient methodologies are evaluated in the next chapter.

2.2.3 **Loss coefficient methodology selection**

Turbine losses are expressed by means of loss coefficients. Loss coefficients either utilize pressure loss coefficients (Y) or enthalpy loss coefficients (ζ). Each loss coefficient methodology relates back to turbine performance in a specific method although a lot of similarities are present.

An example of the this can be observed when comparing the loss coefficient equations for a stator developed by Denton [28], equation [2.1.19], with that of Traupel [29], equation [2.1.20].

$$\zeta'_{Denton} = \frac{h_2 - h_{2s}}{h_{01} - h_2} \quad [2.1.19]$$

$$\zeta'_{Traupel} = \frac{h_2 - h_{2s}}{h_{01} - h_{2s}} \quad [2.1.20]$$

It is possible to incorporate multiple loss coefficients methodologies into a single modelling methodology, provided the methodologies are correctly linked and do not overlap in terms of the effects that are incorporated.

It is possible to convert pressure loss coefficients to enthalpy loss coefficients and vice versa [30], but the implementation of this conversion into a modelling scheme increases the required processing time and tends to create evaluation overlap.

Numerous turbine loss coefficient methodologies have been developed over time. A comprehensive comparison study was conducted by Ning [27]. The most notable methodologies are:

- Soderberg's [31]: developed one of the first loss coefficient methodologies, it incorporated profile and secondary losses. It is often viewed as a foundation for other methodologies.
- Ainley & Mathieson [32]: established, by means of detailed turbine performance experiments, a pressure loss coefficient turbine performance prediction methodology.
- Craig & Cox [33]: developed a methodology based on linear turbine blade cascade testing focused on predicting losses in turbine stages. With the incorporation of "Other losses", a greater overall efficiency accuracy was obtained.
- Dunham & Came [34]: produced a methodology by improving upon the "Ainley & Mathieson" methodology made possible by the improvement of measured experimental data.
- Traupel [35]: developed a one-dimensional empirical modelling methodology that incorporates various flow distributions generated by turbine blades and accompanying turbine blade components. The empirical data was extracted from an array of experiments and data sets.
- Kacker & Okapuu [36]: the methodology is a combination and advancement of the "Ainley & Mathieson" and "Dunham & Came" methodologies, with the incorporation of "Shock losses".
- Denton [28]: produced a methodology based on the relationship between turbine loss causes and the respective increases of entropy. The method is based on the theoretical evaluation of losses formulated from the conservation equations and other turbine specific governing equations.

A selection criterion was developed that compares the amount of functional performance data a loss coefficient methodology would produce compared to the amount of blade geometry it requires. The selection criteria scoring is determined by adding value per turbine loss type and deducting value per blade geometry parameter required relative to the total number of possibilities per section:

$$Score = \left(\frac{Number\_of\_Losses}{Total\_Possible\_Losses} \right) - \left(\frac{Number\_of\_Geometries}{Total\_Blade\_Geometries} \right)$$

A higher score implies that loss coefficient requires an amount of geometrical data input but produces a higher level of detailed loss coefficient result. Table 2-2 provides the loss coefficient methodologies comparison result.

Table 2-3: Loss Coefficient Comparison - Adapted from [27]

Year	*Author*	*Types of losses*	*Design (D) / Off-Design (OD)*	*Score*
1949	Soderberg	TT=PR+SE+TL	D	62%
1951	Ainley & Mathieson	TT=PR+SE+TL+TE	D+OD	53%
1960	Steward et al	PR, SE	D	52%
1965	Smith	TT	OD	55%
1968	Baljé & Binsley	TT=PR+SE+TL	D	60%
1969	Mukhtarov & Krichakin	TT=PR+SE+TL	D+OD	53%
1970	Craig &Cox	TT=PR+SE+OL	D+OD	40%
1970	Dunham & Came	TT=PR+SE+TL+TR	D+OD	60%
1971	Kroon & Tobiasz	TT	D+OD	55%
1977	Traupel	TT=PR+SE+FA+TL+TE+OL	D	74%
1980	Zehner	PR	OD	55%
1981	Macchi & Perdichizzi	TT	D+OD	55%
1982	Kacker & Okapuu	TT=PR+SE+TL+TE	D+OD	51%
1987	Sharma & Butler	SE	D	58%
1990	Moustapha et al	PR, SE	OD	62%
1992	Okan & Gregory-Smith	SE	D	61%
1992	Schobeiri & Abouelkheir	PR	OD	55%
1993	Denton	TT=PR+SE+TL+TE	D	57%

TT - Total losses FA - Fan loss OL - Other losses
PR - Profile loss TL - Tip Leakage loss
SE - Secondary loss TE - Trailing Edge loss

From the comparisons in Table 2-3, it was determined that Traupel [29] is the most advantageous loss coefficient methodology. Traupel's loss coefficient methodology is comprised of profile loss, secondary loss, fan loss, tip leakage loss and trailing edge loss.

Additionally, one can incorporate Last stage blade losses as well as moisture loss into this loss coefficient methodology. It has the benefit of having an enthalpy loss coefficient format that is similar to the Soderberg methodology [1] utilized in the stage-by-stage turbine nozzle-model component.

The disadvantage of the Traupel's methodology is that it does not evaluate turbine losses for off-design conditions. Fortunately, Zehner [24] developed a methodology that provides an off-design correction for Traupel's methodology. Zehner provides an expansion of Traupel's methodologies by integrating turbine blade cascade characteristics and incidence loss into Traupel's profile loss.

Furthermore, the "Moisture loss" used in Traupel's methodology is expanded and improved upon by the incorporations of Gyarmathy's [26] moisture loss calculation, that is based on wet-steam turbine theory, and a correction methodology for moisture loss development compiled by Hiroyuki et al [25].

2.2.4 **Carry-over and reheat analysis**

Turbine “Carry-Over” and “Reheat Factor” do not form part of the primary loss coefficient algorithm but offer an additional performance evaluation methodology. Figure 2-15 provides a visualization of Carry-over and Reheat factor for multiple stages.

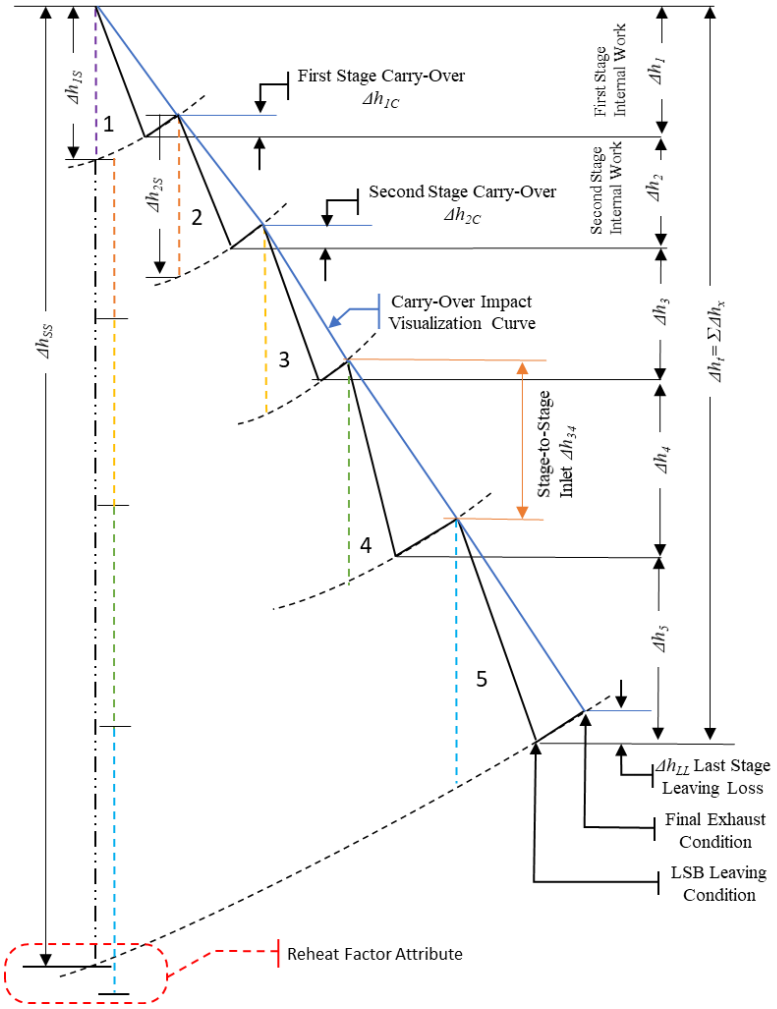

Figure 2-15: 5 Multistage Turbine Carry-over and Reheat Factor Visualization – Adapted from [37]

Carry-over

As the working fluid passes from one stage to the next, point 4 to 1x in Figure 2-16, across the diaphragm (gap), a portion (k_{co}) of the available kinetic energy is lost and converted back into fluid static temperature [37].

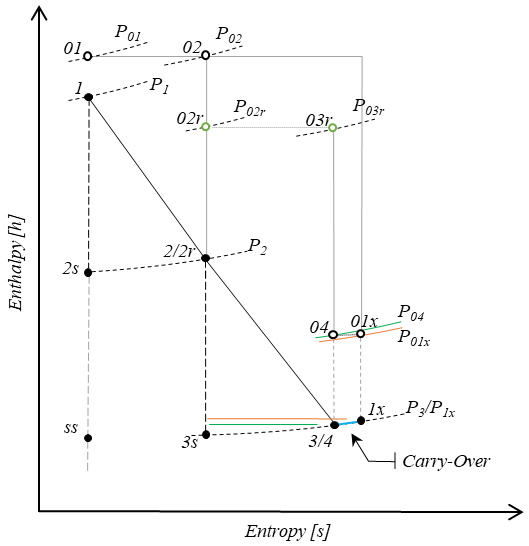

Figure 2-16: Carry-Over Indication

This conversion is caused by the rapid expansion and turbulence of the working fluid leaving a stage. The decrease in working fluid pressure relates to the energy conversion into heat, this generates an increasing of the enthalpy and entropy generally termed stage reheat. This energy conversion is referred to as "Carry-over" ($\Delta h''_C$) [38].

$$v_{1x} = k_{co} \cdot v_4 \qquad [2.1.21]$$

$$\Delta h''_C = h'_{1x} - h''_4 \qquad [2.1.22]$$

Equation [2.1.21] and [2.1.22] govern the Carry-over effect. The Carry-over ($\Delta h''_C$) for a single stage-to-stage can be expressed in terms of the carry-over ratio (k_{co}) as:

$$\Delta h''_C = \left(1 - k_{co}^2\right)\left(\frac{v_4^2}{2}\right) \qquad [2.1.23]$$

The Carry-over effect enables all stages, except the first stage, to benefit to an extent from the inefficiency of the preceding stages. Carry-over is utilized in the stage-by-stage turbine nozzle-model to accommodate for the reheat phenomena as discussed in section 2.2.2 .

Reheat factor

Reheat factor is a measure of inefficiency across multiple stages or a complete turbine of steam turbine resulting from steam's deviation from the ideal gas law. Defined as the ratio of total enthalpy drop relative to ideal enthalpy drop during the expansion phases of a turbine. Reheat factor tends to be between 1.03 and 1.08 for most steam turbines [20]. Reheat factor presents a correlation between isentropic and polytropic turbine efficiencies.

The reheat factor indicates, in part, the overall impact turbine losses have on performance. For a complete turbine consisting of x stages the reheat factor is:

$$RF = \frac{\Delta h_{1s} + \Delta h_{2s} + ... + \Delta h_{xs}}{\Delta h_{ss}} \quad [2.1.24]$$

If the reheat factor is not provided in the in the turbine performance data it can be determined after an initial nozzle-model evaluation has been completed. The Reheat factor indicates that the sum of all the isentropic enthalpy drops across individual stages, of a multi-stage turbine, is greater than the total adiabatic enthalpy drop of the turbine [20]. This can be observed in Figure 2-15 and is characterized by:

$$RF = \frac{\sum_{i=1}^{5} \Delta h_{is}}{\Delta h_{ss}}$$

The reheat factor depends largely on the turbine design with regards to stage loading and expansion design [37]. It is significantly impacted by the initial inlet and exhaust conditions as illustrated in Figure 2-15.

Notably, limited documentation was found on the relationships between Turbine loss, Carry-over and Reheat factor. From obtained literature, it appears that the correlations between the methodologies have not been well researched. Both Carry-over and Reheat factor allow for alternative evaluation of turbine performance.

2.3 Nozzle-model review

Before looking at the inner workings of the stage-by-stage turbine nozzle-model some information is required regarding turbine process modelling. Specifically, the software used and the framework required for the stage-by-stage nozzle-model component.

2.3.1 **Turbine modelling methods**

Turbine blade passages have a notoriously complex design causing a multitude of intricate unsteady fluid flow conditions. Figure 2-17 illustrates a collection of fluid conditions. Almost every combination, of these conditions, is possible across an entire turbine. These combinations, in turn, lead to a variety of physical actions from material stress to shock waves to immense heat transfer [39].

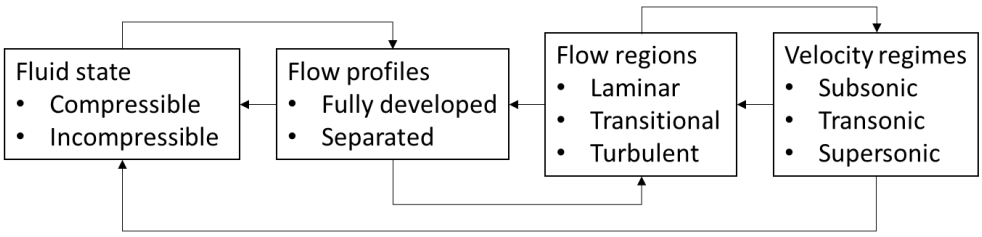

Figure 2-17: Fluid Flow Conditions

Due to the complexity of the thermohydraulic flow through a turbine blade passage, the precise modelling thereof is equally complex. Turbine model formats are primarily defined in the following three categories:

One-dimensional (1D) flow simulation: utilizes velocity triangles as the calculation foundation and applies corrections for losses and efficiencies [19]. Largely empirically based correction factors and loss coefficients improve the accuracy of the modelling methodologies [40]. Loss coefficients and correction factors are reviewed in section 2.2.2

Two-dimensional (2D) cascade simulation: places focus on the angular momentum of the working fluid as it passes through the blade passages. The modelling methodologies either uses an axial-tangential cartesian or a cylindrical coordinate system. Allowing for a row-by-row modelling arrangement (cascade) [41]. Loss coefficients and correction factors are also incorporated for improved accuracy.

Three-dimensional (3D) computational fluid dynamics (CFD): requires exact turbine geometric data as to enable the replication and thus analysis of a turbine. CFD determines the turbine performance losses by calculating the unsteady fluid flow conditions more commonly named secondary flows. Additionally, 3D meshing ads to the complexity of CFD modelling [39]. Most modern research focusses on applying CFD modelling for turbine analysis.

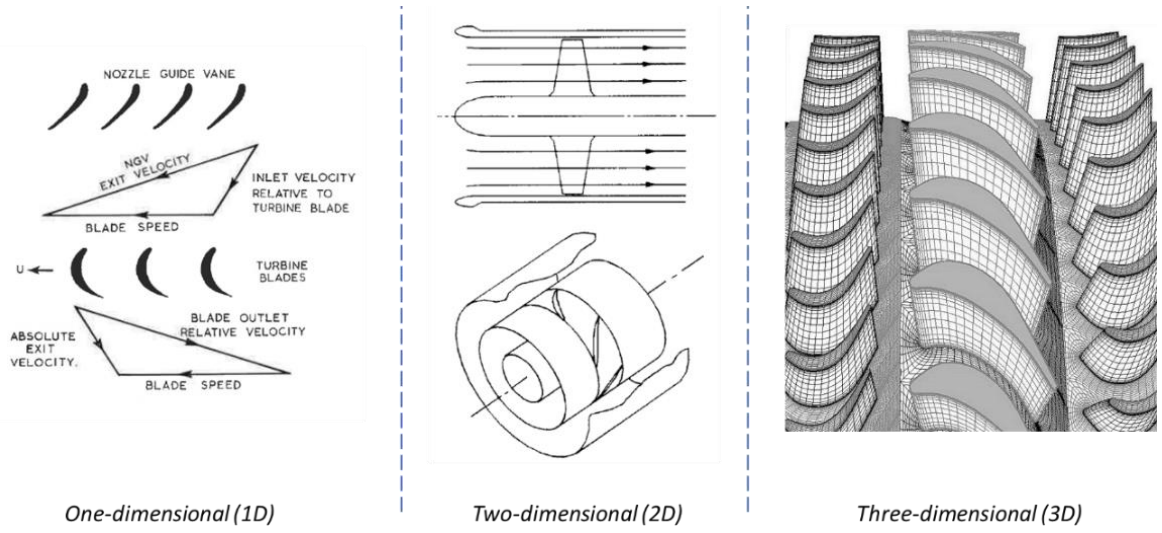

Figure 2-18: 1D, 2D & 3D Modelling - Adapted from [19], [41]& [42] respectively

With each additional dimension, the modelling design complexity increases. This comes at the cost of numerical processing time, advanced modelling knowledge and detailed information required but with the benefit of a possible increased accuracy and fidelity. Although the stage-by-stage turbine nozzle-model methodologies is a 1D modelling method it achieves a high level of accuracy [1].

The incorporation of loss coefficient algorithms into the stage-by-stage turbine nozzle-model aims to add to the accuracy of the turbine performance modelling method, whilst maintaining lower processing time and requiring minimal turbine geometric data.

2.3.2 **Flownex network solver overview**

A brief overview of Flownex SE follows as to provide fundamental background information regarding the stage-by-stage nozzle-model component's workings and compositions. It should be noted that in no way does this overview do justice to the complete workings, complexity or vast capabilities of Flownex.

Flownex SE is defined as a one-dimensional thermo-hydraulic network solver. Flownex utilizes an isolated algorithm solving structure governed primarily by the conservation of mass, energy and momentum equations. It solves these governing equations on a node to node network structure for both steady state and transient simulations. Integrated on top of these equations are component specific algorithms, defining the physics required for their modelling [43].

Once a Flownex network is constructed with all the specific components required for an accurate model, a fluid is assigned to the network. The fluid properties can be drawn from a prepopulated library or customized to requirements. Flownex can integrate Excel, Ansys, Matlab and MathCad into simulations, to mention a few compatible application [43]. The network solver allows for solving criteria to be adjusted, enabling greater model stability, accuracy and control.

A key feature of Flownex is the ability to create a a custom compound component.

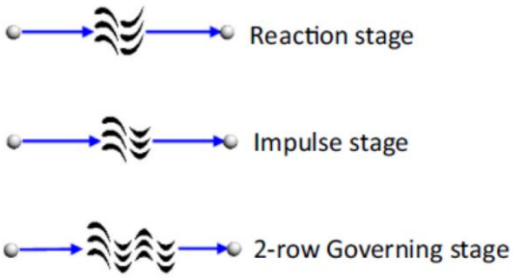

Figure 2-19: Stage-by-stage Nozzle-model Custom Compound Components [1]

The stage-by-stage turbine nozzle-model component was implemented in three custom compound components, illustrated in Figure 2-19, consisting of the components listed in Table 2-4.

Table 2-4: Flownex Component Classification – Images Adapted from [43]

Icon	*Component description*
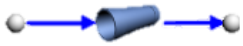	"Pipe" component: Models the flow through a conduit. The component has a multitude of adjustable parameters enabling a vast variety of modelling possibilities. The component can calculate pressure drops, thermal inertias, fluid accelerations and chocked flow to mention a few attributes.
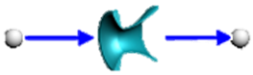	"Restrictor with Loss Coefficient" component: Simulates an ideal nozzle with *Loss coefficient* and *Contraction coefficient* as controlling parameters. The component accurately models the correlation between velocity, flow and pressure changes. This allows for the choking conditions to be correctly determined.
	"Script" component: Is used for the manipulation or assignment of any property associated with the network solver. The script uses the C# programming language.
	"Boundary Condition" component: Used for the control of the network's inlet and outlet conditions. Mostly assigns temperature, pressure or mass flow.
	"Data Transfer Link": Enables the transfer of desired information/data between components, at specific time intervals.
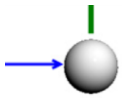	"Nodes": Are the endpoints of components, that encompasses both the volume and energy conservation. If connected to a "Boundary Condition" they act as network boundaries. Capable of adding heat or fixing pressure at any point on a network.

2.3.3 **The Stage-by-stage nozzle model overview**

The Reaction Stage custom compound component illustrated in Figure 2-19 is comprised of the components illustrated in Figure 2-20.

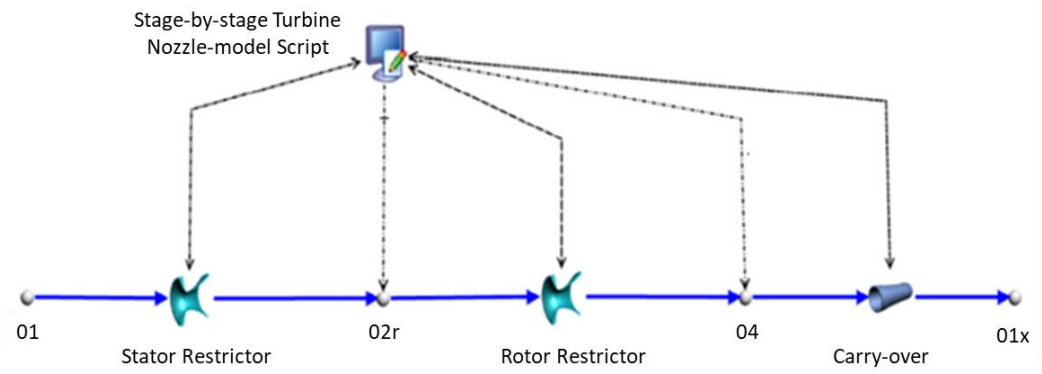

Figure 2-20: Stage-by-stage Nozzle-model Component [1]

The stage-by-stage turbine nozzle-model is grounded on building a turbine stage based on nozzle theory. For the simplification of this concept, a moving nozzle analogy is utilized [1], illustrated in Figure 2-21.

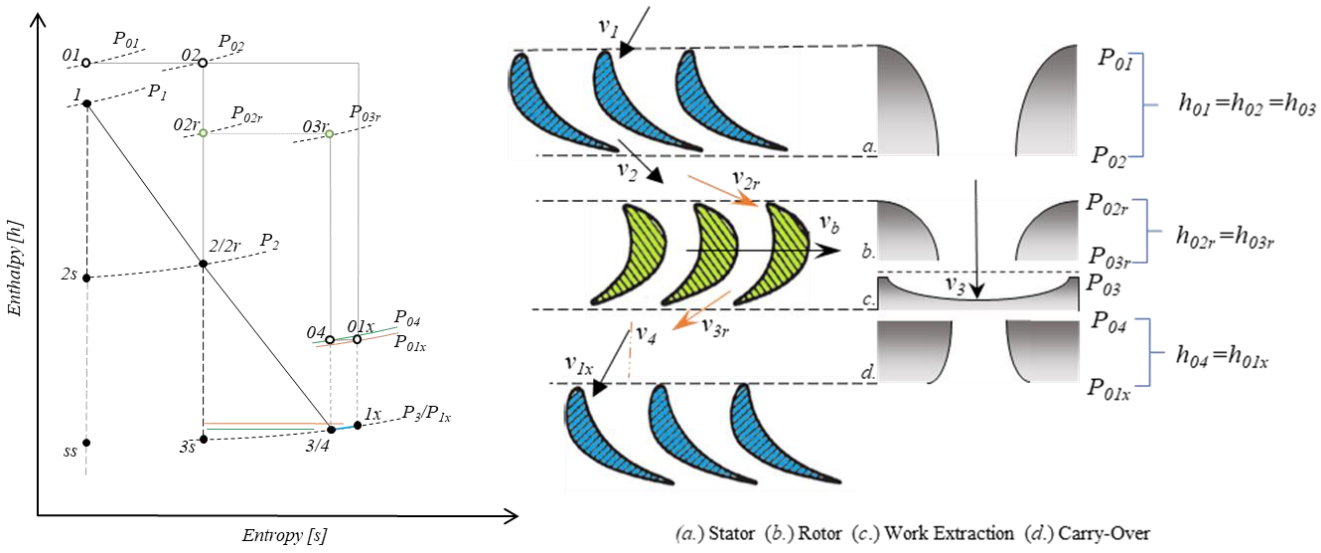

Figure 2-21: Moving Nozzle Analogy - Adapted from [1]

The "Restrictor with Loss Coefficient" component is used to simulate the turbine stator and rotor blade rows. This enables the modelling of a turbine stage as a combination of two nozzles. The restrictor Loss coefficient and Contraction coefficient is used to incorporate the nozzle losses.

The restrictor Loss Coefficient is derived from [43] for a stator and rotor:

$$C'_L = 1 - \frac{\frac{1}{2}\rho_2 v_{2r}^2}{p_{01} - p_2} \quad [2.2.1]$$

$$C''_L = 1 - \frac{\frac{1}{2}\rho_3 v_4^2}{p_{02r} - p_3} \quad [2.2.2]$$

Whilst the Contraction Coefficients are derived by Fuls [1] in terms of row efficiencies and densities for a stator and rotor:

$$C'_D = \frac{\rho_2}{\rho_{2s}}\sqrt{\eta'} \quad [2.2.3]$$

$$C''_D = \frac{\rho_3}{\rho_{3s}}\sqrt{\eta''} \quad [2.2.4]$$

The inclusion of row efficiency allows for the integration of turbine loss coefficients into the nozzle-model. Fuls [1] utilizes a loss coefficient methodology equivalent to equation [2.1.19]. Through algebraic manipulation of [2.1.17] and [2.1.19] the relation between row nozzle-model efficiency (η_{NM}) and turbine loss coefficients (ζ_{NM}) is found as:

$$\eta_{NM} = \frac{1}{1 + \zeta_{NM}} \quad [2.2.5]$$

Notably, this relationship is fundamental to the adaptation of the nozzle-model. The velocity triangle equations expressed in 2.1.3 along with the stage performance visualization of the working fluid, Figure 2-21, contains the basis of the stage-by-stage turbine nozzle-model component. This is facilitated in the “Script” component.

Important calculations performed by the nozzle-model script are for the correction of the relative inlet (v'_{2r}) and exit rotor velocities (v''_{3r}), as they are impacted by the rotor rotational blade speed (u).

Other important calculations performed are that of work extraction (w) and carry-over effect. Before being able to calculate work extraction the nozzle-model script must first calculate the fictitious kinetic energy component (v_3):

$$v_3 = \sqrt{2\left(h_{01} - h_3\right)} \quad [2.2.6]$$

For clarification, up until point 3, no work has been extracted from the working fluid by the nozzle-model. This implies that the total rotor exit enthalpy is identical to that of the inlet condition, although the static enthalpy had decreased. This results in the development of a kinetic energy component (v_3).

The nozzle-model script calculates the fictitious kinetic energy component from the total rotor inlet enthalpy assuming the rotor blades have not extracted any energy from the working fluid.

The work extraction calculation is performed by the "Script" in one of two methods. If blade efficiency (η_b) is known:

$$w = \eta_b \, ½ \, v_3^2 \qquad [2.2.7]$$

Or more practically utilizing the stator and rotor velocities and angles:

$$w = u(v_2 \cos(\alpha_1^{'}) + v_{3r} \cos(\alpha_1^{''}) - u) \qquad [2.2.8]$$

The carry-over effect, discussed in section 2.2.4 , is simulated by a "Pipe" component which acts as a diffuser. The "Pipe" receives variable values from the "Script" enabling the nozzle-model component exit condition correction for the next stage [1]. These variables consist of the derived inlet and outlet diameter:

$$D_{in} = \sqrt{\frac{4}{\pi} \frac{\dot{m}}{\rho_3 v_4}} \qquad [2.2.9]$$

$$D_{out} = \sqrt{\frac{4}{\pi} \frac{\dot{m}}{\rho_{1x} v_4 k_{co}}} \qquad [2.2.10]$$

As well as, a "Pipe" component specific property, a "Pressure drop coefficient" (K_{loss}) that describes an approximation of desired total pressure drop whilst retaining the static pressure

$$K_{loss} = 1 - k_{co}^2 \frac{\rho_{1x}}{\rho_3} \qquad [2.2.11]$$

The continuous control and calculation of corrections, coefficients and variables form part of the "Script" component's function. The timeframe or phase in which the calculations must be performed is reliant upon the "Data Transfer Links" that communicate information between the "Script" and all the other components.

The examination of the workings of the stage-by-stage turbine nozzle-model component enables the development and implementation of an adaption methodology. This is the topic of the next chapter along with the examination and implementation of the selected loss coefficients.

2.4 Case study data classification

Before proceeding, it is required to discuss the categories of data used for the generation and simulation of turbine test cases. Table 2-5 provides a summary.

Table 2-5: Turbine performance data categories

Information	Description
Turbine design data	▪ Original equipment manufacturer (OEM) design information. ▪ Measured information obtained over the lifetime of the component. ▪ Recorded design changes.
Acceptance tests (AT)	▪ Provides a comprehensive data set of the plant design and performance information. ▪ Usually obtained during the commissioning phase of plant life. ▪ Can be used as an ideal plant condition. ▪ Are physical measurements, typically at a higher accuracy than operating plant data.
Heat balance diagrams (HBD)	▪ Heat balance diagrams provide steam cycle overview information. ▪ HBD are often available for various loads. Allowing for off-design or varied operational performance guidelines. ▪ If provided by OEM it may be used as a model verification check. ▪ Are typically predicted, not measured, and would in some cases contain margins of conservatism.
Operational plant data	▪ Operational plant data is actual measurements and observations of plant performance information. ▪ The information is regularly available although less reliable and often incomplete. ▪ Can be utilised for actual plant performance evaluations.

Chapter 3 Research Methodology

This chapter will first describe the adaptation methodology implemented by illustrating the Flownex script architecture. Second, it will evaluate the selected loss coefficients obtained from literature and convert them into a digital/mathematical form for implementation into a programming algorithm. Finally, it will review the results of the adaptation.

3.1 Nozzle model adaptation methodology

A Flownex "Script" is utilized to interact with the nozzle-model component, as illustrated in Figure 3-1. The script consists of the converted turbine loss coefficient algorithms. The C# script code format allows for validation and stability control measure to be implemented in the program architecture.

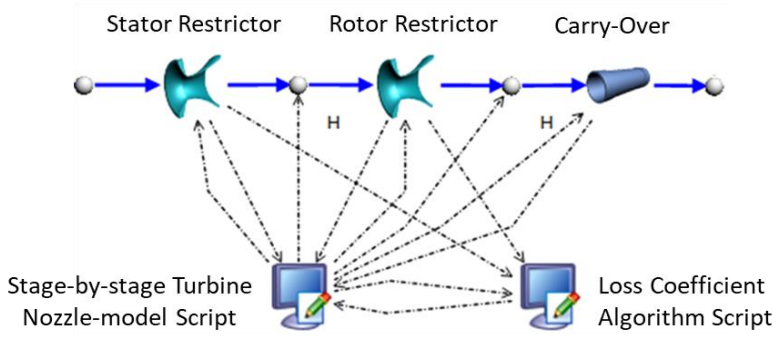

Figure 3-1: Stage-by-stage nozzle-model with Loss Coefficient Algorithm Implemented

The diagram illustrated in Figure 3-2 provides a structural format diagram to indicate the general requirements of the algorithm script.

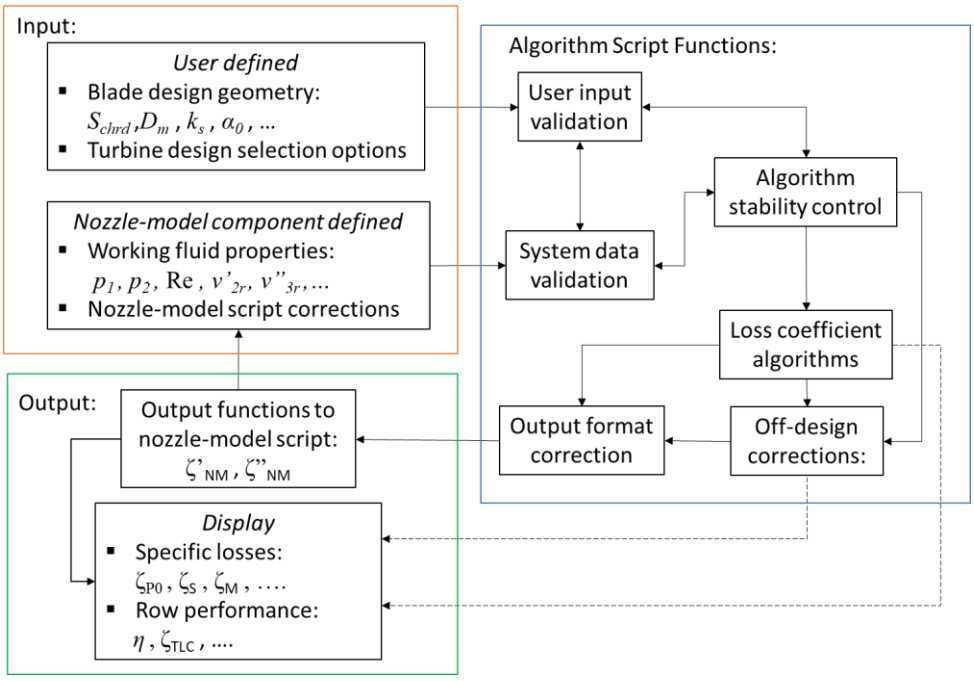

Figure 3-2: Loss Coefficient Algorithm Script Architecture

The loss coefficient algorithm script architecture is comprised of three sections:

- Input: User defined turbine design data and data transfer link information from the nozzle-model components, as indicated in Figure 3-2.
- Script functions: Check validity of data, maintain the script program during processing, calculated loss coefficients and format results to feedback to nozzle-model.
- Output: Returns script values to nozzle-model script per processing step and displays final values obtained.

The following section is comprised first of a description of the turbine loss coefficient input variables, followed by the evaluation and conversion of design and off-design loss coefficient into programmable algorithms.

Notably, the initial loss coefficient algorithms were developed in Mathcad, an engineering calculation software, that was used for methodology verification and validation purposes. An initial attempt to directly implement a MathCad scripts into a Flownex model presented processing complication and delays.

3.2 Loss coefficient input variables

The turbine loss coefficient input variables are comprised of two categories as indicated in Figure 3-2, namely “user defined” and “nozzle model defined”. The working fluid properties required are linked to the stage-by-stage turbine nozzle-model components via data transfer links. The stator and rotor restrictors send working fluid properties to the loss algorithm script as the variables indicated in Figure 3-3.

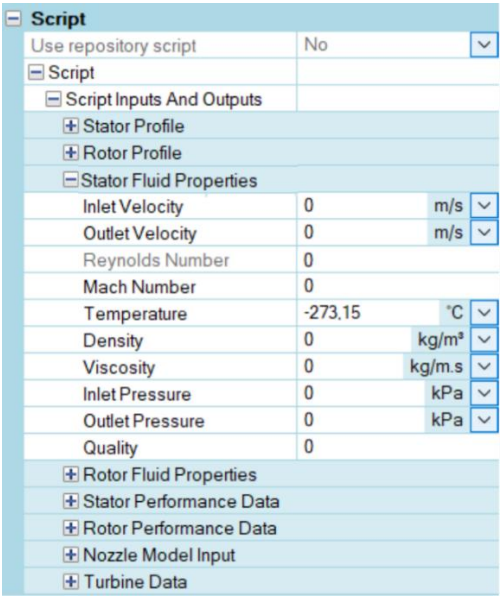

Figure 3-3: Stator Fluid Properties Input Variables

The rotor fluid properties variables are defined and linked similarly to the stator fluid properties variables, illustrated in Figure 3-3, with the exception that the inlet velocity is sourced from the nozzle-model script as it is corrected for blade speed.

The stator and rotor profile input variables, illustrated in Figure 3-4, was developed from section 2.1.2 and the blade design drawings depicted in Figure 2-7 and Figure 2-6. The blade geometries used as input variables are related to the requirements of the selected loss coefficients.

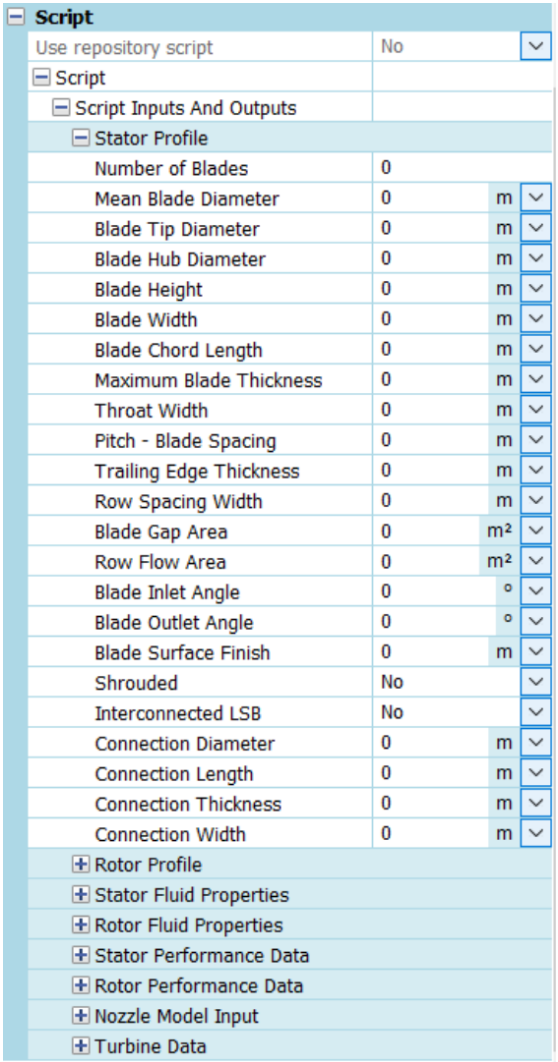

Figure 3-4: Stator Profile Blade Geometry Input Variables

Figure 3-4 depicts the stator profile blade geometries, there is an identical section for the rotor as indicated. The Flownex scripts allow for a customizable user-friendly interface that assists in the evaluation and understanding of the loss coefficient algorithms. Once several comparative models have been executed the correlation between specific turbine losses and turbine blade geometry becomes apparent. Chapter 6 attempts to display some of these correlations.

Notably, section 3.5 discusses the loss coefficient results display, labelled “Performance Data”, and the loss coefficient algorithm script’s output information labelled “Nozzle Model Input”.

3.3 Loss coefficient algorithms

This section will evaluate the selected loss coefficients that are largely comprised of reworkings of Traupel's turbine loss methodology [29] and show how they were systematically adapted into the loss coefficient algorithm script component.

The Traupel enthalpy loss coefficient (ζ_{TLC}) is the sum of a Primary profile loss (ζ_P), a Secondary loss (ζ_S), a Tip Leakage or Seal loss (ζ_{Tl}), a Fan loss (ζ_F), an LSB loss (ζ_{LSB}) and a Moisture loss (ζ_M).

$$\zeta_{TLC} = \zeta_P + \zeta_S + \zeta_{Tl} + \zeta_F + \zeta_{LSB} + \zeta_M \quad [3.3.1]$$

Traupel enthalpy loss coefficient (ζ_{TLC}) relates back to nozzle efficiency by:

$$\eta_{nozzle} = 1 - \zeta_{TLC} \quad [3.3.2]$$

Each enthalpy loss component is evaluated as a collective of its parts.

3.3.1 Primary profile loss

The primary profile loss (ζ_P) is determined by

$$\zeta_P = \zeta_{P0} \cdot \chi_M \cdot \chi_{\mathrm{Re}} + \zeta_{Te} + \zeta_C \quad [3.3.3]$$

ζ_{P0} – Profile loss

χ_M – Mach number correction factor

χ_{Re} – Reynolds number correction factor

ζ_{Te} – Trailing edge loss

ζ_C – Carnot shock loss

Profile loss

The profile loss (ζ_{P0}) is caused by the friction that occurs on the blade surfaces as a result of the flow separation of the boundary layers. A thicker boundary layer creates greater flow separation primarily on the blade suction surface.

The inlet and outlet velocity angles largely impact the boundary layer formation. The profile loss (ζ_{P0}) is obtained from empirical correlations between the inlet and outlet flow angles as illustrated in Figure 3-5.

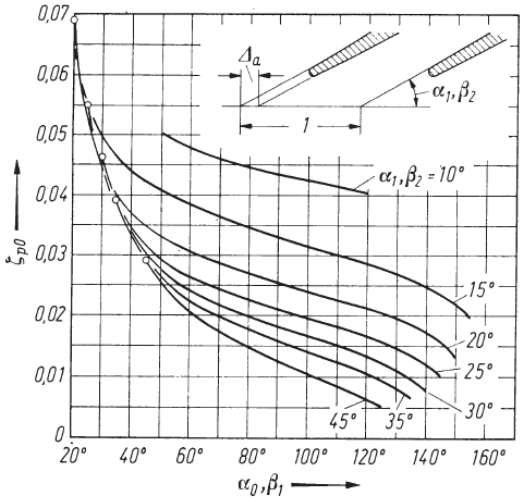

Figure 3-5: Traupel's profile loss chart [29]

The profile loss chart, Figure 3-5, was converted into a series of polynomials which are linearly interpolated for a given angle:

$$M_{P0} = \left[\begin{array}{c|c|c|c|c|c|c} 10 & 0 & 0 & \text{-1.6414*10^-8} & \text{5.22727*10^-6} & \text{-6.49224*10^-4} & \text{7.1513*10^-2} \\ 15 & \text{-7.19149*10^-12} & \text{3.49129*10^-9} & \text{-6.69342*10^-7} & \text{6.34078*10^-5} & \text{-3.13043*10^-3} & \text{1.02567*10^-1} \\ 20 & \text{-1.17977*10^-11} & \text{5.62751*10^-9} & \text{-1.06216*10^-6} & \text{9.92353*10^-5} & \text{-4.74289*10^-3} & \text{1.23335*10^-1} \\ 25 & \text{-1.49757*10^-11} & \text{7.07226*10^-9} & \text{-1.32412*10^-6} & \text{1.23126*10^-4} & \text{-5.8547*10^-3} & \text{1.40457*10^-1} \\ 30 & \text{-1.55815*10^-11} & \text{7.38388*10^-9} & \text{-1.397*10^-6} & \text{1.32036*10^-4} & \text{-6.406*10^-3} & \text{1.51418*10^-1} \\ 35 & \text{-1.96059*10^-11} & \text{9.16953*10^-9} & \text{-1.70609*10^-6} & \text{1.58261*10^-4} & \text{-7.52811*10^-3} & \text{1.69495*10^-1} \\ 45 & \text{-4.23568*10^-11} & \text{1.73797*10^-8} & \text{-2.80328*10^-6} & \text{2.24533*10^-4} & \text{-9.30707*10^-3} & \text{1.84516*10^-1} \end{array}\right]$$

$$\zeta_{P0} = \sum_{i=1}^{7} M_{P0[\alpha_{1\_Position}, i+1]} \cdot \alpha_0^{7-i} \qquad [3.3.4]$$

Equation [3.3.4] is utilized for both stator and rotor with the correct angle orientations required. A model algorithm validation and stability control measure is required at this point to correct for values entered outside of the curve functions indicated in Figure 3-5.

Mach number correction factor

The Mach number correction factor (χ_M) considers the free stream velocity across the blade profile and utilizes the Mach number along with the diagram shown in Figure 3-6.

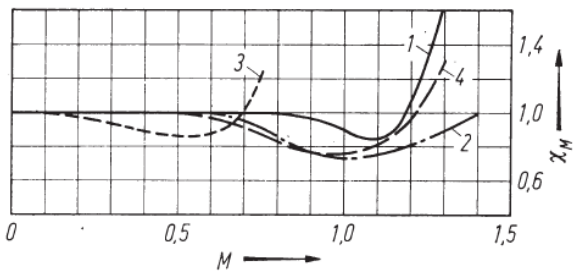

Figure 3-6: Mach number correction factor chart [29]

Mach number correction factor curve types, illustrated in Figure 3-6, are described as:

- Curve 1 - Relates to a conventional high-speed grid
- Curve 2 - Applies to a strongly accelerating grid
- Curve 3 - Corresponds to a constant-pressure impeller grid with rounded entry edge
- Curve 4 - Corresponds to a constant-pressure impeller grid which has a relatively pointed, forward-drawn entry edge for high Mach numbers.

Curve 1 is most often selected in the determinization of the Mach number correction factor. Curve 1 best correlates to the conditions experienced by power utility turbines [35]. The Mach number correction chart is converted into the following algorithms:

$$\chi_M = 1 \text{ for } Ma < 0.8 \qquad [3.3.5]$$

$$\chi_M = -344.9Ma^5 + 1763Ma^4 - 3690.8Ma^3 + 3744.7Ma^2 - 1878.6Ma + 374.2 \text{ for } Ma \geq 0.8 \qquad [3.3.6]$$

The Mach number is determined by Flownex and is linked to the loss coefficient algorithm script.

Reynolds number correction factor

The Reynolds number correction factor (χ_{Re}), determined by utilizing Figure 3-7, describes the influence that the Reynolds number (Re) and surface finish or roughness (k_s) has on the blade profile loss. The relationship between profile loss and the Reynolds number correction factor is indicated by the correlation the Reynolds number has with the boundary layer thickness and the flow separation as defined by classical fluid dynamics [22].

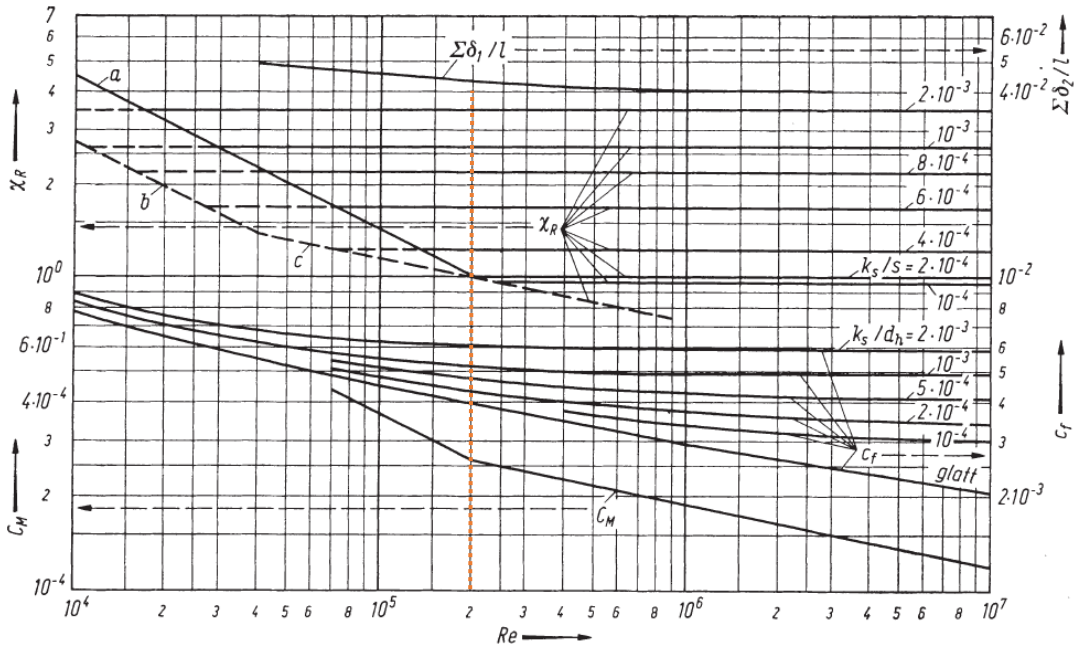

Figure 3-7: Reynolds number correction factor chart [29]

From the chart, it becomes apparent that the Reynolds number correction factor is exclusively dependant on the working fluids Reynolds number below the transition point ($Re<2\cdot10^5$). Whilst above the transition point the turbine blade surface finish will exclusively determine the Reynolds number correction factor. Only line (a) is turbine specific for the Reynolds number correction factor, lines (b) and (c) are used for compressors. A clearer concept of Figure 3-7 is provided in Figure 3-8 and Figure 3-9.

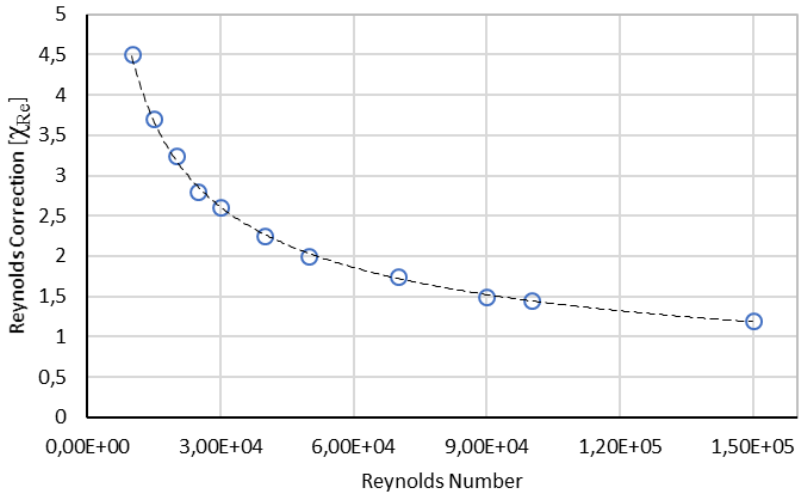

Figure 3-8: Reynolds Correction Curve for $Re<2\cdot10^5$

It is apparent from Figure 3-8 that a lower Reynolds ($Re<2\cdot10^5$) number will increase the profile loss.

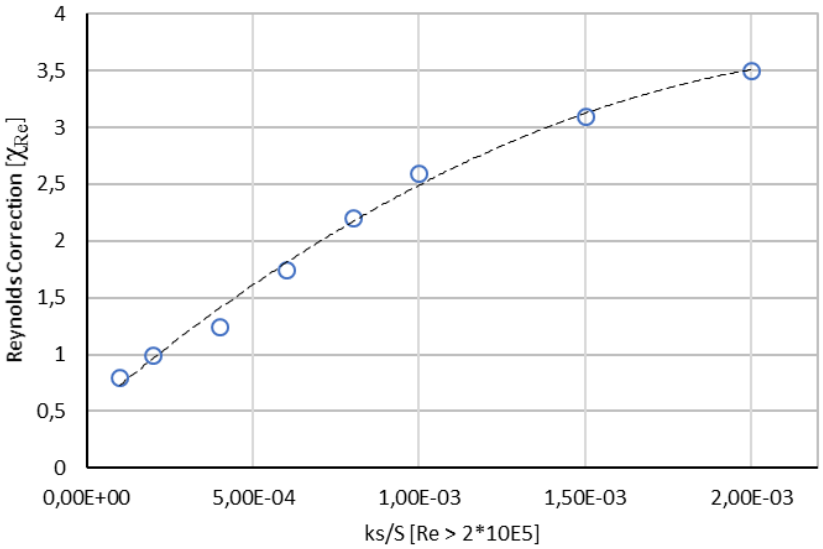

Figure 3-9: Reynolds Correction Curve for $Re>2\cdot10^5$

Figure 3-9 indicates that a larger Reynolds number ($Re>2\cdot10^5$) has no impact on the profile loss but that the relative blade surface finish will increase the profile loss.

The Reynolds number indicates the ratio between inertia and viscous forces within the working fluid flow and is determined by:

$$\mathrm{Re} = \frac{\rho \cdot v \cdot D_{\mathrm{Re}}}{\mu} \quad [3.3.7]$$

ρ – Blade outlet fluid density

v – Blade outlet fluid velocity

D_{Re} – Blade spacing area diameter

μ – Blade outlet dynamic viscosity

The blade spacing area diameter (D_{Re}) is determined for the Reynolds number calculation by converting the blade spacing area (A_{BldGap}), determined by equation [2.1.5], into hydraulic diameter [35]:

$$D_{\mathrm{Re}} = \sqrt{\frac{4 \cdot A_{BldGap}}{\pi}} \quad [3.3.8]$$

Traupel provides a rough guide for surface finishes values to be used [35]:

- 0 to 0.002 mm for ground and polished blades.
- 0.005 to 0.010 mm for standard milled and drawn blades
- 0.01 to 0.03 mm for lightly rusted blades
- 0.03 to 0.06 mm for heavily rusted sheet metal blades
- 0.03 to 0.10 mm for raw casting blades

The Reynolds number correction can then be calculated using the following equation:

For $\mathrm{Re} < 2 \cdot 10^5$

$$\chi_{\mathrm{Re}} = 4.1542 \cdot 10^2 \, \mathrm{Re}^{-0.491718} \quad [3.3.9]$$

For $\mathrm{Re} \geq 2 \cdot 10^5$

$$\chi_{\mathrm{Re}} = -2.04381 \cdot 10^8 \left(\frac{k_s}{S_{chrd}} \right)^3 + 1.34009 \cdot 10^5 \left(\frac{k_s}{S_{chrd}} \right)^2 + 2.00593 \cdot 10^3 \left(\frac{k_s}{S_{chrd}} \right) + 0.565005 \quad [3.3.10]$$

The loss coefficient algorithm section for Mach number and Reynolds number correction factors have validation checks. These checks only allow valid value transfer, thus excluding extreme values fed from the nozzle-model during iteration processes.

Trailing edge loss

The trailing edge loss (ζ_{Te}) is caused by the wake after the trailing edge. First, the trailing edge impact percentage (Δ_a) is determined as the ratio of trailing edge thickness to outlet velocity angle. Figure 3-10 provides an illustration of the impact percentage alongside the trailing edge thickness (δ_{Te}), their connection is defined by equation [3.3.11].

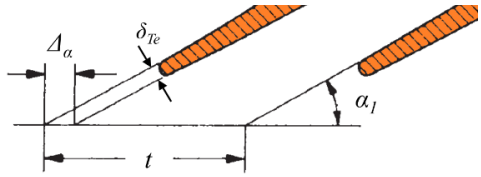

Figure 3-10: Trailing edge area illustration – Adapted from [29]

$$\Delta_a = \frac{\delta_{Te}}{t \cdot \sin(\alpha_1)} \qquad [3.3.11]$$

The trailing edge loss is then defined in section 2.2.2 and determined by utilizing Figure 3-11.

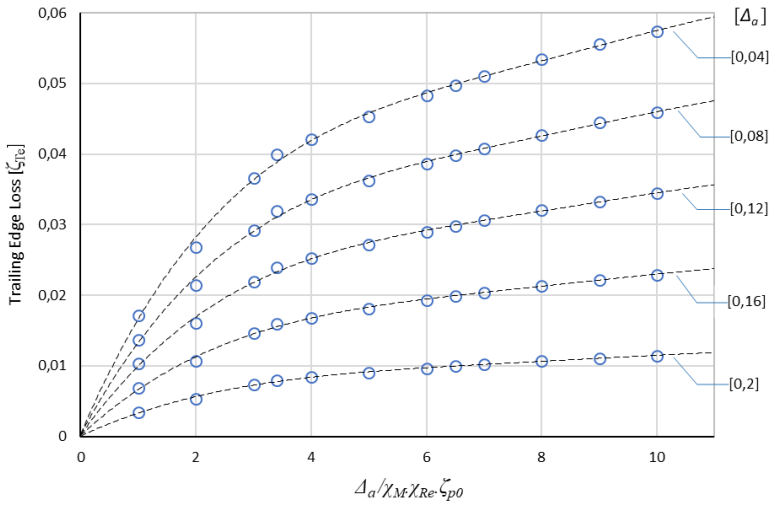

Figure 3-11: Trailing Edge loss diagram [29]

The trailing edge loss diagram depicted was adapted from the Traupel trailing edge loss graph [29]. The trailing edge loss diagram, Figure 3-11, is converted into a set of polynomials:

$$M_{TE} = \begin{bmatrix} 0.04 & -7*10^{-6} & 0{,}0002 & -0{,}003 & 0{,}0191 & 0{,}0004 \\ 0.08 & -6*10^{-6} & 0{,}0002 & -0{,}002 & 0{,}0152 & 0{,}0003 \\ 0.12 & -4*10^{-6} & 0{,}0001 & -0{,}0018 & 0{,}0114 & 0{,}0002 \\ 0.16 & -3*10^{-6} & 9*10^{-5} & -0{,}0012 & 0{,}0076 & 0{,}0002 \\ 0.2 & -1*10^{-6} & 5*10^{-5} & -0{,}0006 & 0{,}0038 & 0{,}00008 \end{bmatrix}$$

$$\zeta_{Te} = \sum_{i=1}^{5} M_{TE[\Delta_{\alpha\_Position},i+1]} \cdot \left(\frac{\Delta_\alpha}{\chi_M \chi_{\mathrm{Re}} \zeta_{P0}} \right)^{5-i} \qquad [3.3.12]$$

An identical matrix and algorithm set is used for both stator and rotor.

Carnot shock loss

The final component required for the profile loss coefficient is the Carnot shock loss (ζ_C). The Carnot shock loss is caused by sudden fluid expansion occurring at the exhaust of the turbine blade passage.

The Carnot shock loss can be viewed as the transition between the two boundaries that follows an elliptical course forming behind the blade trailing edge and is calculated as:

$$\zeta_C = \left(\frac{\Delta_a}{1-\Delta_a} \right)^2 \cdot \sin^2(\alpha_1) \qquad [3.3.13]$$

3.3.2 **Secondary Loss**

The Secondary loss (ζ_S) is determined by

$$\zeta_S = \frac{\zeta_P}{\zeta_{P0}} \cdot \frac{F}{(l/t)_k} + \zeta_a + A \cdot \left(\frac{s_{chord}}{l} - \frac{s_{chord}/t}{(l/t)_k} \right) \qquad [3.3.14]$$

ζ_P – Primary profile loss

ζ_{P0} – Profile loss

F – Flow angle correction factor

$(l/t)_k$ – Critical blade length to pitch ratio

ζ_a – Endwall losses

A – Velocity grid correction coefficient

S_{Chrd} – Blade chord length

The correction factor ratio of ζ_P and ζ_{P0} indicates that the secondary losses are affected by the blade angles, the trailing edge effects, the Mach and the Reynolds numbers. The blade length (l_S) to pitch (t) ratio inclusion takes into consideration the interaction between the secondary vortex on the two endwalls as it relates to the blade chord (S_{Chrd}). This consideration first evaluates the impact of actual (l_S/t) to critical $(l/t)_k$ blade length to pitch ratio as follows:

$$(l/t)_k = B \cdot \sqrt{\zeta_P} \qquad [3.3.15]$$

B – Blade orientation coefficient

The blade orientation coefficient is given as $B = 7$ for a stator and $B = 10$ for a rotor by Traupel [29]. If (l_s/t) is smaller than $(l/t)_k$ then $(l/t)_k$ is used in equation [3.3.14].

Flow correction factor

The change in flow angle correction factor (F) is an indication of how the secondary flow is affected by the difference between the inlet and the outlet flow angles (α_0 ,α_1) and the respective velocities. This relationship is observed in Figure 3-12.

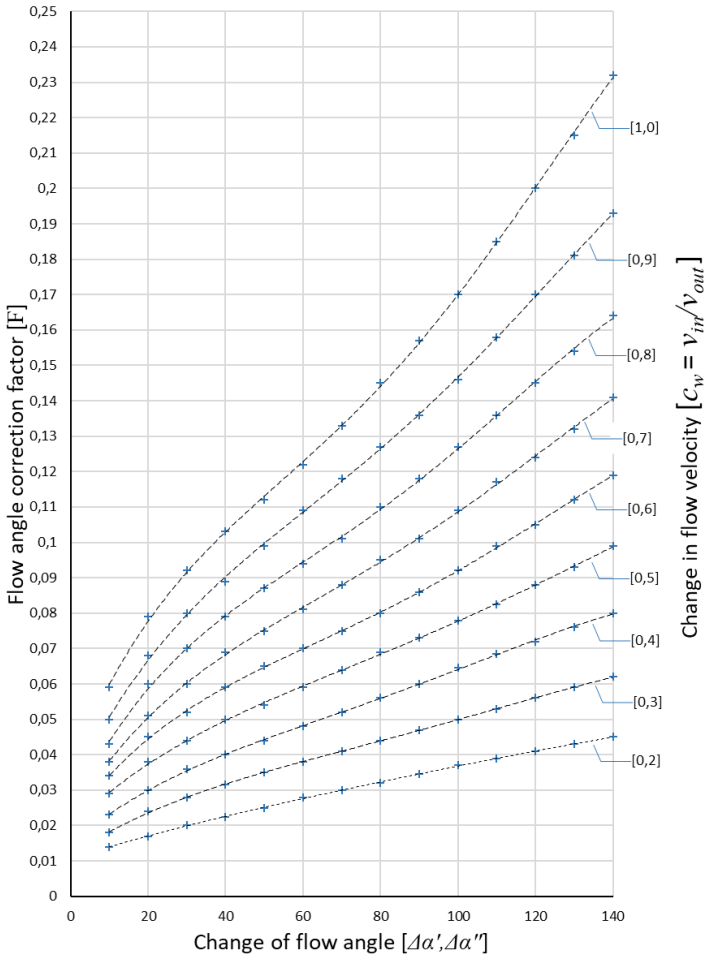

Figure 3-12: Flow correction factor chart – Adapted from [29]

Figure 3-12 indicates that the greater the difference between inlet and outlet angles ($\Delta\alpha$ - change of flow angle) the greater the secondary loss will be impacted by the flow correction factor. Similarly, the smaller the change in flow velocity ratio (c_w) the greater the impact.

$$\Delta\alpha = \alpha_0 - \alpha_1 \quad [3.3.16]$$

$$c_w = v_{in} / v_{out} \quad [3.3.17]$$

The flow correction factor diagram, Figure 3-12, is converted into a set of polynomials applicable to both stator and rotor:

$$F = \sum_{i=1}^{5} M_{F[c_{w\_Position},i+1]} \cdot \Delta\alpha^{5-i} \quad [3.3.18]$$

$M_F =$

1	-9.1269*10^-10	3.23992*10^-7	-3.65469*10^-5	2.66136*10^-3	3.66044*10^-2
0.9	-6.16173*10^-10	2.27701*10^-7	-2.78513*10^-5	2.28791*10^-3	3.03546*10^-2
0.8	-7.17726*10^-10	2.52631*10^-7	-3.00349*10^-5	2.21563*10^-3	2.43801*10^-2
0.7	-4.52489*10^-10	1.69238*10^-7	-2.13194*10^-5	1.75095*10^-3	2.27393*10^-2
0.6	-4.04069*10^-10	1.5065*10^-7	-1.88122*10^-5	1.48852*10^-3	2.10375*10^-2
0.5	-1.85538*10^-10	7.60232*10^-8	-1.05483*10^-5	1.06001*10^-3	1.97787*10^-2
0.4	-2.62881*10^-10	8.98421*10^-8	-1.08292*10^-5	9.40453*10^-4	1.47745*10^-2
0.3	-1.64113*10^-10	5.98948*10^-8	-7.81293*10^-6	7.29054*10^-4	1.16583*10^-2
0.2	-2.80663*10^-11	1.00053*10^-8	-1.5836*10^-6	3.47721*10^-4	1.06541*10^-2

A model algorithm validation and stability control measure is required at this point to correct for values entered outside of curve functions indicated in Figure 3-12.

Endwall loss

The Endwall losses (ζ_a) is a correction for the loss that occurs across the axial distance between the blade rows. These losses are caused by the state of the boundary layers at the endwalls and the unsteady effects (wake) as a result of the rotor-stator interaction.

To determine the Endwall losses the friction coefficient associated with the blade surface condition (k_s) must first be determined. The surface must first be defined as smooth or rough:

$$k_s < k_{s\_Lmt}$$

Where the limit value is set at:

$$k_{s\_Lmt} = 0.042mm$$

Next, the smooth friction coefficient (c_f) value must be determined for the correct surface condition. For a rough surface:

$$c_{f\_rgh} = \left(1.89 + 1.62 \cdot \log\left(\frac{l}{k_s}\right)\right)^{-2.5} \quad [3.3.19]$$

For a smooth surface :

$$c_{f\_smth} = \frac{0.455}{\log(\mathrm{Re})^{2.58}} \quad [3.3.20]$$

Figure 3-7 may be used to determine the friction coefficient (c_f). Equations [3.3.19] and [3.3.20] were used for the loss coefficient algorithm development.

The Endwall losses are determined by:

$$\zeta'_a = \frac{c_f}{\sin(\alpha'_1)} \cdot \left(1 + \frac{l'}{D'_m}\right) \cdot \frac{\delta'_{Gap}}{l'} \quad [3.3.21]$$

$$\zeta''_a = \frac{c_f}{\sin(\alpha''_1)} \cdot \left(1 - \frac{l''}{D''_m}\right) \cdot \frac{\delta''_{Gap}}{l''} \quad [3.3.22]$$

ζ_a – Endwall losses

c_f – Surface friction coefficient

D_m – Mean blade diameter

δ_{Gap} – Blade gap width

Velocity grid correction coefficient

The last component of the Secondary loss is a correction coefficient for the lack of undistributed flow in the blade passage pertaining to low aspect ratio turbines. The Velocity grid correction (A), was determined from experimental data and described by Dejc et. al [44], it has the following approximate the values:

- 0.02 for strongly accelerating and high-velocity grids such as a stator row of a reaction stage
- 0.035 for constant pressure grids such as a rotor row of an impulse stage

3.3.3 **Fan Loss**

The fan loss (ζ_F) is a result of the change in pitch length between the root and tip of the blades causing the spacing between blades to not be constant over the radius. The blade length (l_s) to mean blade diameter (D_m) ratio is used alongside the blade diameter hub to tip ratio (υ) in Figure 3-13 to determine the Fan loss.

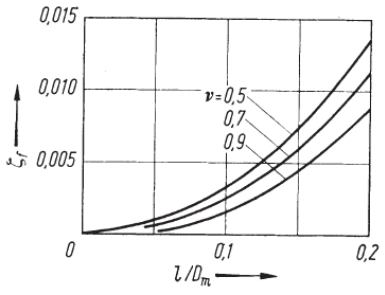

Figure 3-13: Fan loss chart [29]

The blade diameter hub to tip ratio (υ) is determined by

$$\upsilon = D_n / D_s$$

The fan loss increases independently with the increase in blade hub to tip ratio and the blade length to mean diameter ratio. A simple set of polynomials were used for the development of the fan loss component:

$$M_{Fl} = \begin{bmatrix} 0.5 & 3.53074*10^{-1} & -2.08139*10^{-3} & 1.28485*10^{-4} \\ 0.7 & 3.20866*10^{-1} & -7.03983*10^{-3} & 6.39394*10^{-5} \\ 0.9 & 2.99004*10^{-1} & -1.49509*10^{-2} & 7.86364*10^{-5} \end{bmatrix}$$

$$\zeta_F = \sum_{i=1}^{3} M_{Fl[\upsilon_{Position},i+1]} \cdot \left(\frac{l}{D_m}\right)^{3-i} \quad [3.3.23]$$

Due to the sizing of the graph, a stricter control measure is required to restrict extreme values for both stator and rotor.

3.3.4 **Tip Leakage Loss**

The Tip Leakage loss (ζ_{Tl}) is caused by the energy dissipation of the working fluid across the blade tip and the mixing of the tip leakage flow with the exiting main flow. Traupel [29] provides empirical approximations for tip leakage loss for turbine blades, classified into two groups namely unshrouded and shrouded.

Unshrouded

Traupel presents a tip leakage loss approximation function for unshrouded turbine blades based on experimental results obtained from the ETH Institute of Thermal Turbomachinery [29]. The approximation function is comprised of an extensive list of variables. The tip leakage for an unshrouded stator and an unshrouded rotor is determined respectively as:

$$\zeta_{Tl}^{'} = K_{\tau}^{'}\left[\frac{2(1-R)\varphi^{'} + v_1^2}{2\varphi^{'}}\right]\frac{(\tau^{'} - 0.002S_{Chrd}^{'})D_n^{'}}{l^{'}D_m^{'}} \quad [3.3.24]$$

$$\zeta_{Tl}^{''} = K_{\tau}^{''}\left[\frac{2R\varphi^{''} + v_{2r}^2 - u^2 + 1}{2\varphi^{''}}\right]\frac{(\tau^{''} - 0.002S_{Chrd}^{''})D_s^{''}}{l^{''}D_m^{''}} \quad [3.3.25]$$

Where the tip leakage gap mass flow percentage (φ) was determined by relating blade tip area to the blade flow area:

$$\varphi^{'} = \left(\frac{\pi\tau^{'}D_n^{'}}{A_{Flow}}\right) \quad [3.3.26]$$

$$\varphi^{''} = \left(\frac{\pi\tau^{''}D_s^{''}}{A_{Flow}}\right) \quad [3.3.27]$$

An unshrouded correction coefficient (K_{τ}) is used in the approximation function.

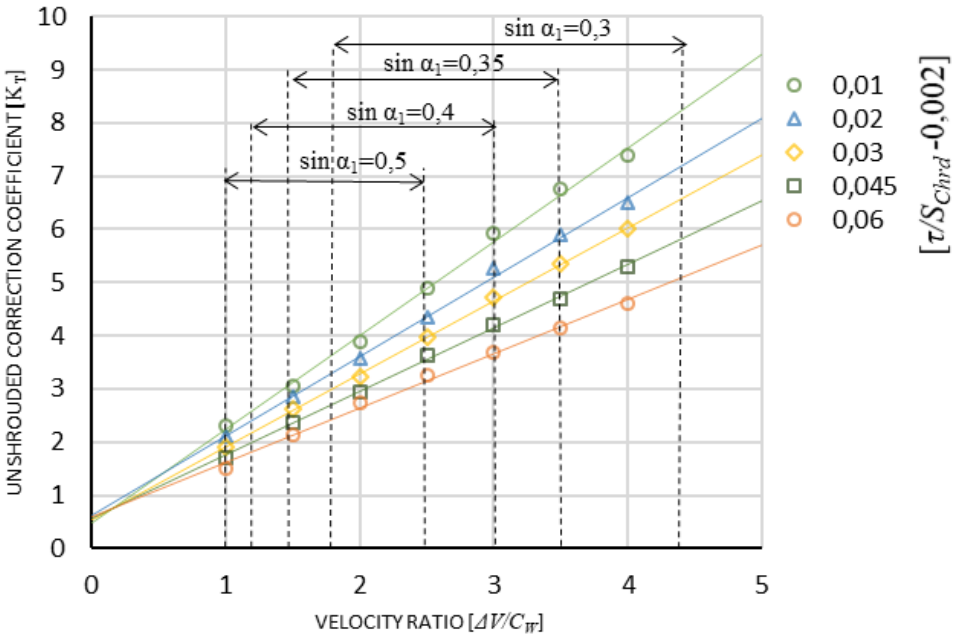

Figure 3-14: Unshrouded Correction Coefficient Chart

The unshrouded correction coefficient can be determined by using Figure 3-14 adapted from 4 diagrams provided by Traupel [29] or approximated using a set of linear curves:

$$M_{K\tau} = \begin{bmatrix} 0{,}01 & 1{,}7643 & 0{,}4821 \\ 0{,}02 & 1{,}497 & 0{,}6205 \\ 0{,}03 & 1{,}3744 & 0{,}5366 \\ 0{,}045 & 1{,}194 & 0{,}5649 \\ 0{,}06 & 1{,}0202 & 0{,}6065 \end{bmatrix}$$

$$K_\tau = \sum_{i=1}^{2} M_{K\tau_{[(\frac{\tau}{S_{Chrd}}-0.002)_{Position},i+1]}} \cdot \left(\frac{\Delta v}{c_w}\right)^{2-i} \qquad [3.3.28]$$

Figure 3-14 provides a reference guide for approximate correct value zones based on the row outlet velocity ($sin\ \alpha_1$), this attribute must be included as a model algorithm validation function.

Shrouded

Tip leakage loss for shrouded blades incorporates the Shrouded tip leakage mass flow ratio (ω); that indicates the portion of mass flow through the seals and the Shrouded tip leakage velocity ratio (Υ); that implements a correction for the tip leakage losses resulting from the inlet-outlet velocity ratio occurring at design inlet and outlet flow angles.

Traupel [35] provides a value estimation table for the shrouded tip leakage velocity ratio (Υ) as it relates to the shrouded tip leakage mass flow ratio and the pressure distribution range between LP and HP turbines.

Both the shrouded tip leakage mass flow ratio and the derived shrouded tip leakage velocity ratio can be determined for the stator and rotor accordingly:

$$\omega = \frac{\varphi}{1-\varphi} \qquad [3.3.29]$$

$$\Upsilon = 1{,}5318\omega^2 + 1{,}3854\omega + 0{,}1244 \qquad [3.3.30]$$

Then the Shrouded tip Leakage loss is calculated as:

$$\zeta'_{Tl} = 2(1-R)\omega' \left[1 - \left(\frac{\Upsilon' - v_2/v_1}{v_2/v_1} \right)^2 \right] \qquad [3.3.31]$$

$$\zeta''_{Tl} = \omega'' \left[1 - \left(\frac{\Upsilon'' - v_{3r}/v_{2r}}{v_{3r}/v_{2r}} \right)^2 \right] \qquad [3.3.32]$$

The Traupel shrouded tip leakage loss coefficient uses a generalized evaluation method and does not incorporate exact blade seal design geometries, illustrated in Figure 3-15, into its determination.

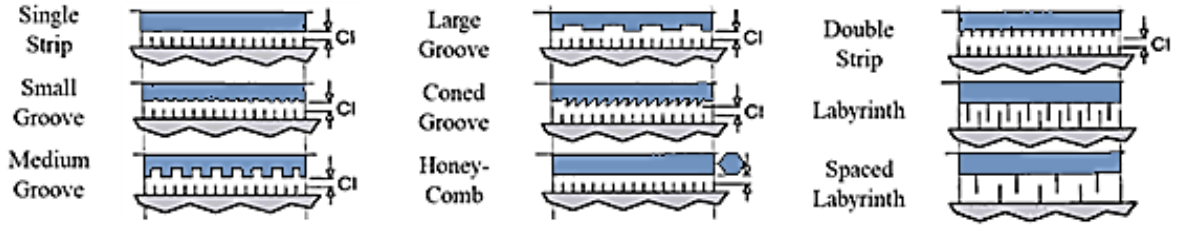

Figure 3-15: Blade Shroud Seal Designs – Adapted from [11]

Notably, due to the complex nature of tip leakage experimental measurements, evaluation and accuracy of theoretical approximations, it is regarded as the weak point for the loss coefficient algorithm. A sensible amount of validation checks and stability corrections have been implemented to improve the tip leakage approximation.

An alternative tip leakage loss modelling method is proposed by Fuls [1]. Gland seal leaks, bypass flows and clearance leaks can be modelled in Flownex's by utilizing a labyrinth seal component in combination with the nozzle components, as illustrated in Figure 3-16.

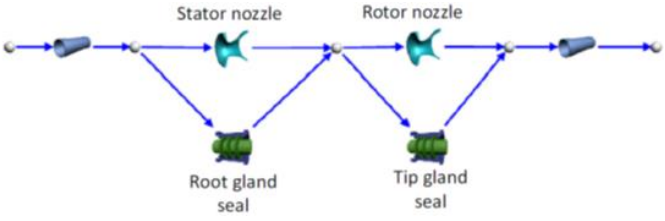

Figure 3-16: Single stage model utilizing Flownex's labyrinth seal component [1]

3.3.5 **Moisture Losses**

Traupel [29] incorporates a Moisture loss coefficient (ζ_M) that was derived in part from the work of Gyarmathy [26]. The moisture loss is determined by:

$$\zeta_M = \zeta_u + \zeta_b + \zeta_s \quad [3.3.33]$$

ζ_u =Thermal loss

ζ_b =Brake loss

ζ_s =Drag loss

Moisture loss can be broken down into two loss groups namely: Thermal loss and Mechanical loss. The Thermal loss (ζ_u) is comprised of the loss occurring due to the heat exchange between the liquid and vapour phases. This heat exchange phenomenon is part of any operational condition that allows for the development of condensation [26]. The magnitude of the thermal loss in comparison to the moisture loss can be observed in Figure 3-17.

The Mechanical loss is comprised of two components: Brake loss (ζ_b) and Drag loss (ζ_s). The brake loss is caused by wet steam components, comprised of steam and various water droplets, having different velocities. The difference in velocities causes a kinetic energy loss as the faster moving steam attempt to move past the slower water droplet [26].

The Drag loss is created by the frictional forces occurring between the steam and the water droplets. Due to the difference in velocities, the larger water droplets form a boundary layer as the steam passes, creating a condition that enables the steam to continuously dissipate kinetic energy on the droplets [26].

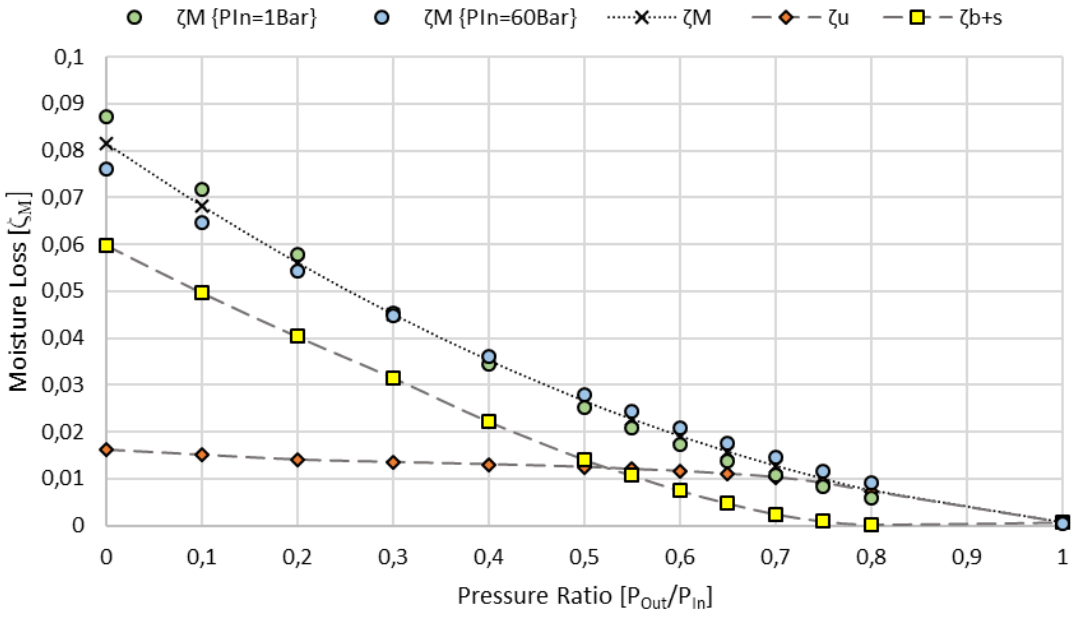

Figure 3-17: Moisture Loss to Pressure Ratio

The work of Gyarmathy [26] and Hiroyuki et. al. [25] was used to improve on the correlation provided by Traupel [35] producing the Moisture loss to pressure ratio chart in Figure 3-17. The Moisture loss can then be determined by:

$$\zeta_M = 0.0581\left(\frac{p_{out}}{p_{in}}\right)^2 - 0.139\left(\frac{p_{out}}{p_{in}}\right) + 0.0815 \qquad [3.3.34]$$

A model algorithm validation function is used to only initiate the Moisture loss function if the steam quality drops below 99% and the pressure ratios are within limits.

Note that the unique phenomenon of supersaturation must be incorporated into the validation function. Supersaturation occurs when the steam state does not follow the exact equilibrium curves when crossing the saturation line whilst travelling inside a blade passage.

This deviation results from the condensation phase experiencing a delay that is followed by a sudden phase shift, creating an instantaneous collapse from steam to droplet state requiring the initiation of the Moisture Loss function.

3.3.6 **LSB Losses**

The Last Stage Blade loss coefficient (ζ_{LSB}), specific to the loss coefficient algorithm, is solely comprised of the loss incurred by the last stage blades interconnections. The loss is based on the frictional and separation flow forces generated by the reduction in flow area and the respective flow disturbance resulting from the interconnection [29]. Figure 3-18 provides an LSB interconnection geometry guide.

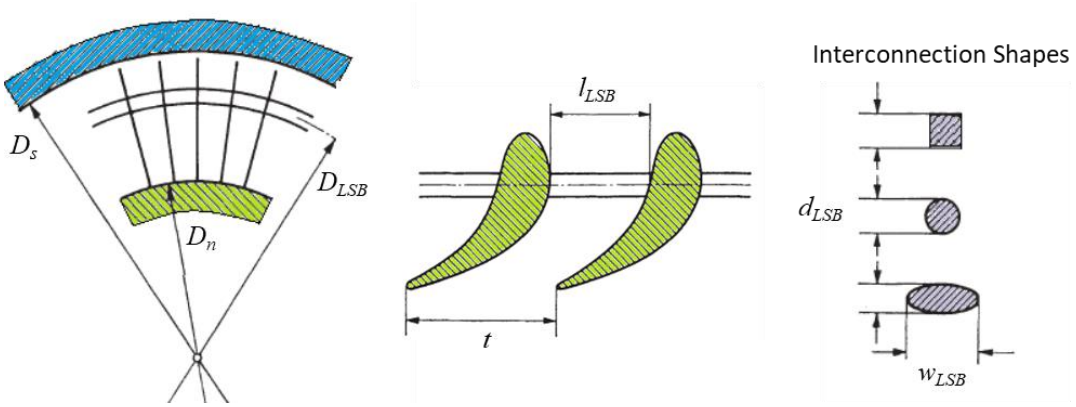

Figure 3-18: LSB Interconnection Geometry – Adapted from [29]

The LSB loss is determined for both stator and rotor by:

$$\zeta_{LSB} = 8x_{LSB} \cdot \mathrm{Sin}^2\,\alpha_1 \cdot \left(\frac{t^2}{l_{LSB}^2}\right)\left[\frac{D_{LSB}d_{LSB}}{D_s^2 - D_n^2}\right] \qquad [3.3.35]$$

The last stage blade interconnection shape specific drag coefficient (x_{LSB}) is determined from the drag coefficient values illustrated in Table 2-1 [35]. The loss coefficient algorithm has a manual input validation check and correction requirement for x_{LSB}.

Table 3-1: LSB Interconnection Drag Coefficient

Shape	$\frac{w_{LSB}}{d_{LSB}}$	x_{LSB}
	1	1,2
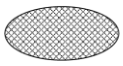	2 4 8	0,64 0,35 0,28
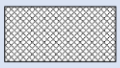	1 5 10	1,18 1,2 1,3
	0,5	1,7

The turbine blade interconnection script input variables are indicated at the end of Figure 3-4

This concludes all the components required for the design condition modelling section of the loss coefficient algorithm. All the loss coefficient components are calculated and combined as indicated in equation [3.3.1] to form the master equation of the loss coefficient algorithm.

3.4 Off-design loss coefficient algorithm

The loss coefficient developed by Traupel [29] can be corrected for off-design conditions by implementing Zehner's [24] loss coefficient methodology. The Zehner loss coefficient (ζ_{P_Z}) focuses on determining turbine performance at off-design conditions. Traupel's loss coefficient is used as the basis for Zehner's loss coefficient, thus utilizing the same primary profile enthalpy loss (ζ_P) coefficient characteristics determined in section 3.3 .

The Zehner loss coefficient applies the following correction on the zero-incidence design profile loss condition determined by Traupel's loss coefficient [24]:

$$\zeta_{P\_Z} = 1-(1-\zeta_P)^{-Z_a \cdot \Delta i^{Z_b}} \qquad [3.3.36]$$

ζ_{P_Z} – Zehner Profile loss coefficient

ζ_P – Traupel Profile loss

Δi – Difference in angle of attack from design

Z_a & Z_b – Cascade geometry character correction

The Zehner correction requires first the determination of the incidence angle (α_{Inc}). Figure 3-19 indicates the working fluid inlet angle conventions for both the rotor and the stator blade rows. The inlet angles are adjusted to illustrate the incidence angles for off-design turbine speeds (-u, +u) with regards to design speed (u).

Notably, the turbine speed and off-design speeds are configured into the loss coefficient algorithm script under the "Turbine Data" section illustrated in Figure 3-4.

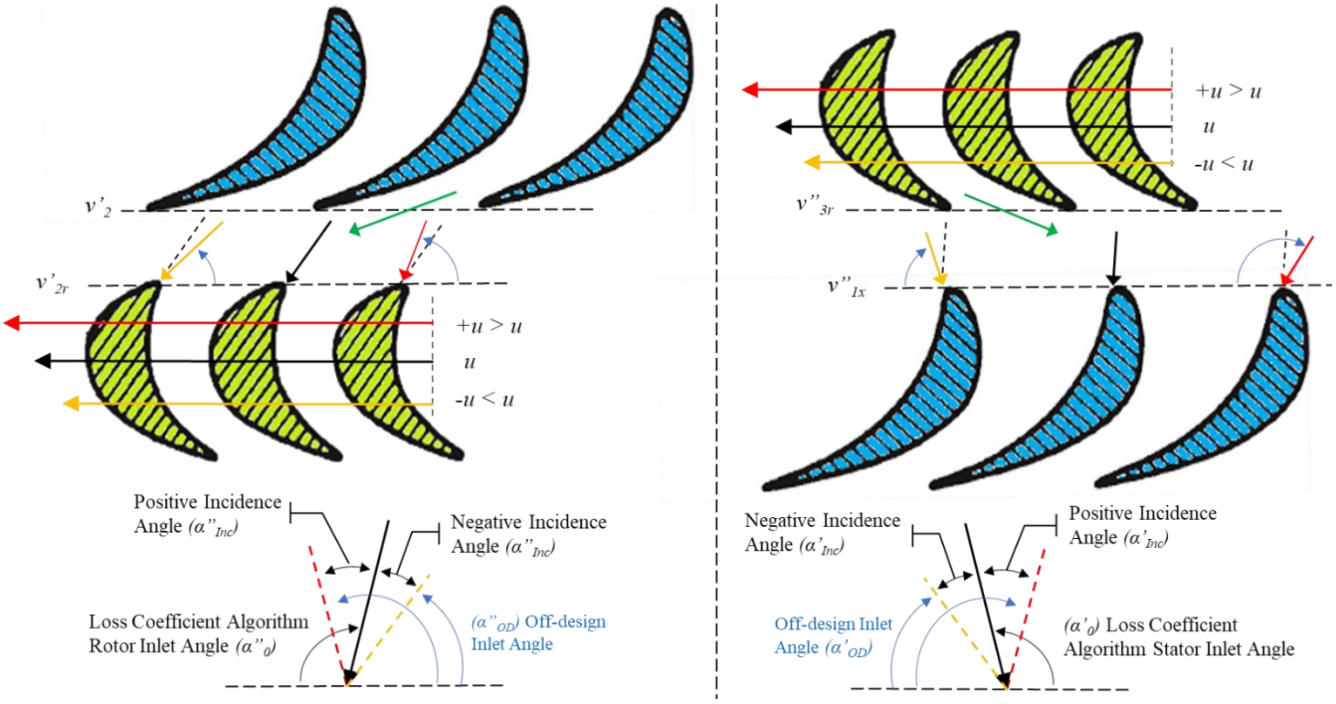

Figure 3-19: Rotor and Stator Inlet Angle Orientation

The negative incidence angles move towards the convex pressure blade surface whilst the positive incidence angle moves towards the concave suction blade surface. The incidence angle is determined as the difference between the converted design inlet angle (α_0) and the off-design inlet angle (α_{OD}):

$$\alpha_{Inc} = (180° - \alpha_0) - \alpha_{OD} \quad [3.3.37]$$

The difference to the design angle of attack (Δi) is then determined with regards to the impact the incidence angle has. If $\alpha_0 - \alpha_{Inc} > 0$, then:

$$\Delta i = \frac{\alpha_0 - \alpha_{Inc}}{180° - \alpha_{Inc}} \quad [3.3.38]$$

Otherwise:

$$\Delta i = \frac{\alpha_0 - \alpha_{Inc}}{-\alpha_{Inc}} \quad [3.3.39]$$

The difference to the design angle of attack (Δi) is now used with cascade geometry character terms (Z_a, Z_b). These are empirical correlations describing the cascade geometry character that utilizes the turbine cascade coefficient (γ_{cas}) and incorporates the blade stagger angle (β_S), the height of the curvature of the camber line (f_{hcc}), the pitch and the blades inlet and outlet angles [24]. This is illustrated in Figure 2-8. The blade stagger angle is determined by:

$$\beta = \sin^{-1}\left(\frac{S_{chrd}}{S_{wdth}}\right) \quad [3.3.40]$$

β – Blade stagger angle

S_{chrd} – Blade chord length

S_{wdth} – Thickest blade width alone chord line

The turbine cascade coefficient is then determined by:

$$\gamma_{cas} = \frac{f_{hcc}}{t} \cdot \sqrt{\beta \cdot (\alpha_0 + \alpha_1)} \quad [3.3.41]$$

γ_{cas} – Cascade coefficient

f_{hcc} – The height of the curvature of the camber line

t – Pitch

Turbine blade profiles that have a higher camberline tend to have thicker boundary layer creating higher loss conditions. A cascade coefficient (γ) reference guide, illustrated in Figure 3-20, for various blade profiles is provided by Zehner.

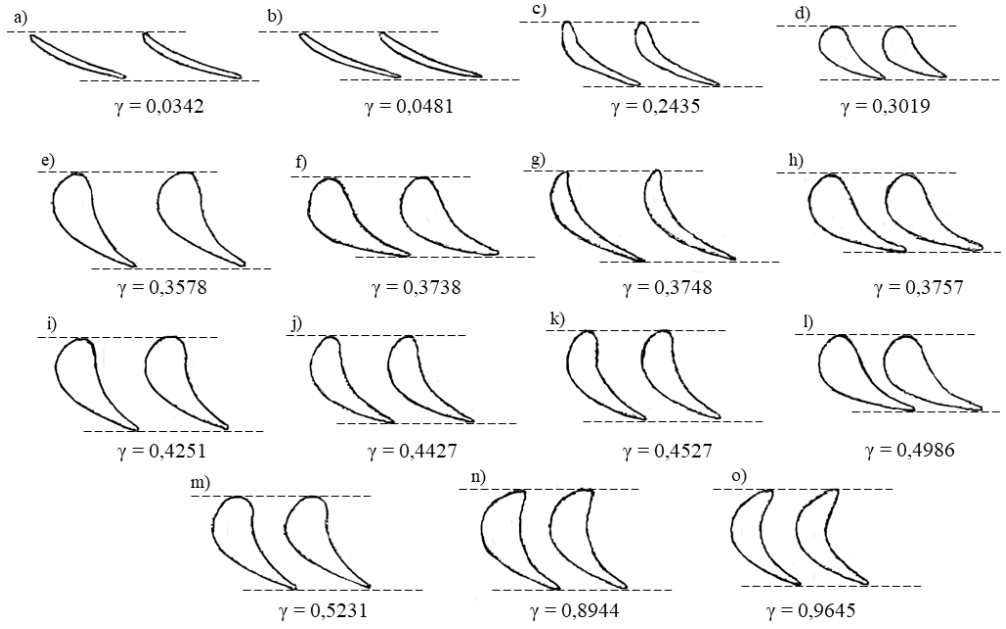

Figure 3-20: Cascade coefficient reference guide – Adapted from [24]

Figure 3-20 is used as a validation check platform. Z_a and Z_b cascade geometry character correlations are determined as follow:

If $\Delta i > 0$, then:

$$Z_a = 2.587 - 0.426 \cdot \gamma_{cas} - 1.21 \cdot \gamma_{cas}^2 \quad [3.3.42]$$

$$Z_b = 4.175 - 10.802 \cdot \gamma_{cas} - 13.881 \cdot \gamma_{cas}^2 \quad [3.3.43]$$

Else

$$Z_a = 0.446 - 3.82 \cdot \gamma_{cas} - 2.899 \cdot \gamma_{cas}^2 \quad [3.3.44]$$

$$Z_b = 2.413 - 10.38 \cdot \gamma_{cas} - 10.116 \cdot \gamma_{cas}^2 \quad [3.3.45]$$

The Off-Design loss coefficient (ζ_{TZLC}) is now determined by rewriting Traupel's enthalpy loss coefficient as a function of Zehner's profile loss correction.

$$\zeta_{TZLC} = \zeta_{P\_Z} + \zeta_S + \zeta_{Tl} + \zeta_F + \zeta_{LSB} + \zeta_M \quad [3.3.46]$$

Additionally, a model algorithm stability function is required to ensure that the incidence angles are within limits and orientated correctly for both stator and rotor. The inlet stator row is excluded from the off-design coefficient algorithm, whilst the remainder has a simple inlet angle check function.

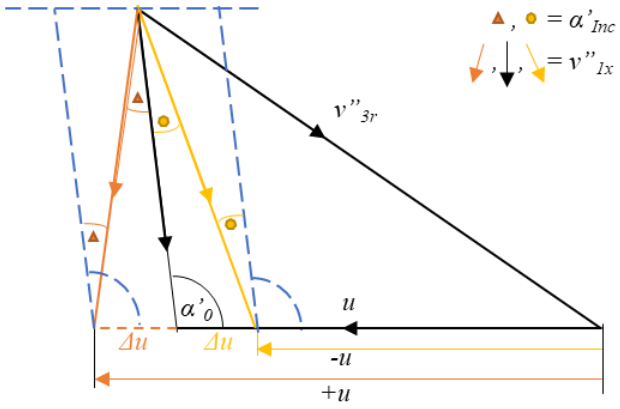

Figure 3-21: Off-design Turbine Stator Inlet Angle Triangles

The check function utilizes Figure 3-21 and the law of sines. For $-u < u$:

$$\frac{\mathrm{Sin}(\alpha'_{Inc})}{\Delta u} = \frac{\mathrm{Sin}(\alpha'_0)}{v''_{1x}} \quad [3.3.47]$$

An equivalent approach is used for the overspeed ($+u > u$) of a turbine and the rotor inlet angle check function.

3.5 Loss coefficient output variables

The implementation of section 3.3 and section 3.4 into the loss coefficient algorithm script in Flownex produces a loss coefficient result output display as illustrated in Figure 3-22.

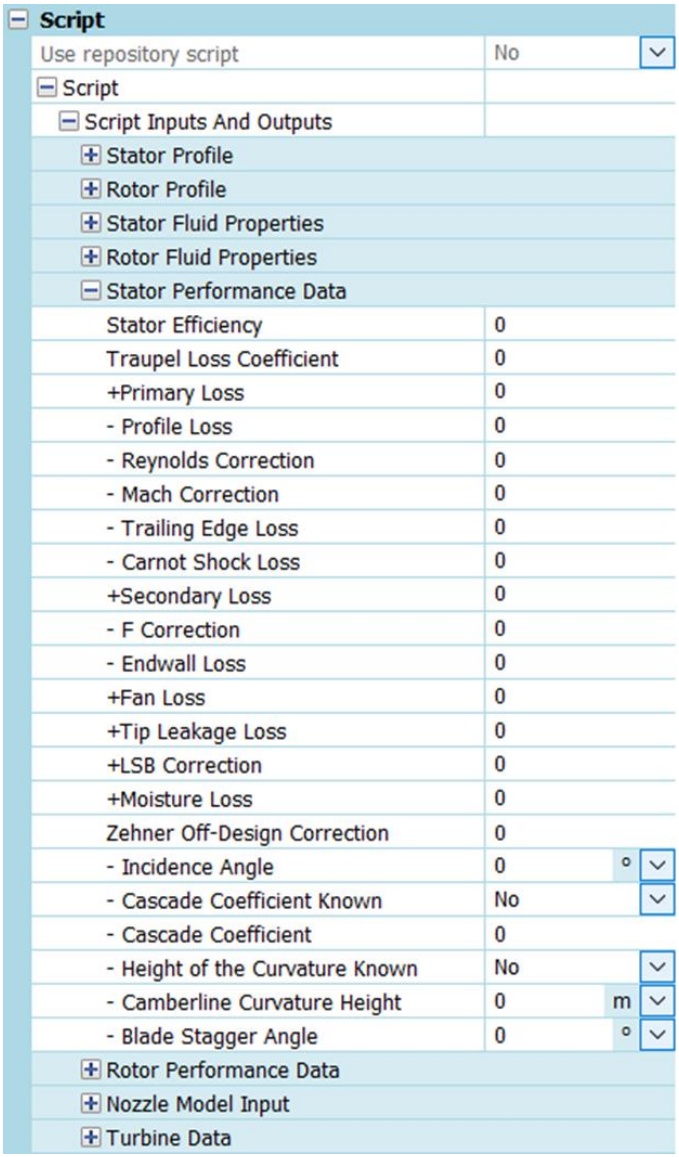

Figure 3-22: Loss Coefficient Algorithm Results Display

All the loss coefficients implemented for both design and off-design can be observed in Figure 3-22, that presents a breakdown of the principle losses into their respective contributing components for a stator. An equivalent display exists for the rotor.

The results obtained from the loss coefficient must be converted to fit back into the original nozzle-model script. Equations [2.2.5] and [3.3.2] state:

$$\eta = \frac{1}{1+\zeta_{NM}} \quad \text{and} \quad \eta = 1-\zeta_{Traupel}$$

Determining the original nozzle-model efficiency and the loss coefficient algorithm efficiency respectively. Whilst the respective stator enthalpy loss coefficients are stated in equations **Error! Reference source not found.** and **Error! Reference source not found.**

$$\zeta'_{NM} = \frac{h_2 - h_{2s}}{h_{01} - h_2} \quad \text{and} \quad \zeta'_{Traupel} = \frac{h_2 - h_{2s}}{h_{01} - h_{2s}}$$

With algebraic manipulation the conversion relationship for both stator and rotor is expressed as:

$$\zeta_{NM} = \frac{\zeta_{Traupel}}{1 - \zeta_{Traupel}} \qquad [3.3.48]$$

Equation [3.3.48] is used as the foundation for all loss coefficient algorithm script output information sent to the original stage-by-stage turbine nozzle-model script. Figure 3-23 illustrates the loss coefficient algorithm script output variables in Flownex.

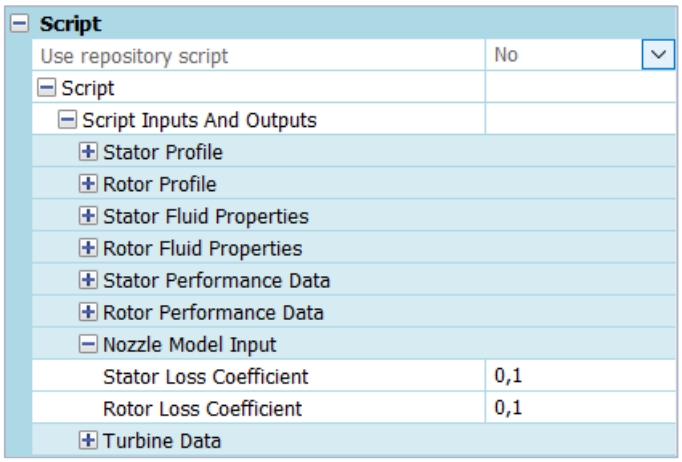

Figure 3-23: Loss Coefficient Algorithm Output Display

This concludes the development methodology used for the creation of the loss coefficient algorithm. The subsequent chapters investigate the attributes of the developed Stage-by-stage Turbine Nozzle-model with Loss Coefficient Algorithm Implemented, illustrated in Figure 3-1.

Chapter 4 Algorithm Validation: AGARD Test Case

This chapter serves as a validation case study for the implementation of the loss coefficient algorithm into the nozzle-model. The stage-by-stage nozzle model was tested against a well calibrated and measured gas turbine test case of the Advisory Group for Aerospace Research and Development (AGARD). The AGARD gas turbine test case presents a rare validation opportunity in the sense that the loss coefficient algorithm could be tested against the stage-by-stage nozzle model [1] and an extensively well-documented turbine validation case [45].

Upon further investigation, it was found that the AGARD report [45] provides a range of different compressor and turbine test cases. The test case utilized for validation (E/TU-4) is an air turbine rig comprised of four stator-rotor stages, illustrated in Figure 4-1. E/TU-4 was predominantly developed for the investigation of industrial turbine characteristics.

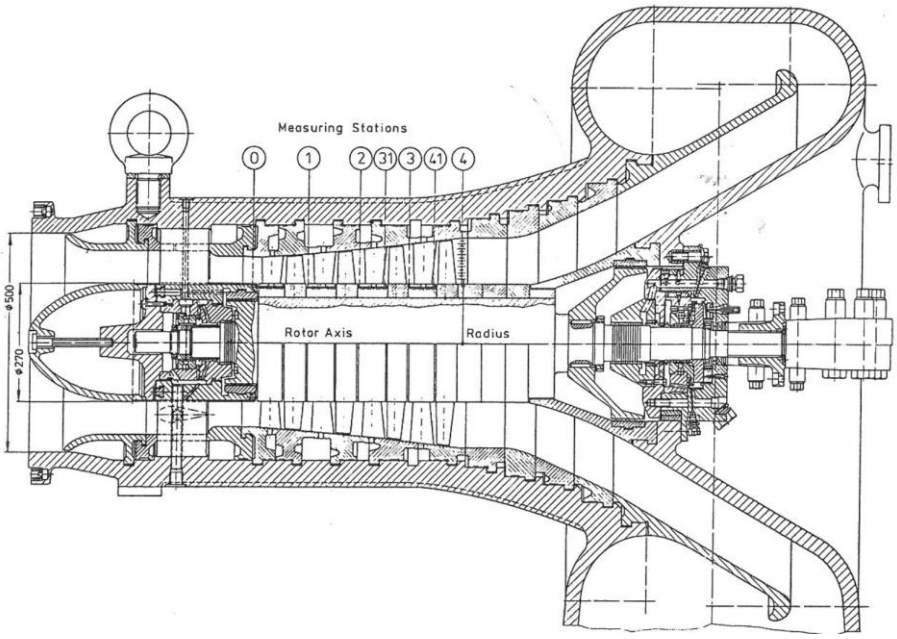

Figure 4-1: AGARD 4-Stage Turbine Cross-section View [45]

The E/TU-4 test case consisted of seven test scenarios. Each scenario investigates the turbine thermodynamic parameters and performance for a specific combination of mass flow rate and turbine rotational speed.

A previous study, conducted by Pottas [40], provides detailed turbine blade geometries for the AGARD E/TU-4 test case. The blade geometries where developed by interpolating various turbine coordinate data points, that describe the blade profiles, obtained from the AGARD report [45].

The AGARD test case E/TU-4 has the following attributes that further justify its use as a validation case:

- The turbine rig has an open loop configuration that measures mass flow upstream from the turbine inlet with a venturi tube.
- The Inlet, exhaust and the inter-stage air pressures, temperatures and flow velocities were measured with a traversing probe.
- Turbine rotational speed and torque are measured in association with a connected dynamometer.
- Each stage has identical blade profile designs.

The development and validation of an equivalent loss coefficient algorithm model aims to show the comparative modelling ability between the original nozzle-model (with calibrated and fixed loss coefficients) and the loss coefficient nozzle-model (with calculated and variable loss coefficients). Additionally, the loss coefficient nozzle model should display additional row specifics information resulting from the inclusion of turbine blade geometry.

The case study evaluation requirements were:

- Validate the loss coefficient stage-by-stage turbine nozzle-model methodology.
- Display additional attributes obtained by the implementation of the loss coefficient algorithms.

Note: The following abbreviations used for the result tables and graphs:

- NM - Stage-by-stage turbine nozzle-model
- LCNM - Loss coefficient stage-by-stage turbine nozzle-model
- Test - AGARD gas turbine test case

Model development

Figure 4-2 depicts the AGARD E/TU-4 loss coefficient nozzle model Flownex configuration.

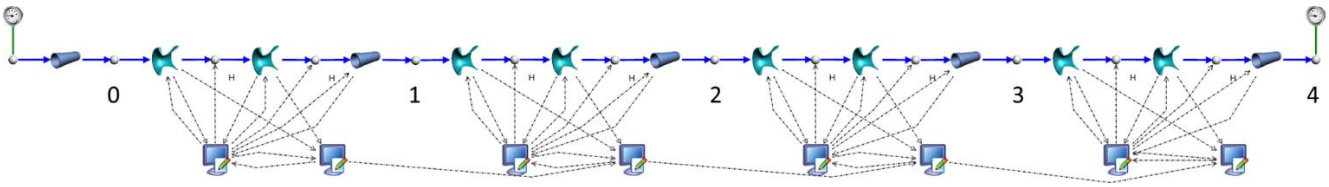

Figure 4-2: AGARD Flownex Model Layout

The turbine geometric information required along with the turbine performance information was obtained from the AGARD test case [45, 40].

The boundary conditions and nozzle areas were set identical to the original nozzle-model [1] and then slightly adjusted to achieve the desired mass flow at the design condition. No calibration was made to the loss coefficients. Carry-over losses were defined the same as for the nozzle model.

AGARD Gas Turbine Boundary Conditions	
Inlet Total Pressure: 257,6 kPa	Working fluid: Air
Inlet Temperature: 131,5 ˚C	Mass flow calibration: 6.45 kg/s
Exhaust Total Pressure: 105 kPa	RPM: 7500

Results and Discussion

The first result reviewed is the comparison of total and static pressure across the turbine stages of Test and LCNM. From Table 4-1 an average total and static pressure error of 0.29% and 0.95% is observed respectively. When comparing LCNM and NM similar results are obtained, an overall deviation of 0.38% is observed.

Table 4-1: AGARD Pressure Result Comparison

Point	Total Pressure [kPa]			Test|LCNM Diff. [%]	NM|LCNM Diff. [%]	Static Pressure [kPa]			Test|LCNM Diff. [%]	NM|LCNM Diff. [%]
	Test	NM	LCNM			Test	NM	LCNM		
0	257,6	257,6	257,5	0,04	0,04	252,9	252,9	253,0	0,05	0,05
1	211,9	212	211,9	0,02	0,06	206,6	209,4	209,5	1,41	0,06
2	170	170,3	169,0	0,61	0,79	165,6	168,0	166,7	0,66	0,77
3	134,6	134,8	133,6	0,77	0,92	130,9	132,8	131,6	0,56	0,87
4	105	105	105,0	0,00	0,00	101,3	103,0	103,4	2,08	0,39

A total and static pressure comparative graph is illustrated in Figure 4-3.

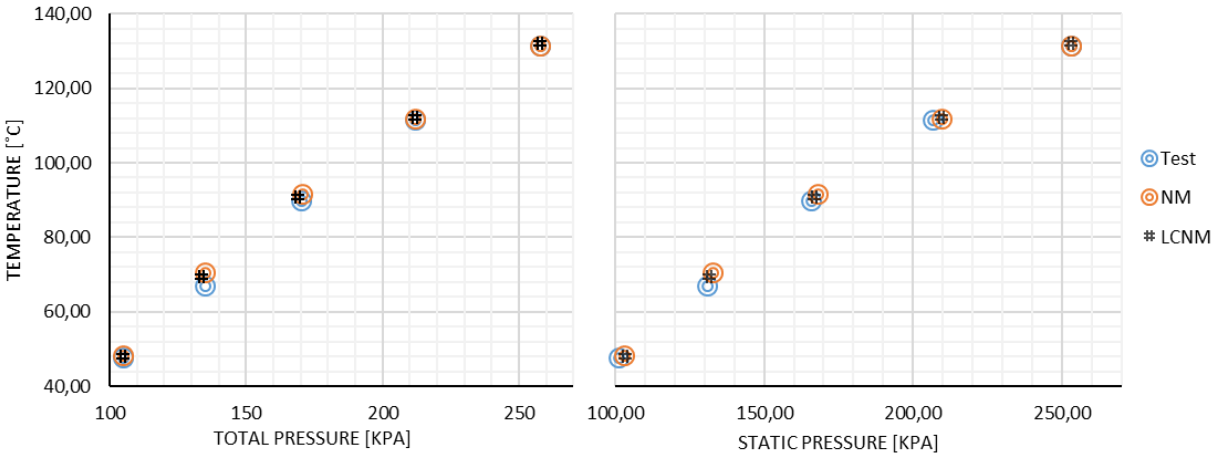

Figure 4-3: AGARD Total & Static Pressure Comparison

Table 4-2 presents a temperature and velocity comparison. The temperature obtained an error range of between 0.28% to a maximum of 3.14%. The comparative studies found that the there is a high level of accuracy obtained by the LCNM. With the only exception is the comparison of velocities, where a sizable average difference of 22% was obtained between Test and LCNM. Whilst an average error of 0.8% is obtained between LCNM and NM.

Table 4-2: AGARD Temperature Result Comparison

Point	Temperature [˚C]			Test|LCNM Diff. [%]	NM|LCNM Diff. [%]	Velocity [m/s]			Test|LCNM Diff. [%]	Test|LCNM Diff. [%]
	Test	NM	LCNM			Test	NM	LCNM		
0	131,5	131,5	132,0	0,38	0,38	65,6	65,5	65,2	0,61	0,46
1	111,7	111,8	112,0	0,28	0,19	75	52,5	51,8	30,93	1,33
2	90,0	91,6	90,7	0,82	0,94	74,8	54,7	54,1	27,67	1,10
3	67,2	70,6	69,3	3,14	1,83	74,2	54,6	55,2	25,61	1,10
4	47,8	48,4	48,0	0,34	0,91	82,7	58,2	58,1	29,75	0,17

The velocity differences can in part be accredited to the slightly larger deviation obtained in the static pressure values compared to the total pressure values. The correlation between static pressure and velocity is significant enough that if the model was to be more finely tuned to better predict static pressure it could be presumed that a better velocity correlation could be obtained. Further investigation of different AGARD E/TU-4 models indicates similar velocity deviation percentages.

Since losses mainly affect the temperatures, one can conclude that the nozzle loss coefficients as calculated by the LCNM are trustworthy. The loss coefficient algorithm additionally produced turbine performance data related to turbine losses, presented in Table 4-3.

Table 4-3: AGARD Turbine Loss Performance Data

Performance Data	Stage 1		Stage 2		Stage 3		Stage 4	
	Stator	Rotor	Stator	Rotor	Stator	Rotor	Stator	Rotor
Efficiency [%]	91,34	91,66	93,05	90,29	92,95	90,58	92,73	89,33
Row Loss Coefficient	0,087	0,083	0,069	0,097	0,071	0,094	0,073	0,107
+Primary Loss	0,034	0,043	0,029	0,057	0,029	0,052	0,028	0,048
- Profile Loss	0,028	0,042	0,027	0,057	0,026	0,052	0,026	0,049
- Reynolds Correction	1,089	0,962	0,925	0,953	0,919	0,944	0,914	0,935
- Mach Correction	1,000	1,000	1,000	1,000	1,000	1,000	1,000	1,000
- Trailing Edge Loss	0,004	0,002	0,004	0,002	0,004	0,002	0,005	0,002
- Carnot Shock Loss	0,0001	0,0002	0,0002	0,0002	0,0002	0,0002	0,0002	0,0002
+Secondary Loss	0,035	0,013	0,022	0,012	0,021	0,012	0,020	0,012
- F Correction	0,049	0,027	0,039	0,030	0,042	0,029	0,042	0,029
- Endwall Loss	0,0004	0,0001	0,0003	0,0001	0,0002	0,0001	0,0002	0,0002
+Fan Loss	0,010	0,012	0,014	0,016	0,018	0,020	0,022	0,024
+Tip Leakage Loss	0,007	0,015	0,004	0,013	0,003	0,011	0,002	0,024

From the turbine loss performance data, it is determined that the overall turbine efficiency is 91.49% that compares favourably with the AGARD Test case data result of 91.3%. The AGARD loss coefficient nozzle-model obtains an efficiency prediction accuracy of 99.3%.

Additionally, a visual turbine overall loss distribution graph is illustrated in Figure 4-4.

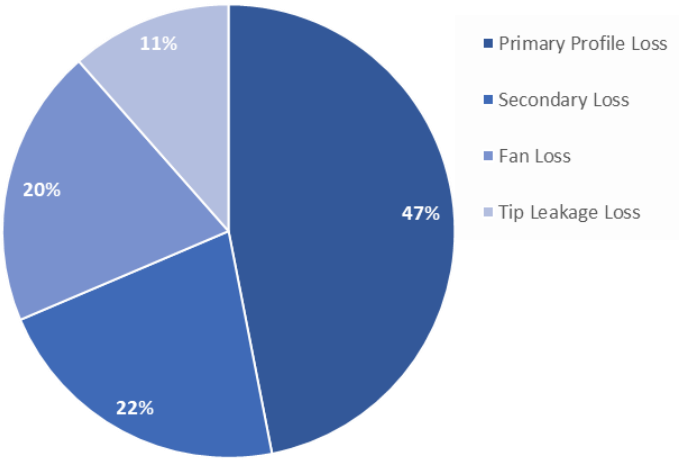

Figure 4-4: AGARD Turbine Loss Distribution

It can be inferred that the largest contributing factors to the turbine performance loss are associated with the losses occurring from boundary layer development and the subsequent kinetic energy losses. This is indicated by the loss distribution illustrated in the turbine losses data, Table 4-3.

Chapter 5 Design and Off-Design Evaluation

This chapter evaluates the ability of the loss coefficient nozzle model, to model an actual steam turbine. The case study compares the performance of the steam turbine model against the actual turbine performance data for both design and off-design conditions.

5.1 Steam turbine model

The LP steam turbine used in this case study was selected based on the availability of design information. The turbine performance data consists of an Acceptance Test, an updated HBD and fragmented design data. The model is developed and calibrated for full load design conditions followed by a partial load condition evaluation. The calibrated full load model is then used in the succeeding section for the evaluation of off-design conditions. The LP steam turbine cross section is illustrated in Figure 5-1.

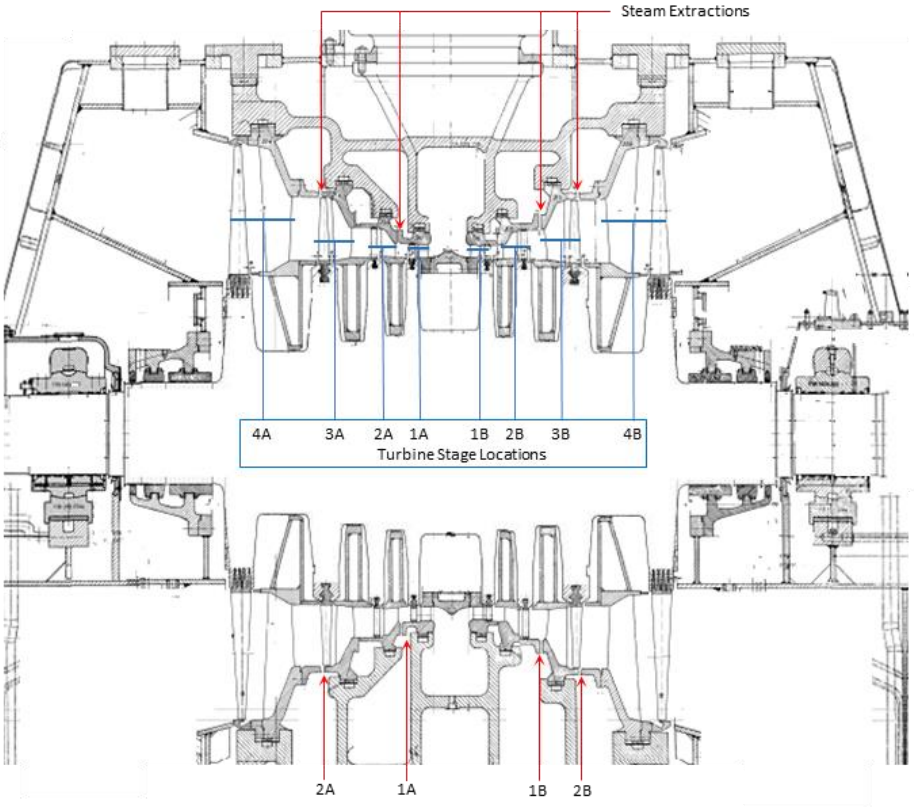

Figure 5-1: LP Turbine Cross-Section - Adapted from [6]

The case study evaluation requirements are:

- Develop and calibrate a full load LP steam turbine model using the loss coefficient stage-by-stage turbine nozzle model to predict the performance.
- Predict partial load performance with the calibrated model.
- Display additional attributes obtained from the loss coefficient algorithms.

Model Development

Figure 5-2 depicts the LP steam turbine loss coefficient nozzle model Flownex configuration. Four distinctive steam extraction points are indicated, correlating to the LP steam turbine design configuration. Note that the double-flow arrangement is modelled as two parallel turbines, each with their individual extractions. This is because the extractions are not symmetrical between the two flows.

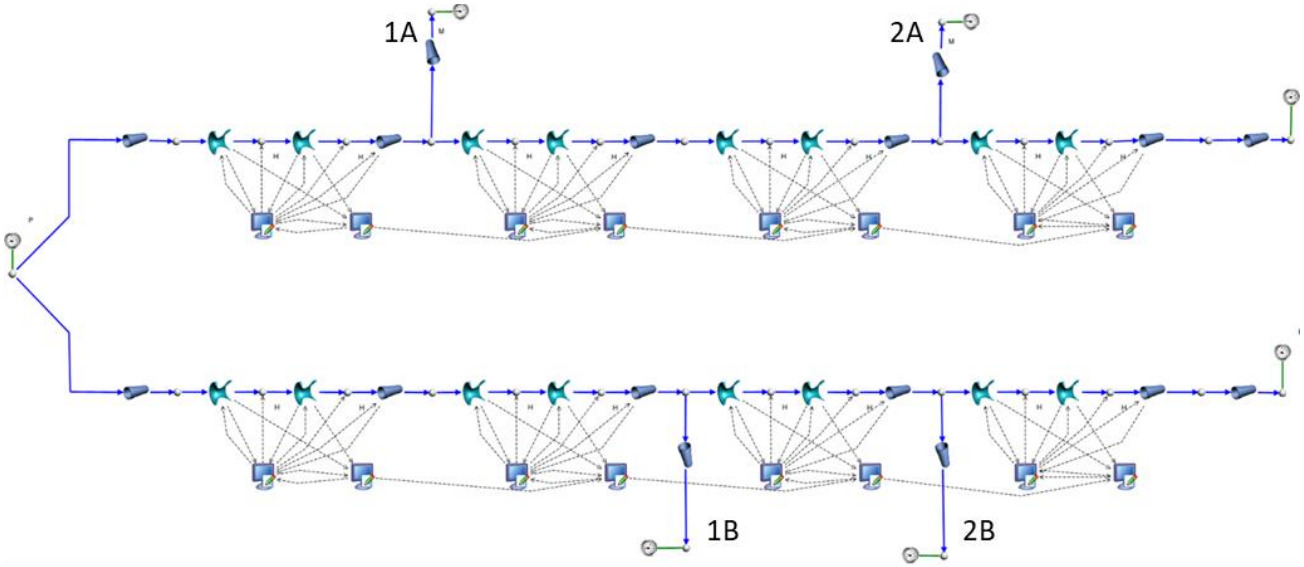

Figure 5-2: LPST Flownex Model Layout

For the determination of the turbine loss coefficients each stage's blade geometry variables are required as per Figure 3-4. The blade geometries were extrapolated using methods discussed in section 2.1.2 from obtained information.

The general turbine rotor, casing and blade diameters, widths and spacings were measured from a turbine cross-section illustration. Further motivation for the use of this specific turbine case was the availability of blade specific information such as the number of blades and the blade surface finish.

The LP turbine the pitch, blade throat, blade chord length and other stator blade profiles parameters were estimated from literature [8]. This enabled the determination of the blade design inlet and outlet angles as well as the remainder of the required blade variables.

The assumption was made to determine the blade angles across the mean blade diameter line. Additionally, the specification and spacing of the blade shrouding were available in the design data along with the LSB interconnection design information.

The model boundary conditions are obtained from the design information and heat balance diagram [6]. The steam temperatures and pressures at the four extraction points are used as validation parameters, whilst the mass flow is used as a boundary condition calibration value.

The design information of the LP turbine indicated identical inlet conditions for both flow directions. Once the model was developed it was calibrated according to the method discussed in section 3.5

LPST Full Load Boundary Conditions	
Inlet Total Pressure: 400 kPa	Working fluid: Steam
Inlet Temperature: 147.9 ˚C	Mass flow calibration: 88.72 kg/s
Exhaust Total Pressure: 5,35 kPa	RPM: 3000
Extraction 1A: 3.867 kg/s	Extraction 2A: 0.967 kg/s
Extraction 1B: 4.136 kg/s	Extraction 2B: 0.967 kg/s

Note: The following abbreviations used for the result tables and graphs:

- LCNM - LPST Loss coefficient stage-by-stage turbine nozzle-model
- LPST – Low-pressure steam turbine acceptance test dated 1970
- HBD – Based on an updated turbine performance review dated 1990
- LCNMPL – Partial load LPST Loss coefficient stage-by-stage turbine nozzle-model

Results and Discussion

The first set of results, presented in Table 5-1, compare the total pressure and temperature for the various boundary points at full load conditions.

Table 5-1: LPST Full Load Result Comparison

Point	Total Pressure [kPa]			LPST-LCNM Diff. [%]	HBD-LCNM Diff. [%]	Temperature [˚C]			LPST-LCNM Diff. [%]	HBD-LCNM Diff. [%]
	LPST	HBD	LCNM			LPST	HBD	LCNM		
Inlet	400	400	400,0	0,00	0,00	150	147,9	147,9	1,40	0,00
Extraction 1a	144	149	148,4	3,07	0,39	110	111,0	110,5	0,46	0,40
Extraction 1b	48,5	48,8	48,6	0,21	0,41	80	80,4	81,2	1,50	1,00
Extraction 2a	15,3	15,7	16,1	5,36	2,68	54	54,7	54,9	1,67	0,46
Extraction 2b	15,3	15,7	16,2	5,95	3,25	54	54,7	54,9	1,67	0,46
Exhaust	5,35	5	5,0	6,54	0,00	33,75	32,0	32,9	2,59	2,73

From Table 5-1 average errors of 1.12%, for total pressure, and 1.55 %, for temperature, are observed between the HDB and the LCNM. The loss coefficient nozzle-model achieves a high level of accuracy against both acceptance test and HBD conditions. The model indicates that the turbine should produce 35.25 MW, which compares reasonably to the initial rating of 36 MW.

Figure 5-3 provides a visual comparison of the total pressure and temperature. Notably, the model produces results comfortably within the range of the of assessment values.

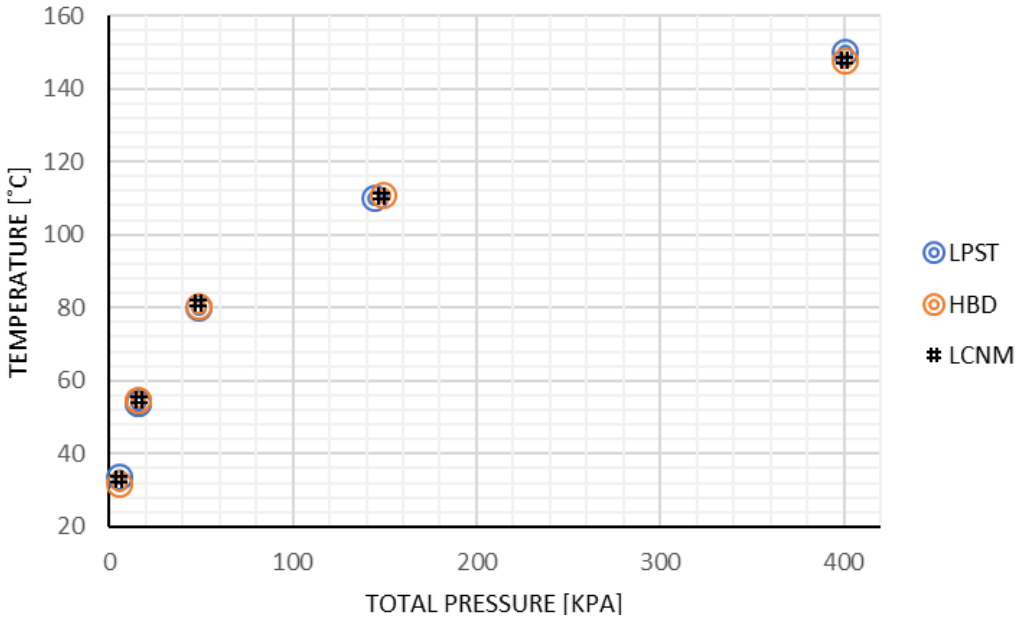

Figure 5-3: Full Load LPST Total Pressure Comparison

In addition to the general thermodynamic parameters, the loss coefficient algorithm produced turbine performance data related to turbine losses. Presented in Table 5-2 is a subset of data comparing the loss profiles for one side of the LP steam turbine, the complete set is provided in Appendix A. Figure 5-4 presents an overall turbine loss distribution.

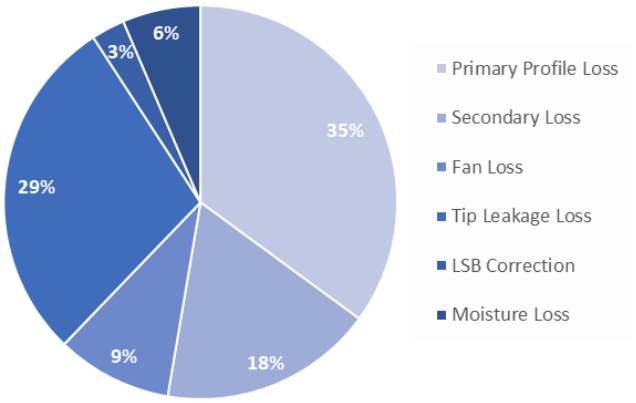

Figure 5-4: Overall Full Load LPST Loss Distribution

Table 5-2: Full Load LPST Section B Loss Performance Data

	Stage 1B		Stage 2B		Stage 3B		Stage 4B	
Performance Data	Stator	Rotor	Stator	Rotor	Stator	Rotor	Stator	Rotor
Efficiency [%]	89,41	83,55	91,15	88,30	94,52	89,44	87,23	81,30
Row Loss Coefficient	0,106	0,165	0,089	0,117	0,055	0,106	0,128	0,187
Primary Loss	0,026	0,048	0,027	0,062	0,022	0,048	0,032	0,044
Secondary Loss	0,056	0,018	0,039	0,010	0,015	0,004	0,011	0,003
Fan Loss	0,000	0,000	0,000	0,001	0,007	0,008	0,026	0,027
Tip Leakage Loss	0,024	0,039	0,023	0,045	0,011	0,026	0,017	0,020
LSB Correction	0,000	0,000	0,000	0,000	0,000	0,000	0,000	0,024
Moisture Loss	0,000	0,000	0,000	0,000	0,000	0,000	0,032	0,069

From Table 5-2 it can be observed that stage 4 rotor has a last stage blade interconnection and the entire stage experiences moisture loss. The moisture loss corresponds to the wet steam indications provided in the HBD. Figure 5-5 presents a comparative turbine loss distribution visualization between stages 3B and 4B.

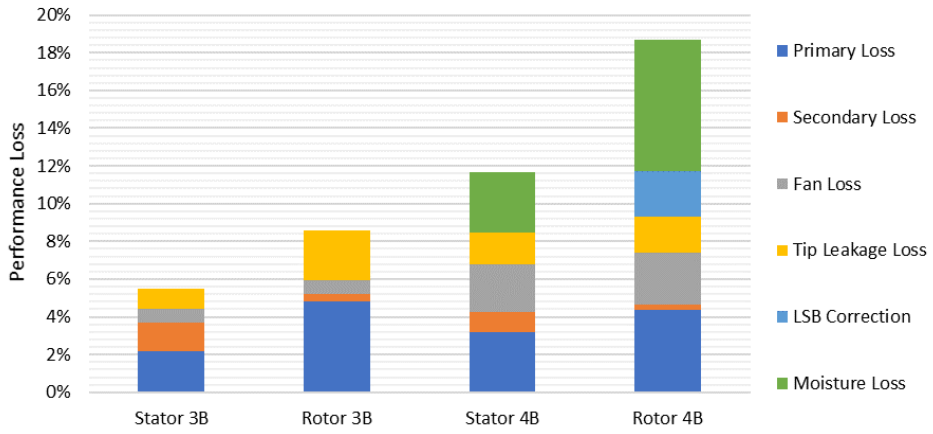

Figure 5-5: LPST Stage 3B & 4B Loss Comparison

The turbine loss performance data determines the overall turbine efficiency is to be 88,85%, that compares well with the rated efficiency value of 89%. The inlet and exhaust stages obtained stage efficiencies of 86,5% and 84,3% respectively. This is lower than the middle stages by comparison and is accredited to the additional loading forces experienced on the inlet and outlet stages. The LPST loss coefficient nozzle-model achieves an overall turbine performance prediction accuracy of 98.8%, at full load conditions.

Partial & Full Load Comparison

Lastly, this case study evaluates the loss coefficient algorithms ability to model partial load operational conditions. A 60% partial load operational condition was selected from the available design information and heat balance diagrams [6]. For the configuration of the partial load evaluation, only the boundary conditions were changed, all other parameters stay identical to the full load evaluation. The steam quality at the four extraction points is used as the primary validation parameter between the model and the heat balance diagram.

LPST 60% Partial Load Boundary Conditions	
Inlet Total Pressure: 240 kPa	Working fluid: Steam
Inlet Temperature: 130˚C	Mass flow: 50.75 kg/s
Exhaust Total Pressure: 4.7 kPa	RPM: 3000
Extraction 1A: 2.11 kg/s	Extraction 2A: 0.8 kg/s
Extraction 1B: 2.36 kg/s	Extraction 2B: 0.8 kg/s

Results and Discussion

The results presented in Table 5-3 compare the total pressure and steam quality for the various boundary points at 60% partial load conditions. The pressure boundary condition results indicate an average error of 2.86%, with the largest deviations occurring at extraction points 2A and 2B. Temperature was excluded from the comparison as the HDB only provides a possible steam quality for the extraction points. The steam quality comparison indicates an approximate error of 1.24%.

Table 5-3: 60% Partial Load LPST Result Comparison

Point	Total Pressure [kPa]		HBD-LCNMPL Diff. [%]	Steam Quality		HBD-LCNMPL Diff. [%]
	HBD	LCNMPL		HBD	LCNMPL	
Inlet	240	240,0	0,00	130˚C	130˚C	0,00
Extraction 1a	88	88,2	0,19	0,96	0,980	1,72
Extraction 1b	29,8	29,5	0,95	0,93	0,938	1,04
Extraction 2a	10,1	10,9	7,59	0,91	0,923	1,41
Extraction 2b	10,1	11,0	8,43	0,91	0,924	1,52
Exhaust	4,7	4,7	0,00	0,89	0,901	1,78

The 60% partial load model indicates a power production of 20,3 MW at an overall turbine efficiency of 87,96%. This equates to 57,7% of the full load 35,25MW LCNM power production. The partial load operational condition reduces the overall LCNM turbine efficiency by 1.1%.

The partial load LCNM results compare favourably with the HBD partial load values. The actual LPST power production rating at 60% partial load is unknown but is estimated to be 21.3MW equating to an estimated 5.9% error made by the 60% partial load LCNM.

Table 5-4 presents the 60% partial load LPST loss performance data comparable to the full load equivalent presented in Table 5-2. It can be observed that both stage 3B and 4B experiences moisture loss. The additional moisture loss corresponds to the increased wet steam condition indicated by the HBD.

Table 5-4: 60% Partial Load LPST Section B Loss Performance Data

	Stage 1B		Stage 2B		Stage 3B		Stage 4B	
Performance Data	Stator	Rotor	Stator	Rotor	Stator	Rotor	Stator	Rotor
Efficiency [%]	89,40	83,63	89,65	88,37	92,22	89,44	87,48	78,88
Row Loss Coefficient	0,106	0,164	0,104	0,116	0,078	0,106	0,125	0,211
Primary Loss	0,026	0,048	0,027	0,062	0,022	0,048	0,038	0,066
Secondary Loss	0,056	0,017	0,039	0,010	0,015	0,004	0,013	0,004
Fan Loss	0,000	0,000	0,000	0,001	0,007	0,008	0,026	0,027
Tip Leakage Loss	0,024	0,039	0,023	0,044	0,011	0,046	0,017	0,020
LSB Correction	0,000	0,000	0,000	0,000	0,000	0,000	0,000	0,024
Moisture Loss	0,000	0,000	0,000	0,000	0,001	0,004	0,043	0,069

Figure 5-6 provides a visual comparison between the 60% partial load (PL) and full load (FL) LPST performance loss distributions presented in Table 5-4 and Table 5-2 respectively.

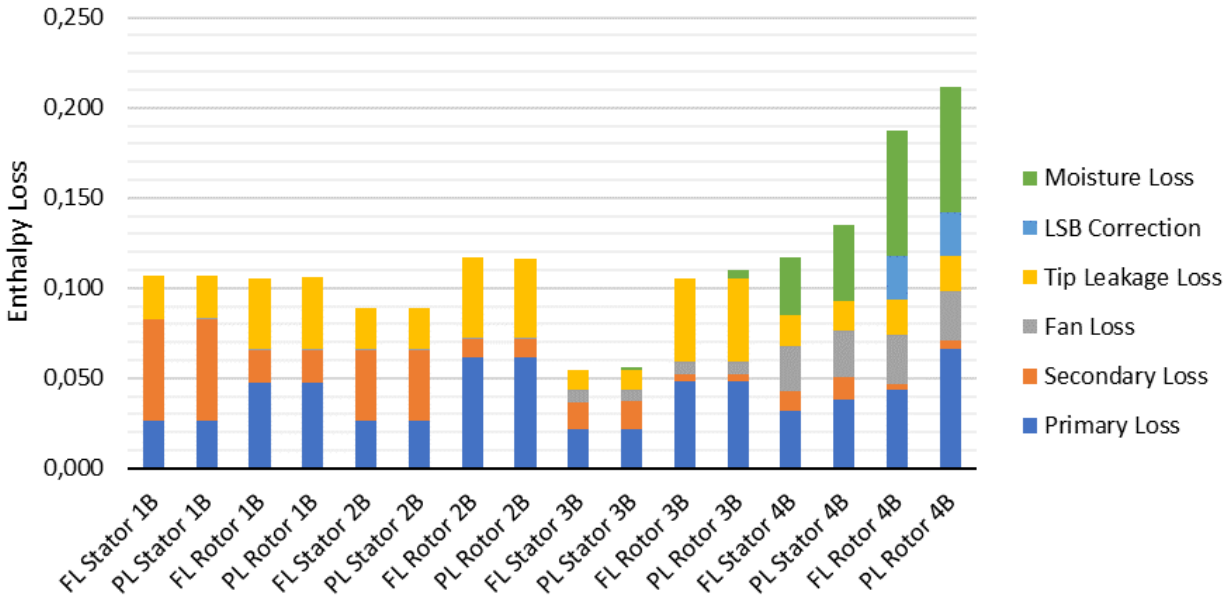

Figure 5-6: Full & Partial Load Section B Loss Distribution Comparison

The largest increase in turbine loss can be observed in the 60% partial load rotor 4B. Whilst an incremental formation of moisture loss can be observed on stator 3B and rotor 3B. The 60% partial load LPST LCNM evaluation presents the loss coefficient algorithms reasonable ability to predict partial load performance with minimal model configuration requirements.

This LPST design case model will be used in the following section as the calibrated model and used for the comparison between design and off-design conditions.

5.2 Off-Design impact assessment

Power utility turbines are often designed to run at only one optimal spin or rotational speed that corresponds to a power grids unique operating frequency. For a 50Hz power grid, the optimal design values are either 3000-rpm or 1500-rpm, depending on whether the generator is a 2-pole or 4-pole machine. When a turbine deviates from design speed it is usually cause for concern.

Most power utilities will allow, for a short correctable time period, a slight deviation in output power frequency. Predetermined trip values, for turbine-generator sets, activate when the unit operates outside of optimal or safe conditions. For a 50Hz network, a deviation of ±5Hz is tolerable for a very limited time period due to the extreme risk associated with the respective operational conditions. For this reason, the off-design conditions corresponding to 45Hz and 55Hz will be investigated here.

The 5% frequency deviation correlates to the turbine critical speeds. Turbine critical speeds are defined as the specific turbine spin speeds that induce turbine shaft resonance. Resonance typically occurs when the frequency, magnitude and orientation of an oscillating excitation force, acting on a rotor, corresponds with a natural frequency. The critical speeds are set at a 10% separation margin from the design speed [46]. For a 3000-rpm turbine, the critical speeds are associated with 2700-rpm and 3300-rpm.

The off-design assessment uses the LP steam turbine model developed for design conditions in the prior section. The Flownex model and actual turbine configurations can be observed in Figure 5-1 and Figure 5-2. The case study evaluation requirements are:

- Predict the performance deviation of a LP steam turbine caused by a change in turbine operational speed. Test for multiple operational conditions comparing to measured Off-Design Condition data
- Display additional attributes obtained by the implementation of the loss coefficient algorithms: Focused on “Incidence Angle”.

Note: The following abbreviations used for the result tables and graphs:

- LCNM – Design condition Loss coefficient stage-by-stage turbine nozzle-model
- 2700, 3300 – Off-design condition Loss coefficient stage-by-stage turbine nozzle-model

Model development

The model boundary conditions are set to heat balance diagram [6] values. No other changes were done to the calibrated design LP steam turbine model. The turbine speed was adjusted to the off-design evaluation parameters. The LP steam turbine model spin speed, for all LCNM components, can be controlled via a Flownex data link that fixes the spin speed to the desired value.

LPST Off-Design Boundary Conditions	
Inlet Total Pressure: 400 kPa	Working fluid: Steam
Inlet Temperature: 147.9 ˚C	Mass flow calibration: 88.725 kg/s
Exhaust Total Pressure: 5 kPa	RPM: 3000
+10% rpm: 3300 [55Hz]	-10% rpm: 2700 [45Hz]

Additionally, the Cascade coefficient input values are required for the determination of the off-design performance losses. The Cascade coefficient plays a significant role in the Zehner correction factor, see section 3.4 . For this the turbine blade profiles can be compared to the Cascade coefficient reference guide, presented in Figure 3-20, or calculated by equation [3.3.41].

Figure 5-7: Cascade Coefficient Determination Example

Results and Discussion

Table 5-5 presents the off-design findings related to total pressure and temperature. From these results an average temperature deviation of 2,49% and 2,97% were observed for the 2700rpm and 3300rpm speeds respectively.

Table 5-5: Off-design Total Pressure & Temperature Comparison

	Total Pressure [kPa]			Temperature [˚C]		
Point	LCNM	2700	3300	LCNM	2700	3300
Inlet	400	399,9	399,9	147,9	148	148,9
Extraction 1a	148,4	143,9	144,1	110,5	109,8	110,1
Extraction 1b	48,60	48,39	48,38	81,2	80,5	80,4
Extraction 2a	16,12	17,06	18,3	54,9	58,5	58,16
Extraction 2b	16,21	18,02	18,7	54,9	57,87	58,8
Exhaust	5	5,2	5,16	32,88	33,58	34,10

The largest pressure deviation occurs at the low-pressure extraction points for different operational speeds, which correspondence to higher temperature conditions.

An interesting comparison between the amount of work produced per stage at various operational speeds are presented in Figure 5-8.

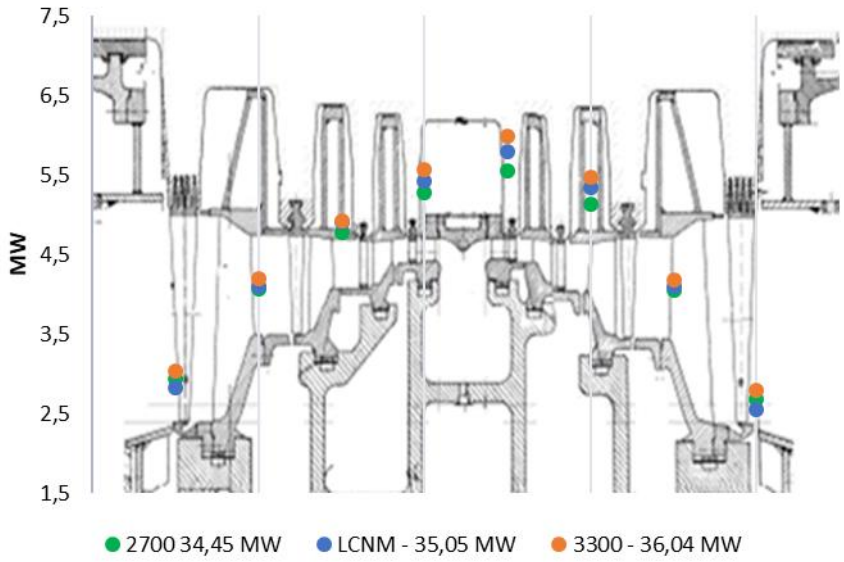

Figure 5-8: Full & Partial Load Work Per Stage Comparison

Both the 3300rpm and 2700rpm operational speeds are less efficient than the turbine design condition efficiency, at 88.3% and 87.8% respectively. Stage 1A produces slightly less power than stage 1B (±0.3MW) this is accredited to the location of the steam extraction point 1A as illustrated in Figure 5-1.

Table 5-6: Off-design LSB Comparison

	LSB LCMN		LSB 2700		LSB 3300	
Performance Data	Stator	Rotor	Stator	Rotor	Stator	Rotor
Efficiency [%]	87,23	81,50	84,65	81,33	84,46	81,4
Primary Loss	0,032	0,044	0,032	0,044	0,032	0,044
Secondary Loss	0,011	0,003	0,011	0,002	0,011	0,002
Fan Loss	0,026	0,027	0,026	0,027	0,026	0,027
Tip Leakage Loss	0,017	0,020	0,030	0,020	0,030	0,020
LSB Correction	0,000	0,024	0,000	0,024	0,000	0,024
Moisture Loss	0,043	0,069	0,042	0,069	0,042	0,069
Zehner Off-Design Correction	0,000	0,000	0,154	0,187	0,155	0,186
Incidence Angle [˚]	0,000	0,000	-30,47	-25,17	30,57	27,20

Table 5-6 evaluates a sample section of the turbine loss performance information tabled in Appendix A. The evaluation compares the last stage blade performances for the three operational speeds. Emphasized are the incidence angles created by the variation from design speed, generating additional off-design losses. It is determined that the overall turbine loss for the last stage blade is increased by 4.67% and 5.26% for 2700rpm [45Hz] and 3300rpm [55Hz] respectively.

Figure 5-9 illustrates the design and off-design turbine rotor inlet angles.

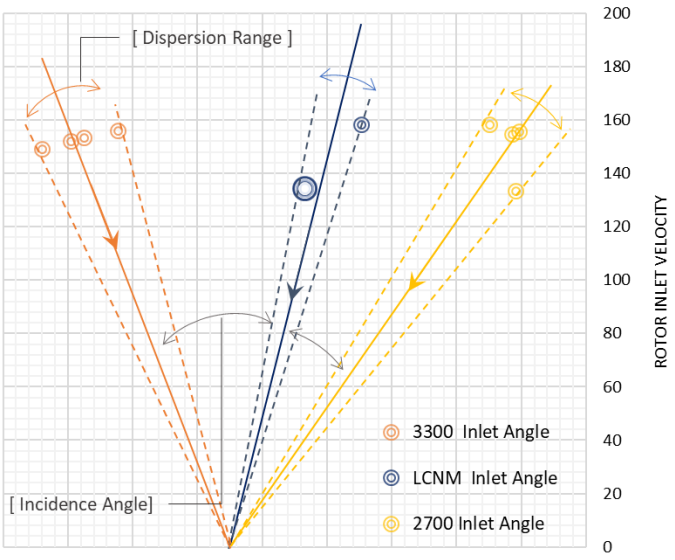

Figure 5-9: LPST Rotors Inlet Angles

The 2700-rpm and the 3300-rpm inlet angles deviate from the design angle by the incidence angle. Figure 3-19 provides an interpretation guide for incidence angle orientation. A dispersion range indicates the design and off-design inlet angle range for the different turbine rotors stages.

Chapter 6 Turbine Blade Design Impact

This chapter investigates the information that can be obtained from a single turbine stage model. The emphasis is placed on the correlation between turbine losses as they relate to specific turbine blade geometry data clusters. Four different case studies are evaluated:

- Blade profile design improvement
- Blade profile degradation
- Blade shrouding variations
- Last stage blades interconnection effects

Each case study examines the impact that deviating from an original blade design has on stage performance. All models developed in this chapter are based on a single stage configuration illustrated in Figure 6-1.

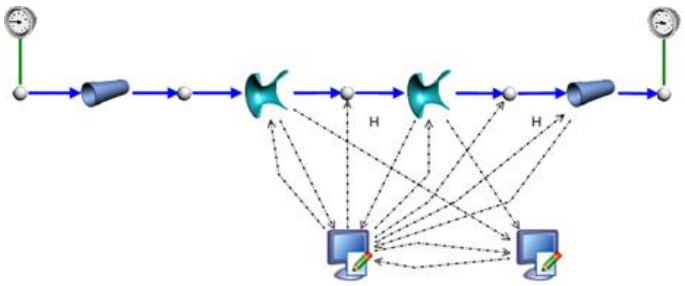

Figure 6-1: Single Stage LCNM

All parameters are kept identical except for the ones required for specific evaluations, thus ensuring the accuracy of compatibility. Each case has unique boundary conditions and evaluation parameters.

6.1 Blade profile design upgrade

This case study aims to show the ability of the loss coefficient nozzle-model to quantify the improvement impact on turbine performance in upgrading a blade profile.

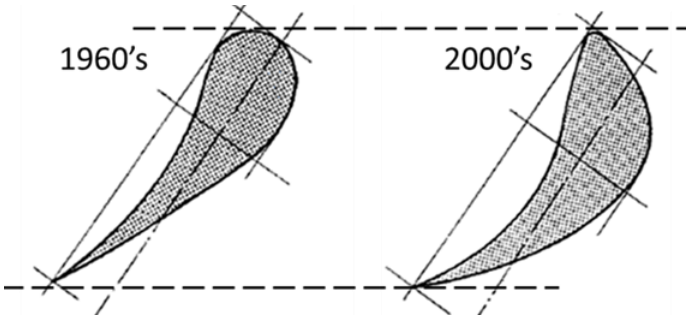

Figure 6-2: Turbine Blade Profile Improvement Example

An actually recorded blade improvement installation is used for the case study [6]. Turbine blading information along with process information was partially available, for both the original and upgraded blades. The remainder of the information was obtained by methods discussed in section 2.1.2 . The case study evaluation requirements are:

- Predict the performance improvement generated by the upgrade of the turbine blade profile.
- Display additional attributes obtained by the implementation of the loss coefficient algorithms: Focused on blade geometry data clusters.

Note: The following abbreviations used for the result tables and graphs:

- 1960 – Original blade design Loss coefficient stage-by-stage turbine nozzle-model
- 2000 – Upgraded blade design Loss coefficient stage-by-stage turbine nozzle-model

All components are identical except for specific blade geometries. The upgraded blade changes consisted of the following properties: Throat, Max blade thickness, Flow area, Trailing Edge Thickness, Blade Chord Length.

Model development

The performance and boundary conditions were obtained, calculated and inferred from design drawings, acceptance tests and HDB's. Only the first stage of the IP steam turbine was evaluated as it consisted of the most complete design. First, the 1960 model nozzle area was calibrated and then used for the 2000 model by means of only adjusting the blade profile properties. The actual turbine blade upgrades improved the overall turbine power output from 365 MW to 400 MW.

Stage Upgrade Boundary Conditions	
Inlet Total Pressure: 3,32 MPa	Working fluid: Steam
Inlet Temperature: 490 ˚C	Mass flow calibration: 148 kg/s
RPM: 3000	IP Steam Turbine

Results & Discussion

Table 6-1 presents a performance comparison between the documented values and the loss coefficient nozzle model. It was determined that an error of between 1 - 2,5% was experienced.

Table 6-1: Blade Upgrade Performance Comparison

Performance Component	1960's	2000's
Actual Overall Turbine MW	365	400
Actual 1st IP ST Stage MW	3,765	4,483
Flownex LCNM 1st Stage MW	3,726	4,373
1st Stage Actual|LCNM MW Diff [%]	1,015	2,455

A stator and rotor row efficiency improvement of 3,34% and 4,07% respectively was observed for the upgraded blade profile, this is illustrated in Table 6-2.

Table 6-2: Blade Upgrade Performance Data

Performance Data	1960 Design		2000 Design		Difference [%]	
	Stator	Rotor	Stator	Rotor	Stator	Rotor
Efficiency [%]	86,61	86,01	89,51	89,51	3,34	4,07
Row Loss Coefficient	0,134	0,140	0,105	0,105	21,59	25,01
Primary Loss	0,030	0,043	0,018	0,030	40,92	30,49
Secondary Loss	0,077	0,048	0,070	0,057	8,58	18,96
Tip Leakage Loss	0,017	0,037	0,007	0,006	60,19	84,11

From the result obtained a clear link is apparent between blade geometries and turbine performance this correlation is presented in Figure 6-3 and Figure 6-4. The exact description and locations of the blade geometries relative to the loss coefficient components are discussed in section 2.2.2 .

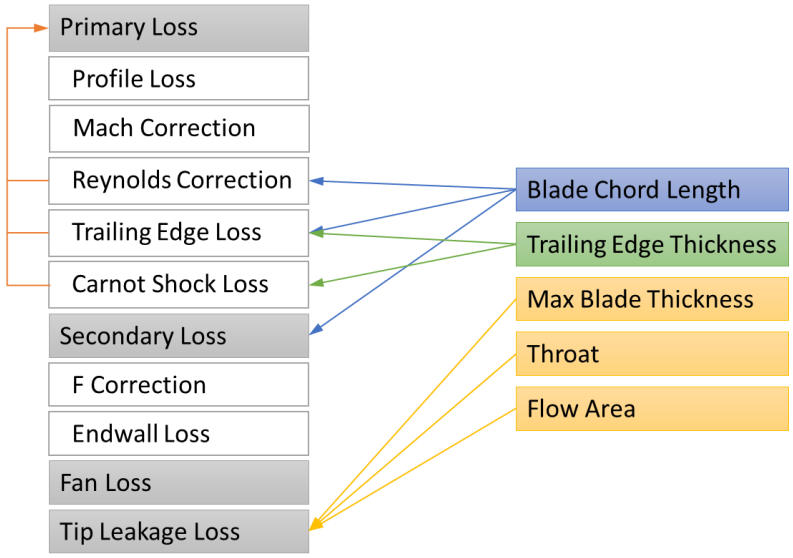

Figure 6-3: Blade Geometry Cluster - Turbine Losses Correlation

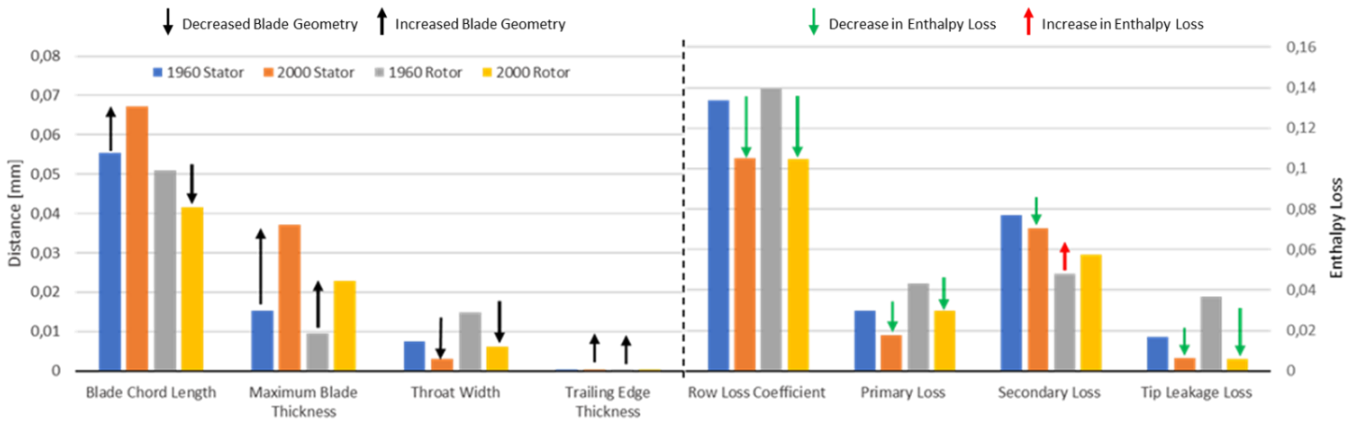

Figure 6-4: Blade Geometry Cluster - Turbine Losses Correlation

Figure 6-4 indicates that the overall stage loss decreases (green arrows) with the upgraded blade design (black arrows). Notably the rotor secondary loss increases (red arrow) with the upgrade. It can be assumed that the overall improvement of the rotor performance justified the additional secondary loss associated with the upgraded blade design.

The results provide clear motivation for the consideration of blade profile improvements. The loss coefficient nozzle-model has shown that it is able to predict possible performance improvements generated by upgraded changes in blade geometries.

6.2 Turbine blade degradation

Various particles can be present in the turbine working fluid creating undesirable operational conditions for turbine components. Solid particle erosion (SPE) is the study of material erosion caused by the surface impact of hard particles. SPE alters the blade profile inlet and discharge areas, on both the stator and rotor, creating undesirable working fluid pressures and velocities.

Figure 6-5: Blade Degradation Illustration - Adapted from [13]

Fouling, on the other hand, describes the accumulation of particles on compromised surface areas. Creating the same performance degradation mechanics associated with SPE. Fouling, Material deformation, SPE, Moisture impact erosion and Corrosive pitting are but a few turbine degradation mechanisms. This case study demonstrates the Loss coefficient stage-by-stage turbine nozzle model's ability to predict performance loss associated with blade profile degradation mechanisms.

The case study evaluation requirements are:

- Predict the performance losses incurred by the fouling and erosion of turbine blades.
- Display additional attributes obtained by the implementation of the loss coefficient algorithms: Focused on "surface finish" and corresponding blade geometries.

Note: The following abbreviations used for the result tables and graphs:

- Polished – Loss coefficient stage-by-stage turbine nozzle-model with design blade conditions
- Fouling – Loss coefficient stage-by-stage turbine nozzle-model with severe deposit formations
- Erosion –Loss coefficient stage-by-stage turbine nozzle-model with severe erosion.

Model development

This case study is a theoretical assessment to test the loss coefficient nozzle model's ability to predict the performance losses incurred by a common plant problem. The maintenance and operation guide produce by Sanders [11] was used in the development of the case studies boundary conditions and blade geometry parameters.

An initial ideal turbine stage was developed against which the two degradations mechanisms, Fouling and Erosion, could be compared. Each degradation mechanism evaluation assumes identical blade area degradation and surface finish deformations on both the stator and rotor. All parameters are identical between the three models with the exception listed in the boundary conditions. The k_s values were conservatively selected from a best practices steam turbine operational guide [47].

Stage Degradation Boundary Conditions	
Inlet Total Pressure: 8000 kPa	Working fluid: Steam
Inlet Temperature: 510 ˚C	Mass flow calibration: 300 kg/s
RPM: 3000	Theoretical Stage Condition
Fouling [k_s]: 0.1μm	Erosion [k_s]: 0.06μm

Results & Discussion

Table 6-3: Blade Fouling Degradation Performance Data

Performance	Polished		Fouling		Polished | Fouling Diff. [%]	
	Stator	Rotor	Stator	Rotor	Stator	Rotor
Work [kW]	10290,4		9594,5		6,76	
Efficiency [%]	86,62	88,30	68,00	73,63	21,5	16,6
Row Loss Coefficient	0,134	0,117	0,320	0,264	139,3	125,4
Primary Loss	0,030	0,043	0,098	0,149	224,9	245,5
Secondary Loss	0,077	0,048	0,195	0,090	153,7	85,7
Fan Loss	0,010	0,012	0,010	0,012	0,000	0,000
Tip Leakage Loss	0,017	0,014	0,017	0,014	3,91	2,38

Table 6-4: Blade Erosion Degradation Performance Data

Performance	Polished		Erosion		Polished | Erosion Diff. [%]	
	Stator	Rotor	Stator	Rotor	Stator	Rotor
Work [kW]	10290,4		10089,0		1,96	
Efficiency [%]	86,62	88,30	71,98	76,90	16,9	12,9
Row Loss Coefficient	0,134	0,117	0,280	0,231	109,5	97,4
Primary Loss	0,030	0,043	0,078	0,124	159,4	187,5
Secondary Loss	0,077	0,048	0,175	0,082	127,7	69,4
Fan Loss	0,010	0,012	0,010	0,012	0,000	0,000
Tip Leakage Loss	0,017	0,014	0,017	0,014	2,82	1,66

Table 6-3 and Table 6-4 compare the turbine stage performance of the Polished stage with the Fouling and Erosion degradation stages respectively. The stage performance experiences a decline of 6,76% caused by Fouling. Whilst a 1,96% decline in performance is caused by blade Erosion. The correlation between stage performance and blade geometry clusters is illustrated in Figure 6-6.

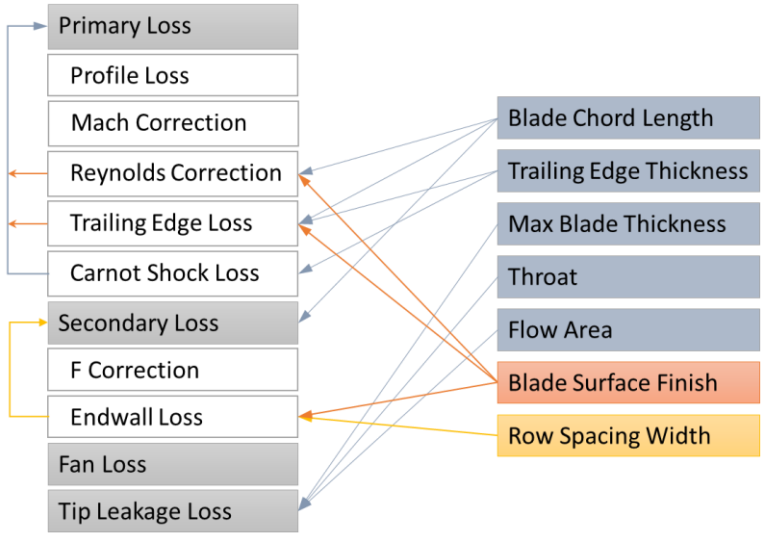

Figure 6-6: Blade Geometry Cluster - Turbine Losses Correlation

Figure 6-7 provides a visual comparison of the turbine loss distribution incurred by blade degradation. It is apparent from the results that minute changes in surface finish and blade profile area may lead to extensive performance losses.

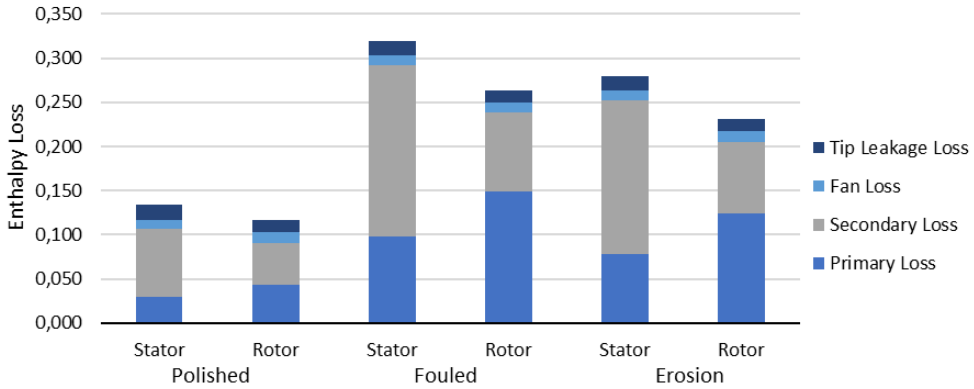

Figure 6-7: Blade Degradation Loss Comparison

Notably from Figure 6-7, it can be observed that the stator experiences a dominant increase in Secondary loss, whilst the rotor experiences a dominant increase in Primary loss (yellow arrows). This is accredited to the specific turbine loss configurations associated with stator and rotor blades as described in section 3.3

Although this case study used extreme theoretical conditions it showed the ability of the loss coefficient algorithm to predict turbine performance loss associated with blade profile degradation mechanisms.

6.3 Turbine blade shrouding variation

This case study evaluates the impact that free-end or unshrouded turbine blades have on stage performance compared to shrouded turbine blades. This case study is a theoretical assessment to evaluate the loss coefficient algorithm's ability to predict the performance difference between shrouded and unshrouded turbine blades.

Figure 6-8: Shrouded and Unshrouded Blade – Adapted from [13]

The case study considers two almost identical blade designs with the only difference being that one is shrouded whilst the other has a free-end. The approach was guided by the work of Singh et. al [8]. Majority of the blade design geometries of the polished blade design, utilized in the prior section, where used from the fundamental design.

The case study evaluation requirements are:

- Predict the performance losses associated with turbine blade shrouding or the lack thereof.
- Display additional attributes obtained by the implementation of the loss coefficient algorithms: Focused on shrouding.

Note: The following abbreviations used for the result tables and graphs:

- Shrouded – Shrouded turbine stage Loss coefficient stage-by-stage turbine nozzle model
- Unshrouded – Unshrouded turbine stage Loss coefficient stage-by-stage turbine nozzle model

Model Development

As a result of the algorithm development for tip leakage loss, discussed in section 3.3 the user input for shrouded configuration is reduced to a simple "yes/no" selection option in the Flownex turbine blade geometry input variables script.

The remainder of the input variables are extracted from the nozzle-model by means of a data-link. The shrouded and unshrouded stage models were configured to imitate identical IP steam turbine stage conditions

The boundary conditions were obtained for an actual first stage IP turbine. The shrouded model was calibrated against the actual first stage values and then evaluated. The mass flow was used as a calibration value, due to the strong relationship between tip leakage loss and mass flow. The unshrouded model only required the deactivation of the "Shrouded" option.

Shrouded/Unshrouded Boundary Conditions	
Inlet Total Pressure: 4000 kPa	Working fluid: Steam
Inlet Temperature: 400 ˚C	Mass flow calibration: 150 kg/s
RPM: 3000	Theoretical Stage Condition

Results & Discussion

Table 6-5 presents the performance comparison between the shrouded and the unshrouded turbine stage models under the theoretical conditions. The results confirm that the shrouded blades enable a turbine stage to produce approximately 1.17% more work than the unshrouded blades under identical conditions. Accordingly, shrouded blades produce an overall better stage efficiency.

Table 6-5: Shrouded and Unshrouded Blade Performance Data

Performance	Shrouded		Unshrouded		Shrouded | Unshrouded Diff. [%]	
	Stator	Rotor	Stator	Rotor	Stator	Rotor
Work [kW]	3840,857		3796,144		1,164	
Efficiency [%]	86,626	88,287	83,787	79,644	3,277	9,789
Row Loss Coefficient	0,134	0,117	0,162	0,204	21,224	73,782
Primary Loss	0,030	0,043	0,030	0,043	0,000	0,000
Secondary Loss	0,077	0,048	0,077	0,048	0,000	0,000
Fan Loss	0,010	0,012	0,010	0,012	0,000	0,000
Tip Leakage Loss	0,017	0,014	0,045	0,100	171,4	614,0

Notably, the removal of the rotor shrouding results in an increase from 0.014 kJ/kg to 0.1 kJ/kg Tip leakage loss. Figure 6-9 convincingly illustrates the impact unshrouded turbine blades have on turbine loss distribution.

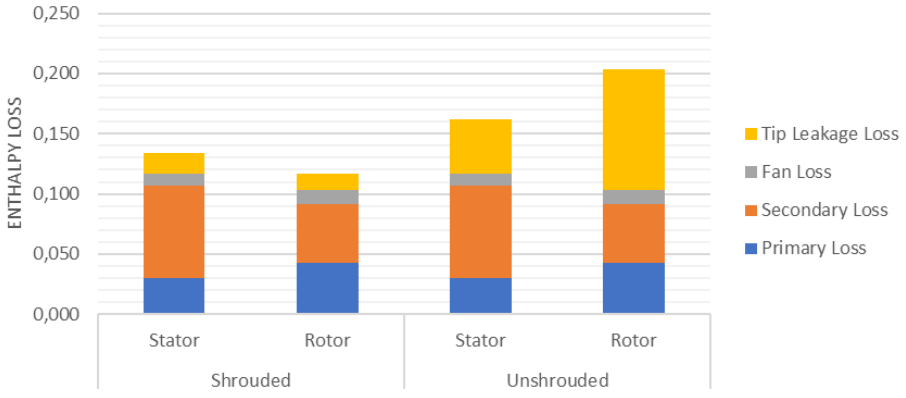

Figure 6-9: Shrouded and Unshrouded Blade Loss Distribution

This case study used reasonable theoretical blade geometries and suitable operational conditions. The ability to predict performance deviation based on tip leakage losses can be finely tuned for actual turbine modelling requirements. The loss coefficient algorithm nozzle-model exhibited the ability to predict turbine performance associated with shrouded and unshrouded blade designs.

6.4 LSB interconnection impact

The last case study of this chapter investigates the impact various last stage blade interconnections have on stage performance. Interconnections are a physical strength and stability requirement, due to the sizing and operational conditions of last stage blades.

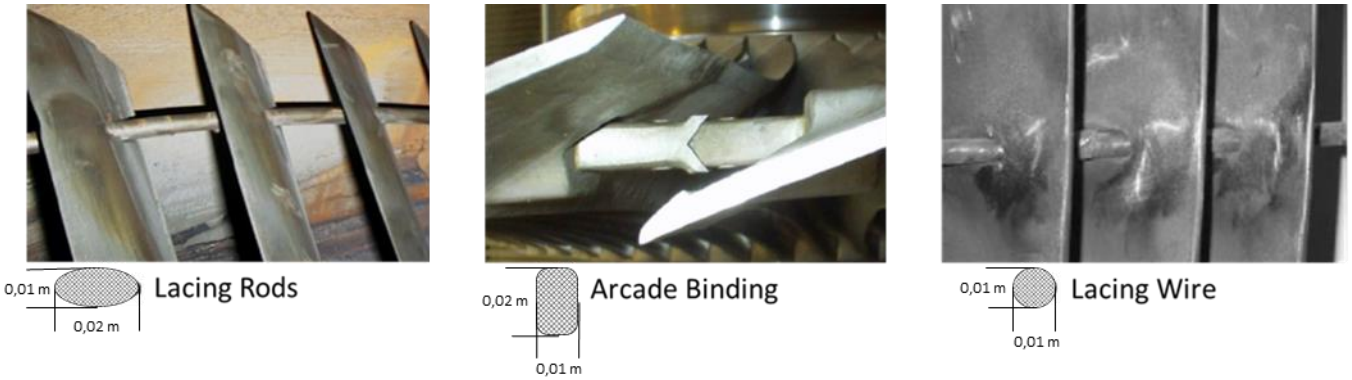

Figure 6-10: LSB Interconnection Types - Adapted from [13]

Figure 6-10 illustrates the three different types of interconnection commonly used by turbine manufactures. The case study compares the three interconnection types against each other in a similar modelling approach as used in the previous section.

The case study evaluation requirements are:

- Predict the stage performances associated with last stage blade interconnections.
- Display additional attributes obtained by the implementation of the loss coefficient algorithms: Focused on LSB interconnection blade geometry illustrated in Figure 3-18.

Note: The following abbreviations used for the result tables and graphs:

- Arcade Binding – Square interconnection LSB Loss coefficient turbine nozzle model
- Lacing Wire – Round interconnection LSB Loss coefficient turbine nozzle model
- Lacing Rods – Oval interconnection LSB Loss coefficient nozzle model

Model development

The last stage models were developed from the last stage blade designs used in Chapter 5 . The three different last stage blade interconnection geometries are based on the design information provided by Singh et. al [8] and EPRI [47]. The interconnection geometries are as follows:

LSB Interconnection Geometry	Arcade Binding	Lacing Wire	Lacing Rods
Connection Thickness [m]	0,02	0,01	0,01
Connection Width [m]	0,01	0,01	0,02

All three interconnection blade designs have the same blade-to-blade length and are located on the same diameter height. For simplification of the test case, only single strand interconnections are evaluated. Only the last stage rotor blades will be interconnected for this case study as per the LPST stage 4B design.

Last stage blade interconnections information is presented in Figure 3-18. The boundary conditions are set to mimic the operational conditions of stage 4B, location illustrated in Figure 5-1.

Last Stage Boundary Conditions	
Stage Inlet Pressure: 15,3 kPa	Working fluid: Steam
Inlet Temperature: 55 ˚C	Turbine Exhaust Pressure: 5,35 kPa
RPM: 3000	Mass flow calibration: 31.5 kg/s

Results & Discussion

Table 6-6 presents a comparison of the LSB interconnection modelling results. The results indicate that Lacing rods are the most beneficial at an 85,45% stage efficiency, followed by Lacing wire at 84,84 %.

Table 6-6: LSB Interconnection Performance Data

	Lacing Rods		Arcade Binding		Lacing Wire	
Performance	Stator	Rotor	Stator	Rotor	Stator	Rotor
Efficiency [%]	91,35	79,56	91,22	74,76	91,32	78,36
Row Loss Coefficient	0,086	0,204	0,088	0,252	0,087	0,216
Primary Loss	0,025	0,055	0,025	0,055	0,025	0,055
Secondary Loss	0,007	0,003	0,007	0,003	0,007	0,003
Fan Loss	0,026	0,027	0,026	0,027	0,026	0,027
Tip Leakage Loss	0,011	0,020	0,011	0,020	0,011	0,020
LSB Correction	0,000	0,024	0,000	0,073	0,000	0,036
Moisture Loss	0,020	0,069	0,022	0,069	0,021	0,069

Figure 6-11 provides a comparative illustration of the LSB interconnection types based on their respective turbine loss distributions. It is apparent that the Arcade Binging interconnection would be the poorest interconnection selection for this specific blade design, based on thermal performance evaluation alone.

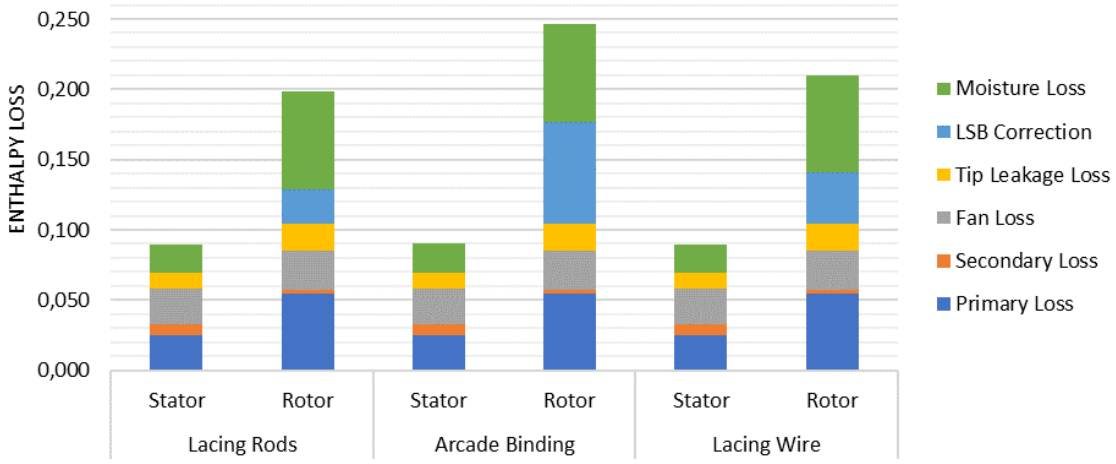

Figure 6-11: LSB Interconnection Turbine Losses Distribution

This case study illustrates the loss coefficient algorithms ability to determine performance deviation based on LSB interconnection geometries, enabling the nozzle-model to more accurately predict last stage performance.

Chapter 7 Conclusion & Recommendation

7.1 Conclusion

The study set out to determine an appropriate loss coefficient model for use in the stage-by-stage turbine nozzle model. Research into turbine loss methodologies produced a functional comparative grouping of turbine loss coefficients that could be used in conjunction with the nozzle model.

The greatest selection criteria for the loss coefficients was integrability and clear correlation to turbine blade geometries. The correlation between losses and geometries are key to obtaining greater functionality from the loss coefficient algorithm.

Traupel's loss coefficient methodology was selected for the loss coefficient algorithm "design" condition section with corrections provided for moisture loss. Zehner's loss correction was used for the development of the loss coefficient algorithm for "off-design" section.

The fundamental group of loss coefficients were comprised of a profile loss, a secondary loss, a fan loss and a tip leakage loss. These losses are associated with the majority of turbine loss methodologies. The second group was aimed at off-design performance predictions and was added as a correction to the fundamental group losses. The final group was focused on specialized losses, specifically last stage blade interconnection losses and moisture loss.

The selected loss coefficients methodologies enabled the development of a loss coefficient algorithm script in Flownex that integrates with the stage-by-stage turbine nozzle model. The algorithm script incorporated structural stability and validation control measures to assist during solving.

Once a model has been developed it requires calibration. Several calibration methods are possible, all dependant on the amount and type of information that is available. Calibration can be performed by fixing the inlet and exhaust pressure and temperature boundary conditions and then configuring the nozzle-model throat area until the correct mass flow is obtained.

A validation and verification case study illustrated the validity of the loss coefficient algorithms by obtaining an average efficiency prediction accuracy of 99.3%. The case study compared the loss coefficient nozzle-model's results to a well-documented actual AGARD gas turbine test case, as well as to the results obtained from the initial stage-by-stage turbine nozzle model.

The validation leads to the successful construction of an operational steam turbine case study model. The low-pressure steam turbine loss coefficient nozzle model obtained an overall performance prediction accuracy of 98.8%. The low-pressure steam turbine model was constructed from an actual operational steam turbine, for which the majority of the design information was available. The test case evaluated both full and partial load operational conditions.

The comparison between full and partial load (60%) results confirmed the loss coefficient algorithm's ability to predict turbine performance as well as turbine loss distributions.

From the low-pressure steam turbine model, an off-design design evaluation became possible. The off-design evaluation investigated the impact of operating a turbine at off-normal spin speeds has on overall turbine performance. The loss coefficient algorithm determined the loss in performance, for (90% and 110%) critical speed operation, by calculating the impact off-design incidence angles have on turbine performance. This, in turn, illustrates the loss coefficient algorithm's ability to model both design and off-design conditions.

Additional case studies displayed the loss coefficient nozzle model's ability to predict offset performance conditions resulting from turbine geometry variance. Four turbine blade design alterations were evaluated. The first evaluation investigated the impact of a change in profile design has on overall stage performance. This was achieved by modelling and comparing the performance of an actual old blade profile designs with its upgrade blade profile design. The loss coefficient nozzle-model was able to predict the change in turbine stage performance resulting from the change in the blade profile design.

The second evaluation investigated the impact of degradation mechanisms have on turbine performance. The evaluation used theoretical Fouling and Erosion blade degradation scenarios. The loss coefficient nozzle-model was able to predict the decline in turbine performance caused by the degradation mechanisms, as well as indicate how the turbine loss distribution related to specific changes in blade profile geometries.

The third evaluation determined the difference in turbine performance related to shrouded and unshrouded blade designs. The focus of this evaluation was to determine the loss coefficient nozzle model's ability to predict tip leakage loss. The final evaluation followed by investigating the impact that last stage blade interconnections have on turbine performance. The third and fourth blade design evaluations displayed the loss coefficient's abilities to predict turbine performance variations related to specific blade design characteristics.

This study has shown that the implementation of the loss coefficient algorithm has enabled the stage-by-stage turbine nozzle model to predict turbine performance, as well as turbine loss distributions, from the incorporation of turbine blade geometries.

7.2 Recommendation

The loss coefficient has the following shortfalls and opportunities for further research:

- The loss coefficient algorithm requires the addition of turbine blade-intercooling into the gas turbine performance analysis methodology.
- Incorporating detail blade shroud design and configurations into the determination of tip leakage instead of a generalized mass flow methodology utilized.
- The implementation of a blade profile selection user interface would further advance the ability of the nozzle-model, similar to the data presented in Figure 3-20.
- The unification of the nozzle-model script and the loss coefficient algorithm script into one streamlined compressed script would improve the overall model processing speed.

References

[1] W. Fuls, “Accurate stage-by-stage modelling of axial turbines using an appropriate nozzle analogy with minimal geometric data,” *Applied Thermal Engineering,* vol. 116, pp. 134-146, 2017.

[2] IEA, “Key World Energy Statistics 2018,” International Energy Agency, Paris, France, 2018.

[3] R. U. ATProM, “Applied Thermofluid Process Modelling,” University of Cape Town, Mechanical Engineering Department, 2018. [Online]. Available: http://www.atprom.uct.ac.za. [Accessed October 2018].

[4] T. Croft, Steam Turbine Principles and Practice 1st Edition, New York: McGraw-Hill Book Company Inc., 1923.

[5] T. Wright, Fluid machinery : performance, analysis, and design, Boca Raton: CRC Press LLC, 1999.

[6] Undisclosed, *Undisclosed Steam Turbine Information,* Undisclosed, 2010.

[7] S. Sandler, Chemical and Engineering Thermodynamics 3rd Edition, Weinheim: John Wiley & Sons Inc, 1999.

[8] M. L. G. Singh, Blade Design and Analysis for Steam Turbines, New York: The McGraw-Hill Companies, 2011.

[9] O. Singh, Applied Thermodynamics 3rd Edition, New Delhi: New Age International (P) Ltd., 2009.

[10] V. Vullo and F. Vivio, Rotors: Stress Analysis and Design, Rome: Springer, 2013.

[11] W. Sanders, “Turbine steam path: Maintenance and Repair Vol.2,” Pennwell Publishing Company, 2002.

[12] H. S. M. Bloch, Steam Turbines: Design, Applications, and Rerating 2nd Edition, Milan: The McGraw-Hill Co., 2009.

[13] F. Woell, *Steam Turbine Thermodynamic Velocity Triangle and Blade Design,* Johannesburg: EPPEI, 2016.

[14] G. Azad, J. Hart and S. Teng, "Heat Transfer and Pressure Distribution on a Gas Turbine Blade," NASA Glenn Research Center, Texas, 2000.

[15] M. Schobeiri, "Turbomachinery Flow Physics and Dynamic Performance 2nd Edition," Springer, Heidelberg, 2012.

[16] S. Egorova, A. Kapitanova and D. Loktevb, "Turbine Blades Profile and Surface Roughness Measurement," *Elsevier, ScienceDirect,* vol. International Conference on Industrial Engineering, 2017.

[17] ISO, "ISO 14661 / ISO 3977 / ISO 2314:2009," International Standard, 2000.

[18] R. Gorla, Turbomachinery Design and Theory, New York: Marcel Dekker Inc., 2003.

[19] M. Smith, "A simple correlation of turbine efficiency," *Journal of Royal Aeronautical Society,* 1965.

[20] S. Dixon and C. Hall, Fluid Mechanics and Thermodynamics of Turbomachinery, Oxford: Elsevier Inc, 2014.

[21] B. Lakshminarayana, Fluid Dynamics and Heat Transfer of Turbomachinery, Chichester: John Wiley & Sons Inc., 1996.

[22] I. Shames, Mechanics of Fluids, 4th Edition, Madrid: McGraw-Hill, 2003.

[23] O. Sharma and T. Butler, "Predictions of Endwall Losses and Secondary Flows in Axial Flow Turbine Cascades," *Journal of Turbomachinery,* vol. 109, no. April, p. 229, 1987.

[24] P. Zehner, "Calculation of Four-Quadrant Characteristics of Turbines," *The American Society of Mechanical Engineers,* no. 80-GT-2, 1980.

[25] K. Hiroyuki, O. Akihiro, S. Naoki and N. Yoshiki, "Development of Moisture Loss Models in Steam Turbines," *Heat Transfer-Asian Research,* vol. 42, no. 10.1002/htj.20395., 2013.

[26] G. Gyarmathy, Grundlagen einer Theorie der Nassdampfturbine, Zürich, Switzerland: ETH Zurich Research Collection, 1962.

[27] N. Wei, “Significance of Loss Models in Aerothermodynamic Simulation for Axial Turbines,” Royal Institute of Technology: Department of Energy Technology - Division of Heat and Power Technology, Stockholm, 2000.

[28] J. Denton, “Loss mechanisms in turbomachines,” *Journal of turbomachinery, ,* vol. 115, 1993.

[29] W. Traupel, Thermische Turbomaschinen: Erster Band, Zürich: Springer Verlag Berlin Heidelberg, 1977.

[30] J. Horlock, Axial Flow Turbine, Butterwoth Published, 1966.

[31] C. Soderberg, “Unpublished Gas Turbine Laboratory notes,” Massachusetts Institute of Technology, 1949.

[32] D. Ainley and G. Mathieson, A Method of performance estimation of axial flow turbines, 1951.

[33] H. Craig and H. Cox, Performance estimation of axial flow turbines., Instititution of mechanical engineers, 1970.

[34] J. Dunham and P. Came, “Improvements to the Ainley-Mathieson method of turbine performance prediction,” *Journal of engineering for power,* vol. 92, pp. 252-256, 1970.

[35] W. Traupel, “Thermische Turbomaschinen: Zweiter Band,” Springer Verlag Berlin Heidelberg, Zürich, 1977.

[36] S. Kacker and U. Okapuu, “A mean line prediction method for axial flow turbine efficiency,” *Journal for engineering for power,* vol. 104, pp. 111-119, 1982.

[37] S. McBrinie, Marine Steam Engines and Turbines 4th Ed, Wellington, New Zealand: The Butterworth Group Ltd, 1980.

[38] W. Kearton, Steam turbine theory and practice, Pitman, 1951.

[39] M. Leonid, Y. Govoruschenko and P. Pagur, “Axial turbine stages design: 1D/2D/3D simulation, experiment, optimization,” in *Turbo Expo*, Nevada, 2005.

[40] R. J. H. Pottas, “A row-by-row axial turbine process model based on a one-dimensional thermofluid network approach,” University of Cape Town, Cape Town, 2016.

[41] R. I. Lewis, Turbomachinary Performance Analysis, Elsevier Science & Technology Books, 1996.

[42] NASA, “NASA Glenn Research Center,” NASA, 2012. [Online]. Available: https://www.grc.nasa.gov/www/5810/rvc/tcgrid.htm. [Accessed 2018].

[43] M-Tech_Industrial, “Flownex Simulation Environment: General User Manual,” May 2017. [Online]. Available: https://www.flownex.com/. [Accessed 2018].

[44] M. Dejc and B. Trojanovskij, “ Untersuchung und Berechnung axialer Turbinenstufen,” Berlin , 1973.

[45] AGARD, “Test Cases for Computation of Internal Flows in Aero Enginre Components,” AGARD: Propulsion and Energetics, NATO Nations, 1990.

[46] API, “API Starndard 612: Special purpose steam turbines for industrial services,” American Petroleum Institute, Washington, 1995.

[47] EPRI, “Collection of Journal Articles on Steam Turbine Blades,” Electrical Power Research Institute.

Appendix A: Experimental Data

AGARD Case Study

	Stage 1		Stage 2		Stage 3		Stage 4	
Description	Stator	Rotor	Stator	Rotor	Stator	Rotor	Stator	Rotor
Number of Blades	39	39	39	39	39	39	39	39
Mean Blade Diameter [m]	0,330379	0,33543	0,34123	0,346281	0,35208	0,357132	0,362931	0,367982
Blade Tip Diameter [m]	0,390758	0,400061	0,412459	0,421762	0,434161	0,443463	0,455862	0,465165
Blade Hub Diameter [m]	0,27	0,27	0,27	0,27	0,27	0,27	0,27	0,27
Blade Height [m]	0,062406	0,067069	0,073281	0,077944	0,084156	0,088819	0,095031	0,099694
Blade Width [m]	0,045455	0,039174	0,046792	0,038393	0,04802	0,037668	0,049135	0,037
Blade Chord Length [m]	0,055294	0,051025	0,056266	0,052215	0,057156	0,05343	0,057963	0,054662
Maximum Blade Thickness [m]	0,015393	0,009459	0,015632	0,008983	0,015847	0,008514	0,016038	0,008053
Throat Width [m]	0,0075	0,0148	0,0107	0,01365	0,01453	0,01359	0,01818	0,01438
Pitch - Blade Spacing [m]	0,035951	0,035334	0,037218	0,036538	0,038448	0,037733	0,039638	0,038909
Trailing Edge Thickness [m]	0,0004	0,00048	0,000482	0,000512	0,000462	0,000526	0,000548	0,000522
Row Spacing Width [m]	0,009673	0,017286	0,008894	0,016532	0,008169	0,015831	0,007492	0,03959
Blade Gap Area [m^2]	0,000453	0,000961	0,000762	0,001034	0,001192	0,001177	0,001688	0,001401
Row Flow Area [m^2]	0,017658	0,037466	0,029714	0,040328	0,046486	0,045895	0,065835	0,054639
Blade Inlet Angle [˚]	79,90363	31,47247	79,90363	24,05564	79,90363	16,13911	79,90363	7,901738
Blade Outlet Angle [˚]	19,53035	67,06804	20,163	67,7347	20,78783	68,37578	21,41185	68,99137
Blade Surface Finish [m]	0,00001	0,00001	0,00001	0,00001	0,00001	0,00001	0,00001	0,00001
Shrouded	Yes	Yes	Yes	Yes	Yes	Yes	Yes	Yes
Interconnected LSB	No	No	No	No	No	No	No	No
Efficiency [%]	91,3387	91,66072	93,05028	90,28629	92,9471	90,5845	92,73315	89,33202
Traupel Loss Coefficient [kJ/kg]	0,086613	0,083393	0,069497	0,097137	0,070529	0,094155	0,072668	0,10668
Primary Loss [kJ/kg]	0,03405	0,043082	0,029479	0,056551	0,028588	0,051531	0,028421	0,047703
Profile Loss [kJ/kg]	0,027808	0,042315	0,026903	0,057016	0,026368	0,052181	0,025833	0,048558
Reynolds Correction	1,089312	0,96174	0,92467	0,952651	0,918966	0,943787	0,914016	0,935209
Mach Correction	1	1	1	1	1	1	1	1
Trailing Edge Loss [kJ/kg]	0,003626	0,002195	0,004421	0,002033	0,004202	0,002083	0,004603	0,002106
Carnot Shock Loss [kJ/kg]	0,000132	0,00019	0,000181	0,000202	0,000155	0,0002	0,000206	0,000185
Secondary Loss [kJ/kg]	0,035312	0,013231	0,022176	0,012455	0,020864	0,01244	0,019631	0,011512
F Correction	0,049498	0,026684	0,039317	0,029591	0,041658	0,02943	0,04238	0,029498
Endwall Loss [kJ/kg]	0,000396	0,000142	0,000296	0,000113	0,00023	9,31E-05	0,000183	0,000202
Fan Loss [kJ/kg]	0,01028	0,011779	0,013944	0,015577	0,01792	0,019659	0,022143	0,023962
Tip Leakage Loss [kJ/kg]	0,006971	0,015302	0,003899	0,012553	0,003157	0,010525	0,002473	0,023502

LPST – Theoretical Geometries[2]

	Stage A1		Stage A2		Stage A3		Stage A4		Stage B1		Stage B2		Stage B3		Stage B4	
Description	Stator	Rotor	Stator	Rotor	Stator	Rotor	Stator	Rotor	Stator	Rotor	Stator	Rotor	Stator	Rotor	Stator	Rotor
Number of Blades	30	30	30	30	30	30	30	30	30	30	30	30	30	30	30	30
Mean Blade Diameter [m]	1,79	1,79	1,81	1,81	1,85	1,85	2,2	2,2	1,79	1,79	1,81	1,81	1,85	1,85	2,2	2,2
Blade Tip Diameter [m]	1,85	1,855	1,97	1,99	2,29	2,34	2,83	2,83	1,85	1,855	1,97	1,99	2,29	2,34	2,83	2,83
Blade Hub Diameter [m]	1,705	1,705	1,71	1,71	1,69	1,68	1,57	1,57	1,705	1,705	1,71	1,71	1,69	1,68	1,57	1,57
Blade Height [m]	0,07	0,07	0,12	0,14	0,3	0,306	0,61	0,63	0,07	0,07	0,12	0,14	0,3	0,306	0,61	0,63
Blade Width [m]	0,056	0,034	0,07	0,034	0,1	0,052	0,16	0,086	0,056	0,034	0,07	0,034	0,1	0,052	0,16	0,086
Blade Chord Length [m]	0,0672	0,0415	0,0861	0,0422	0,125	0,0655	0,208	0,1049	0,0672	0,0415	0,0861	0,0422	0,125	0,0655	0,208	0,1049
Maximum Blade Thickness [r	0,0192	0,0119	0,0246	0,012	0,0357	0,0187	0,0594	0,03	0,0192	0,0119	0,0246	0,012	0,0357	0,0187	0,0594	0,03
Throat Width [m]	0,0095	0,019	0,012	0,018	0,0192	0,0186	0,023	0,0196	0,0095	0,019	0,012	0,018	0,0192	0,0186	0,023	0,0196
Pitch - Blade Spacing [m]	0,0384	0,0384	0,0384	0,0384	0,0386	0,0388	0,041	0,043	0,0384	0,0384	0,0384	0,0384	0,0386	0,0388	0,041	0,043
Trailing Edge Thickness [m]	0,0005	0,0005	0,0005	0,0005	0,0005	0,0005	0,0005	0,0006	0,0005	0,0005	0,0005	0,0005	0,0005	0,0005	0,0005	0,0006
Row Spacing Width [m]	0,018	0,07	0,02	0,11	0,03	0,16	0,076	0,152	0,018	0,07	0,02	0,11	0,03	0,16	0,076	0,152
Blade Inlet Angle [°]	80	30	80	25	82	28	80	25	80	30	80	25	82	28	80	25
Blade Outlet Angle [°]	20	70	20	65	25	72	20	80	20	70	20	65	25	72	20	80
Blade Surface Finish [m]	0,01	0,01	0,01	0,01	0,01	0,01	0,01	0,01	0,01	0,01	0,01	0,01	0,01	0,01	0,01	0,01
Shrouded	Yes	Yes	Yes	Yes	Yes	Yes	No	No	Yes	Yes	Yes	Yes	Yes	Yes	No	No
Interconnected LSB	No	No	No	No	No	No	No	Yes	No	No	No	No	No	No	No	Yes
Connection Diameter [m]	-	-	-	-	-	-	-	2,69	-	-	-	-	-	-	-	2,69
Connection Length [m]	-	-	-	-	-	-	-	0,048	-	-	-	-	-	-	-	0,048
Connection Thickness [m]	-	-	-	-	-	-	-	0,01	-	-	-	-	-	-	-	0,01
Connection Width [m]	-	-	-	-	-	-	-	0,02	-	-	-	-	-	-	-	0,02

LPST - Full Load Case Study

Performance Data	Stage 1A		Stage 2A		Stage 3A		Stage 4A		Stage 1B		Stage 2B		Stage 3B		Stage 4B	
	Stator	Rotor	Stator	Rotor	Stator	Rotor	Stator	Rotor	Stator	Rotor	Stator	Rotor	Stator	Rotor	Stator	Rotor
Efficiency [%]	89,407	84,09	91,146	88,328	94,524	89,441	91,612	81,301	89,407	83,546	91,1474	88,30483	94,52414	89,44059	87,2263	81,30075
Traupel Loss Coefficient [kJ/kg]	0,1059	0,1591	0,0885	0,1167	0,0548	0,1056	0,0839	0,187	0,1059	0,1645	0,088526	0,116952	0,054759	0,105594	0,127737	0,186992
Primary Loss [kJ/kg]	0,0262	0,0477	0,0265	0,0618	0,0218	0,0479	0,0318	0,0437	0,0262	0,0477	0,026514	0,061757	0,021792	0,047902	0,031905	0,043723
Profile Loss [kJ/kg]	0,0252	0,0431	0,0269	0,057	0,0224	0,0522	0,0253	0,0547	0,0252	0,0431	0,026903	0,057016	0,022425	0,052181	0,025315	0,054746
Reynolds Correction	0,8658	1,0535	0,7995	1,0456	0,7262	0,8736	1,0937	0,7572	0,8658	1,0535	0,799469	1,045607	0,726232	0,873555	1,099314	0,757232
Mach Correction	1	1	1	1	1	1	1	1	1	1	1	1	1	1	1	1
Trailing Edge Loss [kJ/kg]	0,0042	0,0021	0,0048	0,002	0,0053	0,0021	0,0039	0,0021	0,0042	0,0021	0,00483	0,001959	0,00531	0,002123	0,003897	0,0021
Carnot Shock Loss [kJ/kg]	0,0001	0,0002	0,0002	0,0002	0,0002	0,0002	0,0002	0,0002	0,0001	0,0002	0,000176	0,000182	0,000196	0,000196	0,000179	0,000168
Secondary Loss [kJ/kg]	0,0561	0,0168	0,039	0,0097	0,0152	0,0041	0,0105	0,0025	0,0561	0,0175	0,038959	0,009715	0,015163	0,004058	0,010548	0,002663
F Correction[2]	0,0981	0,0321	0,1226	0,0312	0,1199	0,0324	0,1209	0,0437	0,0981	0,0335	0,122615	0,031283	0,119928	0,032445	0,120906	0,046672
Endwall Loss [kJ/kg]	0,0004	0,0006	0,0003	0,0004	0,0002	0,0003	0,0003	0,0001	0,0004	0,0006	0,000289	0,000421	0,000168	0,000282	0,000306	0,000118
Fan Loss [kJ/kg]	0,0007	0,0008	0,0005	0,0009	0,0007	0,0008	0,0026	0,0027	0,0007	0,0008	0,000499	0,000859	0,00701	0,007508	0,025623	0,027356
Tip Leakage Loss [kJ/kg]	0,0237	0,0947	0,0226	0,0444	0,0108	0,0461	0,016	0,0196	0,0237	0,0399	0,022555	0,044621	0,010794	0,046125	0,01657	0,019595
LSB Correction [kJ/kg]	0	0	0	0	0	0	0	0,0242	0	0	0	0	0	0	0	0,024169
Moisture Loss [kJ/kg]	0	0	0	0	0	0	0	0	0	0	0	0	0	0	0,04309	0,069486

LPST - 60% Partial Load Case Study

Performance Data	Stage 1B		Stage 2A		Stage 3A		Stage 4A		Stage 1B		Stage 2B		Stage 3B		Stage 4B	
	Stator	Rotor	Stator	Rotor	Stator	Rotor	Stator	Rotor	Stator	Rotor	Stator	Rotor	Stator	Rotor	Stator	Rotor
Efficiency [%]	89,396	83,681	88,587	88,377	92,089	89,439	90,805	85,909	89,396	83,626	89,645	88,375	92,218	89,439	87,476	78,884
Traupel Loss Coefficient [kJ/kg]	0,106	0,163	0,114	0,116	0,079	0,106	0,092	0,141	0,106	0,164	0,104	0,116	0,078	0,106	0,125	0,211
Primary Loss [kJ/kg]	0,026	0,048	0,027	0,062	0,022	0,048	0,038	0,066	0,026	0,048	0,027	0,062	0,022	0,048	0,038	0,066
Profile Loss [kJ/kg]	0,025	0,043	0,027	0,057	0,022	0,052	0,025	0,055	0,025	0,043	0,027	0,057	0,022	0,052	0,025	0,055
Reynolds Correction	0,866	1,054	0,799	1,046	0,726	0,874	1,348	1,167	0,866	1,054	0,799	1,046	0,726	0,874	1,357	1,175
Mach Correction	1,000	1,000	1,000	1,000	1,000	1,000	1,000	1,000	1,000	1,000	1,000	1,000	1,000	1,000	1,000	1,000
Trailing Edge Loss [kJ/kg]	0,004	0,002	0,005	0,002	0,005	0,002	0,003	0,002	0,004	0,002	0,005	0,002	0,005	0,002	0,003	0,002
Carnot Shock Loss [kJ/kg]	0,000	0,000	0,000	0,000	0,000	0,000	0,000	0,000	0,000	0,000	0,000	0,000	0,000	0,000	0,000	0,000
Secondary Loss [kJ/kg]	0,056	0,017	0,039	0,010	0,015	0,004	0,012	0,004	0,056	0,017	0,039	0,010	0,015	0,004	0,013	0,004
F Correction[2]	0,098	0,033	0,123	0,031	0,120	0,032	0,121	0,045	0,098	0,033	0,123	0,031	0,120	0,032	0,121	0,049
Endwall Loss [kJ/kg]	0,000	0,001	0,000	0,000	0,000	0,000	0,000	0,000	0,000	0,001	0,000	0,000	0,000	0,000	0,000	0,000
Fan Loss [kJ/kg]	0,000	0,000	0,000	0,001	0,007	0,008	0,026	0,027	0,000	0,000	0,000	0,001	0,007	0,008	0,026	0,027
Tip Leakage Loss [kJ/kg]	0,024	0,098	0,023	0,044	0,011	0,046	0,016	0,020	0,024	0,099	0,023	0,044	0,011	0,046	0,017	0,020
LSB Correction [kJ/kg]	0,000	0,000	0,000	0,000	0,000	0,000	0,000	0,024	0,000	0,000	0,000	0,000	0,000	0,000	0,000	0,024
Moisture Loss [kJ/kg]	0,000	0,000	0,000	0,000	0,001	0,004	0,032	0,069	0,000	0,000	0,000	0,000	0,001	0,004	0,032	0,069

[2] The LPST geometries displayed are not exact and are in part derived from theory.

							2700									
Efficiency [%]	88,64	83,204	89,908	87,65	93,024	89,423	88,875	88,294	88,64	82,587	89,909	87,621	93,024	89,422	84,648	81,333
Traupel Loss Coefficient [kJ/	0,105	0,1679	0,0883	0,1235	0,0547	0,1058	0,0982	0,117	0,105	0,1741	0,0883	0,1238	0,0547	0,1058	0,1404	0,1866
Primary Loss [kJ/kg]	0,0262	0,0477	0,0265	0,0618	0,0218	0,0479	0,0317	0,0437	0,0262	0,0477	0,0265	0,0618	0,0218	0,0479	0,0319	0,0437
Profile Loss [kJ/kg]	0,0252	0,0431	0,0269	0,057	0,0224	0,0522	0,0253	0,0547	0,0252	0,0431	0,0269	0,057	0,0224	0,0522	0,0253	0,0547
Reynolds Correction	0,8658	1,0535	0,7995	1,0456	0,7262	0,8736	1,091	0,7572	0,8658	1,0535	0,7995	1,0456	0,7262	0,8736	1,0971	0,7572
Mach Correction	1	1	1	1	1	1	1	1	1	1	1	1	1	1	1	1
Trailing Edge Loss [kJ/kg]	0,0042	0,0021	0,0048	0,002	0,0053	0,0021	0,0039	0,0021	0,0042	0,0021	0,0048	0,002	0,0053	0,0021	0,0039	0,0021
Carnot Shock Loss [kJ/kg]	0,0001	0,0002	0,0002	0,0002	0,0002	0,0002	0,0002	0,0002	0,0001	0,0002	0,0002	0,0002	0,0002	0,0002	0,0002	0,0002
Secondary Loss [kJ/kg]	0,0555	0,018	0,039	0,0107	0,0152	0,0042	0,0105	0,0022	0,0555	0,0189	0,039	0,0108	0,0152	0,0042	0,0105	0,0023
F Correction	0,0969	0,0344	0,1226	0,0347	0,1199	0,0339	0,1209	0,0375	0,0969	0,0363	0,1226	0,0349	0,1199	0,0339	0,1209	0,0398
Endwall Loss [kJ/kg]	0,0004	0,0006	0,0003	0,0004	0,0002	0,0003	0,0003	0,0001	0,0004	0,0006	0,0003	0,0004	0,0002	0,0003	0,0003	0,0001
Fan Loss [kJ/kg]	-5E-05	-5E-05	0,0005	0,0009	0,007	0,0075	0,0256	0,0274	-5E-05	-5E-05	0,0005	0,0009	0,007	0,0075	0,0256	0,0274
Tip Leakage Loss [kJ/kg]	0,0234	0,1023	0,0223	0,0501	0,0107	0,0461	0,0303	0,0196	0,0234	0,1075	0,0223	0,0504	0,0107	0,0461	0,0303	0,0196
LSB Correction [kJ/kg]	0	0	0	0	0	0	0	0,0242	0	0	0	0	0	0	0	0,0242
Zehner Off-Design	0,1136	0,168	0,1009	0,1235	0,0698	0,1058	0,1112	0,1171	0,1136	0,1741	0,1009	0,1238	0,0698	0,1058	0,1535	0,1867
Incidence Angle (°)	-25,77	-12,61	-22,77	-11,23	-24,67	-13,88	-30,56	-24,12	-25,77	-12,61	-22,67	-11,17	-24,63	-13,85	-30,47	-25,17
							3330									
Efficiency [%]	88,553	85,836	89,74	88,956	92,865	89,442	88,675	88,349	88,553	85,45	89,74	88,957	92,865	89,442	84,464	81,4
Traupel Loss Coefficient [kJ/	0,1049	0,1416	0,0888	0,1104	0,0548	0,1056	0,0985	0,1164	0,1049	0,1454	0,0888	0,1104	0,0548	0,1056	0,1406	0,1859
Primary Loss [kJ/kg]	0,0262	0,0477	0,0265	0,0618	0,0218	0,0479	0,032	0,0437	0,0262	0,0477	0,0265	0,0618	0,0218	0,0479	0,0321	0,0437
Profile Loss [kJ/kg]	0,0252	0,0431	0,0269	0,057	0,0224	0,0522	0,0253	0,0547	0,0252	0,0431	0,0269	0,057	0,0224	0,0522	0,0253	0,0547
Reynolds Correction	0,8658	1,0535	0,7995	1,0456	0,7262	0,8736	1,1021	0,7572	0,8658	1,0535	0,7995	1,0456	0,7262	0,8736	1,109	0,7572
Mach Correction	1	1	1	1	1	1	1	1	1	1	1	1	1	1	1	1
Trailing Edge Loss [kJ/kg]	0,0042	0,0021	0,0048	0,002	0,0053	0,0021	0,0039	0,0021	0,0042	0,0021	0,0048	0,002	0,0053	0,0021	0,0039	0,0021
Carnot Shock Loss [kJ/kg]	0,0001	0,0002	0,0002	0,0002	0,0002	0,0002	0,0002	0,0002	0,0001	0,0002	0,0002	0,0002	0,0002	0,0002	0,0002	0,0002
Secondary Loss [kJ/kg]	0,0554	0,0144	0,039	0,0087	0,0152	0,004	0,0106	0,0016	0,0554	0,015	0,039	0,0087	0,0152	0,004	0,0106	0,0016
F Correction	0,0968	0,0274	0,1226	0,0278	0,1199	0,0322	0,1209	0,0272	0,0968	0,0284	0,1226	0,0278	0,1199	0,0322	0,1209	0,0272
Endwall Loss [kJ/kg]	0,0004	0,0006	0,0003	0,0004	0,0002	0,0003	0,0003	0,0001	0,0004	0,0006	0,0003	0,0004	0,0002	0,0003	0,0003	0,0001
Fan Loss [kJ/kg]	-5E-05	-5E-05	0,0005	0,0009	0,007	0,0075	0,0256	0,0274	-5E-05	-5E-05	0,0005	0,0009	0,007	0,0075	0,0256	0,0274
Tip Leakage Loss [kJ/kg]	0,0234	0,0795	0,0228	0,0391	0,0108	0,0461	0,0303	0,0196	0,0234	0,0828	0,0228	0,0391	0,0108	0,0461	0,0303	0,0196
LSB Correction [kJ/kg]	0	0	0	0	0	0	0	0,0242	0	0	0	0	0	0	0	0,0242
Zehner Off-Design	0,1145	0,1416	0,1026	0,1104	0,0713	0,1056	0,1133	0,1165	0,1145	0,1455	0,1026	0,1104	0,0713	0,1056	0,1554	0,186
Incidence Angle (°)	25,812	12,789	22,823	11,727	24,754	14,298	30,654	25,88	25,812	12,789	22,708	11,666	24,694	14,262	30,574	27,195

Blade Design Upgrade

Description	1960's		2000's	
	Stator	Rotor	Stator	Rotor
Number of Blades	39	39	39	39
Mean Blade Diameter [m]	0,330379	0,33543	0,330379	0,33543
Blade Tip Diameter [m]	0,390758	0,400061	0,390758	0,400061
Blade Hub Diameter [m]	0,27	0,27	0,27	0,27
Blade Height [m]	0,062406	0,067069	0,062406	0,067069
Blade Width [m]	0,045455	0,039174	0,056	0,034
Blade Chord Length [m]	0,055294	0,051025	0,0672	0,04148
Maximum Blade Thickness [m]	0,015393	0,009459	0,03714	0,022822
Throat Width [m]	0,0075	0,0148	0,003109	0,006134
Pitch - Blade Spacing [m]	0,035951	0,035334	0,0384	0,0384
Trailing Edge Thickness [m]	0,0004	0,00048	0,00045	0,000475
Row Spacing Width [m]	0,009673	0,017286	0,009673	0,017286
Blade Inlet Angle [˚]	79,90363	31,47247	79,90363	31,47247
Blade Outlet Angle [˚]	19,53035	67,06804	19,53035	67,06804
Blade Surface Finish [m]	0,00001	0,00001	0,00001	0,00001
Shrouded	Yes	Yes	Yes	Yes
Efficiency [%]	0,031905	0,043723	0,031854	0,043723
Row Loss Coefficient [kJ/kg]	0,010548	0,002663	0,010531	0,002288
Primary Loss [kJ/kg]	0,025623	0,027356	0,025623	0,027356
Secondary Loss [kJ/kg]	0,01657	0,019595	0,03034	0,019595
Tip Leakage Loss [kJ/kg]	0,04309	0,069486	0,042082	0,069486

Blade Degradation

	Polished		Fouled		Erosion	
Description	Stator	Rotor	Stator	Rotor	Stator	Rotor
Number of Blades	39	39	39	39	39	39
Mean Blade Diameter [m]	0,330379	0,33543	0,330379	0,33543	0,330379	0,33543
Blade Tip Diameter [m]	0,390758	0,400061	0,390758	0,400061	0,390758	0,400061
Blade Hub Diameter [m]	0,27	0,27	0,27	0,27	0,27	0,27
Blade Height [m]	0,062406	0,067069	0,062406	0,067069	0,062406	0,067069
Blade Width [m]	0,045455	0,039174	0,045455	0,039174	0,043	0,038
Blade Chord Length [m]	0,055294	0,051025	0,055294	0,051025	0,053	0,048
Maximum Blade Thickness [m]	0,015393	0,009459	0,016	0,01	0,015	0,009
Throat Width [m]	0,0075	0,0148	0,007	0,013	0,0078	0,0175
Pitch - Blade Spacing [m]	0,035951	0,035334	0,035951	0,035334	0,035951	0,035334
Trailing Edge Thickness [m]	0,0004	0,00048	0,00042	0,0005	0,00039	0,00046
Row Spacing Width [m]	0,009673	0,017286	0,009673	0,017286	0,0098	0,0175
Blade Inlet Angle [˚]	79,90363	31,47247	79,90363	31,47247	79,90363	31,47247
Blade Outlet Angle [˚]	19,53035	67,06804	19,53035	67,06804	19,53035	67,06804
Blade Surface Finish [m]	0,00001	0,00001	0,0001	0,0001	0,00006	0,00006
Efficiency [%]	86,62435	88,2997	67,99743	73,6261	71,97822	76,89786
Row Loss Coefficient [kJ/kg]	0,133757	0,117003	0,320026	0,263739	0,280218	0,231021
Primary Loss [kJ/kg]	0,03001	0,043082	0,097514	0,148841	0,077844	0,123869
Secondary Loss [kJ/kg]	0,076873	0,048191	0,194988	0,089501	0,175031	0,081654
Fan Loss [kJ/kg]	0,01028	0,011779	0,01028	0,011779	0,01028	0,011779
Tip Leakage Loss [kJ/kg]	0,016594	0,013951	0,017243	0,013619	0,017063	0,013719

Shrouded & Unshrouded Case Study

	Shrouded		Unshrouded	
Description	Stator	Rotor	Stator	Rotor
Number of Blades	52	52	52	52
Mean Blade Diameter [m]	0,330379	0,33543	0,340481	0,345532
Blade Tip Diameter [m]	0,390758	0,400061	0,409363	0,418665
Blade Hub Diameter [m]	0,27	0,27	0,27	0,27
Blade Height [m]	0,062406	0,067069	0,071731	0,076394
Blade Width [m]	0,045455	0,039174	0,045455	0,039174
Blade Chord Length [m]	0,055294	0,051025	0,055294	0,051025
Maximum Blade Thickness [m]	0,015393	0,009459	0,015393	0,009459
Throat Width [m]	0,0075	0,0148	0,0075	0,0148
Pitch - Blade Spacing [m]	0,035951	0,035334	0,035951	0,035334
Trailing Edge Thickness [m]	0,0004	0,00048	0,0004	0,00048
Row Spacing Width [m]	0,009673	0,017286	0,009673	0,017286
Blade Inlet Angle [˚]	79,90363	31,47247	79,90363	31,47247
Blade Outlet Angle [˚]	19,53035	67,06804	19,53035	67,06804
Blade Surface Finish [m]	0,00001	0,00001	0,00001	0,00001
Shrouded	Yes	Yes	No	No
Efficiency [%]	86,62574	88,28655	83,78714	79,64409
Traupel Loss Coefficient [kJ/kg]	0,133743	0,117135	0,162129	0,203559
Primary Loss [kJ/kg]	0,03001	0,043082	0,03001	0,043082
Profile Loss [kJ/kg]	0,027808	0,042315	0,027808	0,042315
Reynolds Correction	0,930957	0,96174	0,930957	0,96174
Mach Correction	1	1	1	1
Trailing Edge Loss [kJ/kg]	0,003989	0,002195	0,003989	0,002195
Carnot Shock Loss [kJ/kg]	0,000132	0,00019	0,000132	0,00019
Secondary Loss [kJ/kg]	0,076896	0,0482	0,076896	0,048199
F Correction	0,123266	0,09807	0,123266	0,09807
Endwall Loss [kJ/kg]	0,000263	9,48E-05	0,000263	9,47E-05
Fan Loss [kJ/kg]	0,01028	0,011779	0,01028	0,011779
Tip Leakage Loss [kJ/kg]	0,016557	0,014075	0,044943	0,1005

LSB Interconnection Case Study

	Lacing Rods		Arcade Binding		Lacing Wire	
Description	Stator	Rotor	Stator	Rotor	Stator	Rotor
Number of Blades	30	30	30	30	30	30
Mean Blade Diameter [m]	2,2	2,2	2,2	2,2	2,2	2,2
Blade Tip Diameter [m]	2,83	2,83	2,83	2,83	2,83	2,83
Blade Hub Diameter [m]	1,57	1,57	1,57	1,57	1,57	1,57
Blade Height [m]	0,61	0,63	0,61	0,63	0,61	0,63
Blade Width [m]	0,16	0,086	0,16	0,086	0,16	0,086
Blade Chord Length [m]	0,208	0,10492	0,208	0,10492	0,208	0,10492
Maximum Blade Thickness [	0,059429	0,029977	0,059429	0,029977	0,059429	0,029977
Throat Width [m]	0,023	0,0196	0,023	0,0196	0,023	0,0196
Pitch - Blade Spacing [m]	0,041	0,043	0,041	0,043	0,041	0,043
Trailing Edge Thickness [m]	0,00053	0,00055	0,00053	0,00055	0,00053	0,00055
Row Spacing Width [m]	0,076	0,152	0,076	0,152	0,076	0,152
Blade Inlet Angle [˚]	80	25	80	25	80	25
Blade Outlet Angle [˚]	20	80	20	80	20	80
Blade Surface Finish [m]	0,01	0,01	0,01	0,01	0,01	0,01
Shrouded	Yes	No	Yes	No	Yes	No
Interconnected LSB	No	Yes	No	Yes	No	Yes
Connection Diameter [m]	-	2,69	-	2,69	-	2,69
Connection Length [m]	-	0,048	-	0,048	-	0,048
Connection Thickness [m]	-	0,01	-	0,02	-	0,01
Connection Width [m]	-	0,02	-	0,01	-	0,01
Efficiency [%]	91,35111	79,55595	91,2166	74,75997	91,31794	78,35657
Traupel Loss Coefficient [kJ/	0,086489	0,204441	0,087834	0,2524	0,086821	0,216434
Primary Loss [kJ/kg]	0,022418	0,061012	0,022418	0,06062	0,022418	0,060918
Profile Loss [kJ/kg]	0,025315	0,054746	0,025315	0,054746	0,025315	0,054746
Reynolds Correction	0,661731	1,076321	0,661731	1,069095	0,661731	1,074581
Mach Correction	1	1	1	1	1	1
Trailing Edge Loss [kJ/kg]	0,005487	0,00192	0,005487	0,001923	0,005487	0,00192
Carnot Shock Loss [kJ/kg]	0,000179	0,000168	0,000179	0,000168	0,000179	0,000168
Secondary Loss [kJ/kg]	0,007482	0,002822	0,007482	0,002835	0,007482	0,002825
F Correction	0,120906	0,035455	0,120906	0,03587	0,120906	0,035559
Endwall Loss [kJ/kg]	0,000285	0,000125	0,000285	0,000124	0,000285	0,000125
Fan Loss [kJ/kg]	0,025623	0,027356	0,025623	0,027356	0,025623	0,027356
Tip Leakage Loss [kJ/kg]	0,010774	0,019595	0,010782	0,019595	0,010776	0,019595
LSB Correction [kJ/kg]	0	0,024169	0	0,072508	0	0,036254
Moisture Loss [kJ/kg]	0,020191	0,069486	0,021528	0,069486	0,020521	0,069486

Appendix B: Abbreviated Loss Coefficient Algorithms

Loss Coefficient Algorithm C# Script

```
//Flow Area Calculation
sAbgp.Value=Math.Atan(sO/sDm)*(sDs*sDs-sDn*sDn)/4;
sAf.Value=sAbgp*sNb;
rAbgp.Value=Math.Atan(rO/rDm)*(rDs*rDs-rDn*rDn)/4;
rAf.Value=rAbgp*rNb;

//Traupel Loss Coefficient Calculations
sζ.Value=sPL+sSL+sFL+sTL+sLSB+sML;
rζ.Value=rPL+rSL+rFL+rTL+rLSB+rML;

//Primary Loss
sPL.Value=(sPrf*sReC*sMaC)+sTe+sCs;
rPL.Value=(rPrf*rReC*rMaC)+rTe+rCs;

//Profile Loss
double []α0={sα0,rα0};
double []α1={sα1,rα1};
double []Prf={sPrf,rPrf};
{double [,]PrfM={    {(Math.PI*10/180),0,0,-1.6414*10E-9,5.22727*10E-7,-6.49224*10E-5,7.1513*10E-3}
      ,{(Math.PI*15/180),-7.19149*10E-13,3.49129*10E-10,-6.69342*10E-8,6.34078*10E-6,-3.13043*10E-4,1.02567*10E-2}
      ,{(Math.PI*20/180),-1.17977*10E-12,5.62751*10E-10,-1.06216*10E-7,9.92353*10E-6,-4.74289*10E-4,1.23335*10E-2}
      ,{(Math.PI*25/180),-1.49757*10E-12,7.07226*10E-10,-1.32412*10E-7,1.23126*10E-5,-5.8547*10E-4,1.40457*10E-2}
      ,{(Math.PI*30/180),-1.55815*10E-12,7.38388*10E-10,-1.397*10E-7,1.32036*10E-5,-6.406*10E-4,1.51418*10E-2}
      ,{(Math.PI*35/180),-1.96059*10E-12,9.16953*10E-10,-1.70609*10E-7,1.58261*10E-5,-7.52811*10E-4,1.69495*10E-2}
      ,{(Math.PI*45/180),-4.23568*10E-12,1.73797*10E-9,-2.80328*10E-7,2.24533*10E-5,-9.30707*10E-4,1.84516*10E-2}};

for (int i = 0; i < Prf.Length; i++)
{  double x0,x1;
double []PrfX= new double[6];
double []PrfY= new double[6];
   if (α1[i]<=PrfM[0,0])
       {  for (int k = 1; k < 7; k++)
      { PrfX[k-1]=PrfM[0,k]*Math.Pow((α0[i]*180/Math.PI),6-k); }
      Prf[i]=PrfX[0]+PrfX[1]+PrfX[2]+PrfX[3]+PrfX[4]+PrfX[5];}
   else if (α1[i]>=PrfM[6,0])
      { for (int k = 1; k < 7; k++)
      { PrfX[k-1]=PrfM[6,k]*Math.Pow((α0[i]*180/Math.PI),6-k);}
      Prf[i]=PrfX[0]+PrfX[1]+PrfX[2]+PrfX[3]+PrfX[4]+PrfX[5];  }
   else
      {for (int j = 0; j < 5; j++)
         {if ((α1[i]>=PrfM[j,0]) && (α1[i]<PrfM[j+1,0]))
         {for (int k = 1; k < 7; k++)
         {PrfX[k-1]=PrfM[j,k]*Math.Pow((α0[i]*180/Math.PI),6-k);
         PrfY[k-1]=PrfM[j+1,k]*Math.Pow((α0[i]*180/Math.PI),6-k);}
         x0=PrfX[0]+PrfX[1]+PrfX[2]+PrfX[3]+PrfX[4]+PrfX[5];
         x1=PrfY[0]+PrfY[1]+PrfY[2]+PrfY[3]+PrfY[4]+PrfY[5];
         Prf[i]=((x1-x0)*(α1[i]-PrfM[j,0])/(PrfM[j+1,0]-PrfM[j,0]))+x0;}}}}}
sPrf.Value=Prf[0];
rPrf.Value=Prf[1];
```

```
//Reynolds Number Correction
double []Re={sRe,rRe};
double []Ks={sksf/sSchrd,rksf/rSchrd};
double []ReC=new double[2];
sRe.Value=sρ*V2*(Math.Sqrt(sAbgp/Math.PI))/sμ;
rRe.Value=rρ*V3*(Math.Sqrt(rAbgp/Math.PI))/rμ;
   for (int i = 0; i < Re.Length; i++)
      {if (Re[i]<200000)
      {ReC[i]=415.42*Math.Pow(Re[i],-0.491718);}
      else
      {ReC[i]=(-2.04381*10E7*Ks[i]*Ks[i]*Ks[i])+(1.34009*10E4*Ks[i]*Ks[i])+(2.00593*10E2*Ks[i])+(0.565005);}}
sReC.Value=ReC[0];
rReC.Value=ReC[1];

//Mach Number Correction
double []Ma={sMa,rMa};
double []MaC=new double[2];
   for (int i = 0; i < Ma.Length; i++)
      {if (Ma[i]>0.8)
      {MaC[i]=(-344.92*Math.Pow(Ma[i],5))+(1796.3*Ma[i]*Ma[i]*Ma[i]*Ma[i])+(-
3690.8*Ma[i]*Ma[i]*Ma[i])+(3744.7*Ma[i]*Ma[i])+(-1878.6*Ma[i])+374.2;}
      else
      {MaC[i]=1.0;}}
sMaC.Value=MaC[0];
rMaC.Value=MaC[1];

//Trailing Edge Loss
double []Tep=new double[2];
double []Te=new double[2];
double []δte={sδte,rδte};
double []t={st,rt};
double []TeX=new double[2];
double []TeY=new double[2];

   for (int i = 0; i < Te.Length; i++)
      {Tep[i]=δte[i]/(t[i]*Math.Sin(α1[i]));
      TeX[i]=Tep[i]/(Prf[i]*ReC[i]*MaC[i]);
      if (TeX[i]<3.4)
      {TeY[i]=0.9697*TeX[i]+0.7461;}
      else
      {TeY[i]=-0.014548*TeX[i]*TeX[i]+0.457829*TeX[i]+2.61156;}}

double [,]TeM={{0.04,500,-6*10E-17},{0.08,250,-6*10E-17},{0.12,166.6667,0},{0.16,125,-6*10E-17},{0.2,100,4*10E-17}};
   for (int i = 0; i < Te.Length; i++)
   {double x0,x1;
      if (Tep[i]<=TeM[0,0])
      {Te[i]=(TeY[i]-TeM[0,2])/TeM[0,1];   }
      else if (Tep[i]>=TeM[4,0])
      {Te[i]=(TeY[i]-TeM[4,2])/TeM[4,1];   }
      else
         {for (int j = 0; j < 3; j++)
            {if ((Tep[i]>=TeM[j,0]) && (Tep[i]<TeM[j+1,0]))
            {x0=(TeY[i]-TeM[j,2])/TeM[j,1];
            x1=(TeY[i]-TeM[j+1,2])/TeM[j+1,1];
            e[i]=((x1-x0)*(Tep[i]-TeM[j,0])/(TeM[j+1,0]-TeM[j,0]))+x0;}}}}

sTe.Value=Te[0];
rTe.Value=Te[1];
```

```
//Carnot Shock Loss
double []Cs={sCs,rCs};

sCs.Value=(Tep[0]/(1-Tep[0]))*(Tep[0]/(1-Tep[0]))*Math.Sin(sα1)*Math.Sin(sα1);
rCs.Value=(Tep[1]/(1-Tep[1]))*(Tep[1]/(1-Tep[1]))*Math.Sin(rα1)*Math.Sin(rα1);
//-----Primary Loss Complete----//

//Secondary Loss
sSL.Value=(sPL/sPrf)*(sFc/ltx[0])+sEw+0.02*((sSchrd/sls)-((sSchrd/st)/ltx[0]));
rSL.Value=(rPL/rPrf)*(rFc/ltx[1])+rEw+0.02*((sSchrd/sls)-((sSchrd/st)/ltx[1]));
double []B={7,10};          //B=7 for Stator, B=10 for Rotor
double []    lt={(sls/st),(rls/rt)};
double []ltk={(B[0]*Math.Sqrt(sPL)),(B[1]*Math.Sqrt(rPL))};
double []ltx=new double[2];
for (int i = 0; i < lt.Length; i++)
{ltx[i]=ltk[i]>lt[i]?ltk[i]:lt[i];}
// Coefficient A = 0.02 for strongly accelerating and high velocity grids & 0.035 for constant pressure impeller grids

// F Correction
double []Fc=new double[2];
double []cw={(V1/V2),(V2r/V3)};    //!!!!!!!Check research for accuracy
double []dα={((α0[0]-α1[0])*180/Math.PI),((α1[1]-α0[1])*180/Math.PI)};
{double [,]FcM={{1,-9.1269*10E-11,3.23992*10E-8,-3.65469*10E-6,2.66136*10E-4,3.66044*10E-3},
            {0.9,-6.16173*10E-11,2.27701*10E-8,-2.78513*10E-6,2.28791*10E-4,3.03546*10E-3},
            {0.8,-7.17726*10E-11,2.52631*10E-8,-3.00349*10E-6,2.21563*10E-4,2.43801*10E-3},
            {0.7,-4.52489*10E-11,1.69238*10E-8,-2.13194*10E-6,1.75095*10E-4,2.27393*10E-3},
            {0.6,-4.04069*10E-11,1.5065*10E-8,-1.88122*10E-6,1.48852*10E-4,2.10375*10E-3},
            {0.5,-1.85538*10E-11,7.60232*10E-9,-1.05483*10E-6,1.06001*10E-4,1.97787*10E-3},
            {0.4,-2.62881*10E-11,8.98421*10E-9,-1.08292*10E-6,9.40453*10E-5,1.47745*10E-3},
            {0.3,-1.64113*10E-11,5.98948*10E-9,-7.81293*10E-7,7.29054*10E-5,1.16583*10E-3},
            {0.2,-2.80663*10E-12,1.00053*10E-9,-1.5836*10E-7,3.47721*10E-5,1.06541*10E-3}};

  for (int i = 0; i < Fc.Length; i++)
  {double x0,x1;
  double []FcX= new double[5];
  double []FcY= new double[5];
    if (cw[i]>=FcM[0,0])
      { for (int k = 1; k < 6; k++)
      {FcX[k-1]=FcM[0,k]*Math.Pow(dα[i],5-k);}Fc[i]=FcX[0]+FcX[1]+FcX[2]+FcX[3]+FcX[4];}
    else if (cw[i]<=FcM[8,0])
      { for (int k = 1; k < 6; k++)
      {FcX[k-1]=FcM[8,k]*Math.Pow(dα[i],5-k);}
      Fc[i]=FcX[0]+FcX[1]+FcX[2]+FcX[3]+FcX[4];}
    else
      {for (int j = 0; j < 8; j++)
        {if ((cw[i]<FcM[j,0]) && (cw[i]>=FcM[j+1,0]))
        {for (int k = 1; k < 6; k++)
        {FcX[k-1]=FcM[j,k]*Math.Pow(dα[i],5-k);
        FcY[k-1]=FcM[j+1,k]*Math.Pow(dα[i],5-k);}
        x0=FcX[0]+FcX[1]+FcX[2]+FcX[3]+FcX[4];
        x1=FcY[0]+FcY[1]+FcY[2]+FcY[3]+FcY[4];
        Fc[i]=((x1-x0)*(cw[i]-FcM[j,0])/(FcM[j+1,0]-FcM[j,0]))+x0;}}}}}
sFc.Value=Fc[0];

rFc.Value=Fc[1];
```

```
//Endwall Loss
double ksfL=0.042;
double []ksf={sksf,rksf};
double []ls={sls,rls};
double []Dm={sDm,rDm};
double []cf=new double[2];
   {for (int i = 0; i < cf.Length; i++)
      {if (ksf[i]<ksfL)
      {cf[i]=0.445/Math.Pow((Math.Log(Re[i])),2.58);}
      else
      {cf[i]=Math.Pow((1.89+1.62*(Math.Log((ls[i]/ksf[i])))),-2.5);}}    }

sEw.Value=(cf[0]/Math.Sin(sα1))*(1+(sls/Dm[0]))*(sδgp/sls);
rEw.Value=(cf[1]/Math.Sin(rα1))*(1-(rls/Dm[1]))*(rδgp/rls);
//----Secondary Loss Complete----//


//Fan Loss
double []υ={(sDn/sDs),(rDn/rDs)};
double []lsD={(sls/sDm),(rls/rDm)};
double []FL=new double[2];
double [,]FLM={{0.5,3.53074*10E-2,-2.08139*10E-4,1.28485*10E-5},
      {0.7,3.20866*10E-2,-7.03983*10E-4,6.39394*10E-6},
      {0.9,2.99004*10E-2,-1.49509*10E-3,7.86364*10E-6}};
   for (int i = 0; i < FL.Length; i++)
   {double x0,x1;
   double []FLX= new double[5];
   double []FLY= new double[5];
      if (υ[i]>=FLM[2,0])
         { for (int k = 1; k < 4; k++)                {
         FLX[k-1]=FLM[2,k]*Math.Pow(lsD[i],3-k);}
         FL[i]=FLX[0]+FLX[1]+FLX[2];}
      else if (υ[i]<=FLM[0,0])
         { for (int k = 1; k < 4; k++)
         {FLX[k-1]=FLM[0,k]*Math.Pow(lsD[i],3-k);}
         FL[i]=FLX[0]+FLX[1]+FLX[2];}
      else
         {for (int j = 0; j < 2; j++)
         {if ((υ[i]>=FLM[j,0]) && (υ[i]<FLM[j+1,0]))
            {for (int k = 1; k < 4; k++)
            {FLX[k-1]=FLM[j,k]*Math.Pow(lsD[i],3-k);
            FLY[k-1]=FLM[j+1,k]*Math.Pow(lsD[i],3-k);}
            x0=FLX[0]+FLX[1]+FLX[2];
            x1=FLY[0]+FLY[1]+FLY[2];
            FL[i]=((x1-x0)*( υ[i]-FLM[j,0])/(FLM[j+1,0]-FLM[j,0]))+x0;}}}}

sFL.Value=FL[0];
rFL.Value=FL[1];
//
```

```
//Tip Leakage Loss
double []Shrd=new double[2];
double []UShrd=new double[2];
double []Dδ={sDn/sDm,rDs/rDm};
double []δgp={sδgp,rδgp};
{double []kδ=new double[2];
double []m=new double[2];
   for (int i = 0; i < 2; i++)
   {m[i]=0.5*(δgp[i]/ls[i])*Dδ[i]*(1/Math.Tan(α1[i]));
   kδ[i]=m[i]+0.99-0.0125*(t[i]/ls[i])*(1/Math.Tan(α1[i]));}
// Shrouded & Unshrouded Calculations
   double []v={1.5318* ψ[0]/(1- ψ[0])+1.854* ψ[0]/(1- ψ[0])+0.1244,
            1.5318* ψ[1]/(1- ψ[1])+1.854* ψ[1]/(1- ψ[1])+0.1244};
   double []ψ={3.1415* sδgp*sDn/sAf, 3.1415* rδgp*rDn/rAf };
   Shrd[0]=2*(1-R)* ψ[0]/(1- ψ[0])*(1-Math.Pow((v[0]-(V2/V1))/(V2/V1),2));
   Shrd[1]= ψ[0]/(1- ψ[0])*(1-Math.Pow((v[1]-(V3/V2r))/(V3/V2r),2));
   UShrd[0]=kδ[0]*((sδgp-0.002*sSchrd)*sDn/(sls*sDm))*(2* ψ[0]-2*R *ψ[0]+ V2* V2)/(2*ψ[0]));
   UShrd[1]=kδ[1]*((0.2*rδgp-0.002*rSchrd)*rDs/(rls*rDm))*(( 2*R* ψ[0]+ V2* V2-u*u+1)/(2*ψ[1]));}

sTL.Value=(sShrd.Value)?Shrd[0]:UShrd[0];
rTL.Value=(rShrd.Value)?Shrd[1]:UShrd[1];
//

//Moisture Loss Correction
double []Prt={sPout/sPin,rPout/rPin};

sML.Value=((Prt[0]<1) && (Prt[0]>0) && (sQ<1))?(0.0581*Prt[0]*Prt[0]-0.139*Prt[0]+0.0815):0;
sML.Value=((Prt[1]<1) && (Prt[1]>0) && (rQ<1))?(0.0581*Prt[1]*Prt[1]-0.139*Prt[1]+0.0815):0;
//

//Last Stage Blade Correction
double []Intd={sIntd,rIntd};
double []Intw={sIntw,rIntw};
double []Intx=new double[2];
   for (int i = 0; i < 2; i++)
   {Intx[i]=Intw[i]<=Intd[i]?1.2:0.8;}

sLSB.Value=(sIntC.Value)?(8*Intx[0]*Math.Sin(sα1)*Math.Sin(sα1)*((st*st)/(sIntL*sIntL))*(sIntD*sIntd/(sDs*sDs-sDn*sDn))):0;
rLSB.Value=(rIntC.Value)?(8*Intx[1]*Math.Sin(rα1)*Math.Sin(rα1)*((rt*rt)/(rIntL*rIntL))*(rIntD*rIntd/(rDs*rDs-rDn*rDn))):0;
//
```

```
//Zehner Off-Design Correction
double []za=new double[2];
double []zb=new double[2];
double sZPL,rZPL;
double []ΔαInc=new double[2];
double []ΔInc=new double[2];
   if (rpm<Drpm)
   {sαInc.Value=-(180/Math.PI)*(Math.Asin(Math.Sin(Math.PI-sα0)*(Drpm-rpm)*(Math.PI*sDm/60)/V1));
   rαInc.Value=-(180/Math.PI)*(Math.Asin(Math.Sin(rα0)*(Drpm-rpm)*(Math.PI*sDm/60)
/(Math.Sqrt(V2*V2+(Math.PI*rDm*rpm/60)*(Math.PI*rDm*rpm/60)-2*V2*(Math.PI*rDm*rpm/60)*Math.Cos(sα1)))));}
   else if (Drpm<rpm)
   {sαInc.Value=(180/Math.PI)*(Math.Asin(Math.Sin(sα0)*(rpm-Drpm)*(Math.PI*sDm/60)/V1));
   rαInc.Value=(180/Math.PI)*(Math.Asin(Math.Sin(Math.PI-rα0)*(rpm-Drpm)*(Math.PI*sDm/60)
/(Math.Sqrt(V2*V2+(Math.PI*rDm*rpm/60)*(Math.PI*rDm*rpm/60)-2*V2*(Math.PI*rDm*rpm/60)*Math.Cos(sα1)))));}
   else
   {sαInc.Value=0;    rαInc.Value=0;}
double []αInc={sαInc*Math.PI/180,rαInc*Math.PI/180};
sβstag.Value=Math.Asin(sSw/sSchrd);
rβstag.Value=Math.Asin(rSw/rSchrd);
sfhcc.Value=(sfhccT.Value)?sfhcc.Value:sδbt;
rfhcc.Value=(rfhccT.Value)?rfhcc.Value:rδbt;
sCas.Value=(sCasT.Value)?sCas.Value:(sfhcc*(Math.Sqrt(sβstag*(sα0-sα1)))/st);
rCas.Value=(rCasT.Value)?rCas.Value:(rfhcc*(Math.Sqrt(rβstag*(rα1-rα0)))/rt);
double []Cas={sCas,rCas};
   for (int i = 0; i < 2; i++)
   {ΔαInc[i]=α0[i]+αInc[i];
   if (αInc[i]==0)
   {ΔInc[i]=0;    za[i]=0;    zb[i]=0;}
   else if (ΔαInc[i]>0)
   {ΔInc[i]=(ΔαInc[i]/(Math.PI-αInc[i]));
   za[i]=2.587-0.426*Cas[i]-1.216*Cas[i]*Cas[i];
   zb[i]=4.175+10.802*Cas[i]-13.881*Cas[i]*Cas[i];}
   else if (ΔαInc[i]<0)
   {ΔInc[i]=(ΔαInc[i]/(-αInc[i]));
   za[i]=0.446+3.82*Cas[i]-2.899*Cas[i]*Cas[i];
   zb[i]=2.413+10.38*Cas[i]-10.116*Cas[i]*Cas[i];}}
   sZPL=1-(1-sPL)*Math.Pow(Math.E,(-za[0]*Math.Pow(ΔInc[0],zb[0])));
   rZPL=1-(1-rPL)*Math.Pow(Math.E,(-za[1]*Math.Pow(ΔInc[1],zb[1])));

sζZ.Value=sZPL+sSL+sFL+sTL+sLSB+sML;
rζZ.Value=rZPL+rSL+rFL+rTL+rLSB+rML;
// ---- Off-Design Loss Complete---- //

//Efficiency & Nozzle Model Input
if (rpm>Drpm || rpm<Drpm)
{sη.Value=(100*(1-sζZ));
rη.Value=(100*(1-rζZ));
zs.Value=(sζZ/(1-sζZ));
zr.Value=(rζZ/(1-rζZ));    }
else
{sη.Value=(100*(1-sζ));
rη.Value=(100*(1-rζ));
zs.Value=(sζ/(1-sζ));
zr.Value=(rζ/(1-rζ));}

zs.Value = ((zs<=0) || (zs>1) || (double.IsNaN(zs)))?0.1:zs.Value;
zr.Value = ((zr<=0) || (zr>1) || (double.IsNaN(zr)))?0.1:zr.Value;}
```

Loss Coefficient Algorithm Script Variables Definitions

Blade Geometry Input Variables

sNb_=_StatorProfile_:_NumberofBlades
sDm_=_StatorProfile_:_MeanBladeDiameter
sDs_=_StatorProfile_:_BladeTipDiameter
sDn_=_StatorProfile_:_BladeHubDiameter
sls_=_StatorProfile_:_BladeHeight
sSw_=_StatorProfile_:_BladeWidth
sSchrd_=_StatorProfile_:_BladeChordLength
sδbt_=_StatorProfile_:_MaximumBladeThickness
sO_=_StatorProfile_:_ThroatWidth
st_=_StatorProfile_:_Pitch-BladeSpacing
sδte_=_StatorProfile_:_TrailingEdgeThickness
sδgp_=_StatorProfile_:_RowSpacingWidth
sAbgp_=_StatorProfile_:_BladeGapArea
sAf_=_StatorProfile_:_RowFlowArea
sα0_=_StatorProfile_:_BladeInletAngle
sα1_=_StatorProfile_:_BladeOutletAngle
sksf_=_StatorProfile_:_BladeSurfaceFinish
Bool_sShrd_=_StatorProfile_:_Shrouded
Bool_sIntC_=_StatorProfile_:_InterconnectedLSB
sIntD_=_StatorProfile_:_ConnectionDiameter
sIntL_=_StatorProfile_:_ConnectionLength
sIntd_=_StatorProfile_:_ConnectionThickness
sIntw_=_StatorProfile_:_ConnectionWidth

rNb_=_RotorProfile_:_NumberofBlades
rDm_=_RotorProfile_:_MeanBladeDiameter
rDs_=_RotorProfile_:_BladeTipDiameter
rDn_=_RotorProfile_:_BladeHubDiameter
rls_=_RotorProfile_:_BladeHeight
rSw_=_RotorProfile_:_BladeWidth
rSchrd_=_RotorProfile_:_BladeChordLength
rδbt_=_RotorProfile_:_MaximumBladeThickness
rO_=_RotorProfile_:_ThroatWidth
rt_=_RotorProfile_:_Pitch-BladeSpacing
rδte_=_RotorProfile_:_TrailingEdgeThickness
rδte_=_RotorProfile_:_RowSpacingWidth
rAbgp_=_RotorProfile_:_BladeGapArea
rAf_=_RotorProfile_:_RowFlowArea
rα0_=_RotorProfile_:_BladeInletAngle
rα1_=_RotorProfile_:_BladeOutletAngle
rksf_=_RotorProfile_:_BladeSurfaceFinish
Bool_rShrd_=_RotorProfile_:_Shrouded
Bool_rIntC_=_RotorProfile_:_InterconnectedLSB
rIntD_=_RotorProfile_:_ConnectionDiameter
rIntL_=_RotorProfile_:_ConnectionLength
rIntd_=_RotorProfile_:_ConnectionThickness
rIntw_=_RotorProfile_:_ConnectionWidth

Fluid Properties

V1_=_StatorFluidProperties_:_InletVelocity
V2_=_StatorFluidProperties_:_OutletVelocity
sRe_=_StatorFluidProperties_:_ReynoldsNumber
sMa_=_StatorFluidProperties_:_MachNumber
sT_=_StatorFluidProperties_:_Temperature
sρ_=_StatorFluidProperties_:_Density
sμ_=_StatorFluidProperties_:_Viscosity
sPin_=_StatorFluidProperties_:_InletPressure
sPout_=_StatorFluidProperties_:_OutletPressure

V2r_=_RotorFluidProperties_:_InletVelocity
V3_=_RotorFluidProperties_:_OutletVelocity
rRe_=_RotorFluidProperties_:_ReynoldsNumber
rMa_=_RotorFluidProperties_:_MachNumber
rT_=_RotorFluidProperties_:_Temperature
rρ_=_RotorFluidProperties_:_Density
rμ_=_RotorFluidProperties_:_Viscosity
rPin_=_RotorFluidProperties_:_InletPressure
rPout_=_RotorFluidProperties_:_OutletPressure

Calculated Loss Coefficients

sη_=_StatorPerformanceData_:_StatorEfficiency
sζ_=_StatorPerformanceData_:_TraupelLossCoefficient
sPL_=_StatorPerformanceData_:_+PrimaryLoss
sPrf_=_StatorPerformanceData_:_-ProfileLoss
sReC_=_StatorPerformanceData_:_-ReynoldsCorrection
sMaC_=_StatorPerformanceData_:_-MachCorrection
sTe_=_StatorPerformanceData_:_-TrailingEdgeLoss
sCs_=_StatorPerformanceData_:_-CarnotShockLoss
sSL_=_StatorPerformanceData_:_+SecondaryLoss
sFc_=_StatorPerformanceData_:_-FCorrection
sEw_=_StatorPerformanceData_:_-EndwallLoss
sFL_=_StatorPerformanceData_:_+FanLoss
sTL_=_StatorPerformanceData_:_+TipLeakageLoss
sLSB_=_StatorPerformanceData_:_+LSBCorrection
sML_=_StatorPerformanceData_:_+MoistureLoss
sζZ_=_StatorPerformanceData_:_ZehnerOff-DesignCorrection
sαInc_=_StatorPerformanceData_:_-IncidenceAngle
Bool_sCasT_=_StatorPerformanceData_:_-CascadeCoefficientKnown
sCas_=_StatorPerformanceData_:_-CascadeCoefficient
sCasBool_sfhccT_=_StatorPerformanceData_:_-HeightoftheCurvatureKnown
sfhcc_=_StatorPerformanceData_:_-CamberlineCurvatureHeight
sβstag_=_StatorPerformanceData_:_-BladeStaggerAngle

rη_=_RotorPerformanceData_:_RotorEfficiency
rζ_=_RotorPerformanceData_:_TraupelLossCoefficient
rPL_=_RotorPerformanceData_:_+PrimaryLoss
rPL_=_RotorPerformanceData_:_-ProfileLoss
rReC_=_RotorPerformanceData_:_-ReynoldsCorrection
rMaC_=_RotorPerformanceData_:_-MachCorrection
rTe_=_RotorPerformanceData_:_-TrailingEdgeLoss
rTerCs_=_RotorPerformanceData_:_-CarnotShockLoss
rSL_=_RotorPerformanceData_:_+SecondaryLoss
rFc_=_RotorPerformanceData_:_-FCorrection
rEw_=_RotorPerformanceData_:_-EndwallLoss
rFL_=_RotorPerformanceData_:_+FanLoss
rTL_=_RotorPerformanceData_:_+TipLeakageLoss
rLSB_=_RotorPerformanceData_:_+LSBCorrection
rML_=_RotorPerformanceData_:_+MoistureLoss
rζZ_=_RotorPerformanceData_:_ZehnerOff-DesignCorrection
rαInc_=_RotorPerformanceData_:_-IncidenceAngle
Bool_rCasT_=_RotorPerformanceData_:_-CascadeCoefficientKnown
rCas_=_RotorPerformanceData_:_-CascadeCoefficient
Bool_rfhccT_=_RotorPerformanceData_:_-HeightoftheCurvatureKnown
rfhcc_=_RotorPerformanceData_:_-CamberlineCurvatureHeight
rβstag_=_RotorPerformanceData_:_-BladeStaggerAngle

Loss Coefficient Algorithm Output Variables

zs_=_NozzleModelInput_:_StatorLossCoefficient
zr_=_NozzleModelInput_:_RotorLossCoefficient
Drpm_=_TurbineData_:_TurbineDesignSpeed
rpm_=_TurbineData_:_OperatingSpeed
sQ_=_StatorFluidProperties_:_Quality
rQ_=_RotorFluidProperties_:_Quality

Appendix C: Ethics in Research Assessment

Application for Approval of Ethics in Research (EiR) Projects
Faculty of Engineering and the Built Environment, University of Cape Town

APPLICATION FORM

Please Note:
Any person planning to undertake research in the Faculty of Engineering and the Built Environment (EBE) at the University of Cape Town is required to complete this form **before** collecting or analysing data.The objective of submitting this application *prior* to embarking on research is to ensure that the highest ethical standards in research, conducted under the auspices of the EBE Faculty, are met. Please ensure that you have read, and understood the **EBE Ethics in Research Handbook**(available from the UCT EBE, Research Ethics website) prior to completing this application form: http://www.ebe.uct.ac.za/usr/ebe/research/ethics.pdf

APPLICANT'S DETAILS		
Name of principal researcher, student or external applicant		Alton Marx
Department		Mechanical Engineering
Preferred email address of applicant:		altonmarx@gmail.com
If a Student	Your Degree: e.g., MSc, PhD, etc.,	MSc. Mechanical Engineer
	Name of Supervisor (if supervised):	Prof. Wim Fuls
If this is a researchcontract, indicate the source of funding/sponsorship		EPPEI
Project Title		A stage-by-stage steam turbine process model based on nozzle theory

I hereby undertake to carry out my research in such a way that:

- there is no apparent legal objection to the nature or the method of research; and
- the research will not compromise staff or students or the other responsibilities of the University;
- the stated objective will be achieved, and the findings will have a high degree of validity;
- limitations and alternative interpretations will be considered;
- the findings could be subject to peer review and publicly available; and
- I will comply with the conventions of copyright and avoid any practice that would constitute plagiarism.

SIGNED BY	Full name	Signature	Date
Principal Researcher/ Student/External applicant	Alton Marx	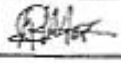	2017/01/18

APPLICATION APPROVED BY	Full name	Signature	Date
Supervisor (where applicable)	Prof. **Wim** Fuls	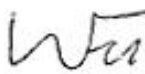	2017/1/18
HOD (or delegated nominee) Final authority for all applicants who have answered NO to all questions in Section1; and for all Undergraduateresearch (Including Honours).	Prof. T. Bello-Ochende		02/02/2017
Chair : Faculty EIR Committee For applicants other than undergraduate students who have answered YES to any of the above questions.			

Page 1 of 1